UNIVERSITY OF CALIFORNIA, SAN DIEGO

Improvement of unnatural amino acid technology and its in vivo application via light-activatable potassium channels

A dissertation submitted in partial satisfaction of the requirements for the degree
Doctor of Philosophy

in

Biology

by

Ji-Yong Kang

Committee in Charge:

Professor Lei Wang, Chair
Professor Edward M. Callaway
Professor Alexander Hoffmann
Professor Ratnesh Lal
Professor Roberto Malinow
Professor Paul A. Slesinger

2013

The Dissertation of Ji-Yong Kang is approved, and it is acceptable in quality and form for publication on microfilm and electronically:

_____

_____

_____

_____

_____

_____
Chair

University of California, San Diego

2013

DEDICATION

This thesis is dedicated to my loving family. Since I was a newborn, my mother has dreamed of me wearing lab coat and doing experiments at the bench. My father always wishes if he continued his study after college, and he is very happy to see me doing research. My brother has always thought of me as his role model and he is my number one fan.

TABLE OF CONTENTS

LIST OF FIGURES

LIST OF ABBREVIATIONS

5-HT_3R	Serotonin receptor
aaRS	Amino acyl synthetase
AAV	Adenovirus-Associated Virus
AME	Acetoxymethyl ester
AMPAR	*α*-Amino-3-hydroxy-5-methyl-4-isoxazolepropionic acid receptor
ANOVA	Analysis of variance
Arch	Archaeorhodopsin-3
Azi	*p*-Azido-phenylalanine
cDNA	Complementary DNA
ChR2	Channelrhodopsin-2
Cmn	4,5-Dimethoxy-2-nitrobenzyl Cysteine
CNS	Central Nervous System
DanAla	2-Amino-3-(5-(dimethylamino)naphthalene-1-sulfonamide) propanoic acid
DCM	Dichloromethane
DIPEA	N,N-Diisopropylethylamine
DIV	Days *in vitro*
DMAP	4-Dimethylaminopyridine
DMEM	Dulbecco's modified Eagle's medium
DMF	N,N-Dimethylformamide
DMSO	Dimethyl sulfoxide
DNA	Deoxy-ribonucleic acid
ESI-TOF	Electrospray ionization-Time of flight
FACS	Fluorescence Activated Cell Sorting
FBS	Fetal Bovine Serum
FCC	Flash Column Chromatography
$GABA_A$R	γ-Aminobutyric acid receptor
GC	Genome Copy

GFP	Green Fluorescent Protein
GHK	Goldman-Hodgkin-Katz
GIRK	G-protein gated Inwardly Rectifying potassium channels
GPCR	G-Protein Coupled Receptor
HEK	Human Embryonic Kidney
HH	Hamburger and Hamilton
HRMS	High-Resolution Mass Spectrometry
HSV-1	Herpes Simplex Virus-1
I_{Kir}	Ba^{2+} sensitive current
IVM	Ivermectin
Kir	Inwardly rectifying potassium channel
KcsA	Potassium crystallographically-sited activation channel
LeuRS	Leucyl synthetase
LC-MS	Liquid Chromatography-Mass spectrometry
LGIC	Ligand-Gated Ion Channel
LV	Lentivirus
mCit	mCitrine, an enhanced yellow fluorescent protein
MEM	Minimum Essential Medium
MOI	Mode Of Infection
MscL	Mechanosensitive channel of Large conductance
nAChR	Nicotinic acetylcholine receptor
NMDAR	N-Methyl-D-Aspartic acid Receptor
NMM	N-Methylmorpholine
NMR	Nuclear Magnetic Resonance
Npg	2-(Nitrophenyl)glycine
NpHR	*Natronomonas pharaonis* Halorhodopsin
OMeY	*o*-Methyltyrosine
pBPA	*p*-Benzoylphenilalanine
PEI	Polyethylenimine
PI	Propidium iodide

PIRK	Photo-activatable Inwardly Rectifying potassium channel
RCF	Relative Centrifugal Force
RNA	Ribonucleic acid
ssRNA	Single-stranded RNA
TeNT	Tetanus neurotoxin light chain
TFA	Trifluoroacetic acid
TLC	Thin Layer Chromatography
tRNA	Transfer RNA
TyrRS	Tyrosyl synthetase
Uaa	Unnatural amino acid
YFP	Yellow Fluorescent Protein

ACKNOWLEDGEMENTS

First and foremost, I would like to express my sincere gratitude to my mentor, Lei Wang. From the time I first started my project, he has been extremely supportive in many possible ways. He gave me complete liberty to ask any scientific question I would like to have answers for. And he always had trust in me that I could solve problems in the journey of my studies. With his support, I could push through many obstacles and I was able to access lots of resources from neighboring laboratories and facilities at Salk Institute and UCSD. Again, I thank him for giving me the opportunity to study in his laboratory and I believe I have grown as a better scientist in his laboratory.

I would also like to thank Paul Slesinger. My studies would have not been accomplished without him and his laboratory. He taught me how to conduct electrophysiology and how to analyze its data. He has always challenged me with intruiging scientific questions and trained me to be a comprehensive scientist. At the same time, I enjoyed sharing fun stories with him and he has been my friend. Members in his laboratory always welcomed me in their working space and offered me with helpful discussions. I thank Michaelanne Munoz, Bartosz Balana, Karthik Bodhinathan, Natalie Taylor, Claire Padgett, and Laia Bahima, for their generosity and friendship.

I am honesly grateful that the UCSD Biology graduate program gave me the fantastic opportunity to study in this rich life science ecosystem. My committee members, Paul Slesinger, Edward Callaway, Roberto Malinow, Alexander Hoffman, and Ratnesh Lal have guided me throughout my studies with constructive discussions and generous supply of resources. I acknowledge all of my past and present members of my laboratory for helping me throughout my studies. Bin Shen, Jeff Takimoto, David Johnson, Angela Parrish, Vanessa Lacey, Xingyu She, Irene Coin, Zheng Xiang, Sam Ulin, Haiyan Ran, Hanjun Kim, and Xiaohua Chen have helped me scientifically and as good friends. I would like to thank Edward Callaway, Roberto Malinow, Sam Pfaff, and Inder Verma for providing me with their laboratory resources and helpful advices. I would specially like to thank Daichi Kawaguchi for his excellent work on *in utero* experiments. He has been a great coworker with positivity and leadership. I also thank Salk Viral Vector Core and Dan Gibbs for helping me with his expertise in viral vectors. CBPL has been home to my research throughout my graduate school. I thank all of the CBPL family, especially Marianne Bowman and June Brennan, for helping me do my research in friendly and efficient environment.

My family has always been supportive for me to complete my studies. They encouraged me to take this great opportunity to study at UCSD even before I made my decision to come to USA, and they have since brought me up to have positivity and confidence whenever they could. Above all, I thank my parents for all their sacrifices to provide a better life for my brother and me. My brother,

Joong Keon Kang, has always been my great friend and has encouraged me throughout my journey. I truly thank Matt Zones, who has been at my side through the ups and downs of graduate school. I would not be this far in my journey without his consistent love and support.

Chapter 2, in part, has been submitted for publication of the material as it may appear in Kang, J.Y., Kawaguchi, D., Coin, I., Xiang, Z., O'Leary, D.D.M., Slesinger, P.A., and Wang, L. (2013) Neuron. The dissertation author was the first author, and the chair of my thesis committee was the senior author of this paper. Chapter 3, in part, is a reprint of the material as it appears in Takimoto, J. K., Xiang, Z., Kang, J. Y., and Wang, L. (2010) Chembiochem. The dissertation author was the third author, and the chair of my thesis committee was the senior author of this publication. Permission to use this work as a part of my dissertation has been obtained from all the co-authors.

VITA

EDUCATION

Ph.D.	**University of California, San Diego** Biology	2013
M.S.	**Seoul National University** Chemistry	2007
B.A.	**Seoul National University** Double majored in Biology & Chemistry	2005

TEACHING

Teaching assitant

- Structural biochemistry class at UCSD 2009
- Recombinant DNA techniques laboratory class at UCSD 2008
- General chemistry laboratory class at Seoul National University 2006
- Biochemistry laboratory class at Seoul National University 2005

RESEARCH

Lei Wang Lab, Salk Institute of Biological Science, La Jolla, CA 2008–2013

- Ph.D. student researcher
- Focuses on neuroscience, biotechnology, structural biology, molecular & cell biology
- Developed an original ion channel that can control neuronal activity with light irradiation
- Pioneered new technology to apply unnatural amino acid in vivo using rodent brains
- Engineered a *de novo* protein with quadruple unnatural amino acid incorporation
- Improved unnatural amino acid incorporation in mammalian cells

Se Won Suh Lab, Seoul National University, South Korea 2005–2007

- Master's student researcher, Thesis: "Overexpression, crystallization & preliminary X-ray crystallographic analysis of a putative transposase from *Thermoplasma acidophilum* encoded by the Ta0474 gene"
- Focused on structural proteomics using X-ray crystallography
- Revealed the structure of two prokaryotic proteins & one human protein

Jeong bin Yim Lab, Seoul National University, South Korea 2003

- Undergraduate researcher, Project: The elucidation of the biosynthetic route of drosopterin, an accessory eye pigment in *Drosophila melanogaster*
- Characterized eye pigment enzymes using biochemistry assays

FELLOWSHIPS AND AWARDS

- University of California, San Diego 2011
  Received the H.A. & Mary K. Chapman Charitable Trust Award
- Seoul National University 2005-2007
  Awarded the Brain Korea 21 program Fellowship
- Seoul National University 2003-2004
  Awarded tuition scholarship

PUBLICATION

- **Kang, J. Y.**, Kawaguchi, D., Coin, I., Xing, Z., O'Leary, D. D., Slesinger, P. A., and Wang, L. *in review*
- Yoon, H. J., **Kang, J. Y.**, Mikami, B., Lee, H. H., and Suh, S. W. (2011). Mol. Cells, *32*, 431−5.
- Takimoto, J. K., Xiang, Z., **Kang, J. Y.**, and Wang, L. (2010). Chembiochem, *11*, 2268−72.
- Lee, H. H., Yoon, H. J., **Kang, J. Y.**, Park, J. H., Kim, do J., Choi, K. H., Lee, S. K., Song, J., Kim, H. J., and Suh, S.W. (2009). Acta Crystallogr. Sect. F Struct. Biol. Cryst. Commun. *65*, 987−91.
- Lee, H. H., Kim, H. S., **Kang, J. Y.**, Lee, B. I., Ha, J. Y., Yoon, H. J., Lim, S. O., Jung, G., and Suh, S. W. (2007). Proteins, *69*, 672−8.
- **Kang, J. Y.**, Lee, H. H., Kim, do J., Han, S. H., Kim, O., Kim, H. S., Lee, S. J., and Suh, S. W. (2006). Acta Crystallogr. Sect. F Struct. Biol. Cryst. Commun. *62*, 1147−9.
- **Kang, J. Y.**, Lee, H. H., Yoon, H. J., Kim, H. S., and Suh, S. W. (2006). Acta Crystallogr. Sect. F Struct. Biol. Cryst. Commun. *62*, 1131−3.
- Lee, H. H., Yoon, J. Y., Kim, H. S., **Kang, J. Y.**, Kim, K. H., Kim, D. J., Ha, J. Y, Mikami, B., Yoon, H. J., and Suh, S.W. (2006). J. Biol. Chem. *281*, 4261−6.
- Han, S. H., Ha, J. Y., Kim, K. H., Oh, S. J., Kim, do J, **Kang, J. Y.**, Yoon, H. J., Kim, S. H., Seo, J. H., Kim, K. W., and Suh, S. W. (2006). Acta Crystallogr. Sect. F Struct. Biol. Cryst. Commun. *62*, 127−30.

ABSTRACT OF THE DISSERTATION

Improvement of unnatural amino acid technology and its in vivo application via light-activatable potassium channels

by

Ji-Yong Kang

Doctor of Philosophy in Biology

University of California, San Diego, 2013

Professor Lei Wang, Chair

Unnatural amino acid (Uaa) technology has broken new ground in the protein research and introduced a plethora of chemical groups that can be incorporated to the existing proteins for new functionality. Here, we incorporated

4,5-dimethoxy-2-nitrobenzyl-Cysteine (Cmn) into the pore region of inwardly rectifying potassium channel Kir2.1 to make a Photo-activatable Inwardly Rectifying Potassium channel, or PIRK. Bulky side chains of Cmn block the channel pore physically, which leaves the channel non-functional. After brief UV irradiation however, 4,5-dimethoxy-2-nitrobenzyl groups are released from Cmn to reactivate the channel. When PIRK was introduced in rat hippocampal primary neurons, the neuronal activity was completely suppressed with a brief UV pulse. We also expressed functional PIRK in the mice embryonic neocortex to present the successful *in vivo* application of the method. This strategy is directly transferrable to other ion channels and receptors, and its application has great potential in unraveling mechanisms of native and diseased brain circuitry. On the other hand, we improved Uaa uptake rate and intracellular concentration in mammalian cells using noncanonical side chains where the Uaa is masked by selected ester groups. This result can boost Uaa incorporation efficiency in mammalian cells, thus reducing the amount of Uaas required.

Chapter 1

INTRODUCTION

1.1 Unnatural amino acid technology

1.1.1 Development of unnatural amino acids

To challenge the limits set by the number of canonical amino acids, unnatural amino acids (Uaas) are introduced to existing proteins to add or modify their function. More than two decades ago, P. Schultz and coworkers first reported site-specific incorporation of a Uaa into *β*-lactamase (Noren, 1989). Intensive exploration in the field has since elaborated the technology to incorporate over 70 different Uaas in a variety of proteins (Liu, 2010).

Some Uaas acted as probes in the incorporated proteins. For example, Uaas with unique NMR signals or IR/X-ray diffraction signatures were adopted to reveal protein structure (Cellitti, 2008; Schultz, 2006). Fluorescent Uaas were incorporated to label proteins' location in cells or to monitor proteins' folding status (Lacey, 2011; Lee, 2009). Other Uaas had their own biophysical properties. Redox-sensitive Uaas (Seyedsayamdost, 2007), back-bone mutated Uaas (Guo, 2008), photo-caged Uaas (Lemke, 2007), or photo-crosslinking Uaas (Coin, 2011) are some examples. Specifically, site-specific photocrosslinking enabled by genetically encoded Uaas, such as *p*-benzoylphenilalanine (pBpA) and *p*-azido-phenylalanine (Azi), helped to uncover protein interactions in cells (Coin, 2011; Hino, 2005; Schlieker, 2004). Uaas are also utilized in protein therapeutics. Immunogenic amino acids can be used to generate therapeutic vaccines (Grunewald, 2008). Moreover, new protein conjugates can be produced using Uaas containing bioorthogonal reactive functional groups (Deiters, 2004).

Uaas are genetically encoded using the orthogonal tRNA/amino acyl synthetase (aaRS) pair (Wang, 2009). The fundamental strategy behind the method first entails genetic mutation of single amino acid in the protein of interest to TAG, the amber stop codon. The gene construct encoding the TAG-mutated protein will be introduced into cells. In a similar manner, the suppressor tRNA encoding anticodon CUA to read through UAG, and its partner aaRS to acylate a unique Uaa with amber-suppressor tRNA will be introduced to the cells using genetic recombinant technique. Upon exogenous addition of Uaas into the cells, suppressor tRNA/aaRS pair will incorporate the Uaa into the TAG-mutated residue in the protein of interest. The characteristics of this 'Uaa-incorporated protein' can be tested using multiple different assays.

1.1.2 Unnatural amino acids in neuroscience

Unique Uaas endowed neuronal proteins with novel properties in living cells. Fluorescent Uaas were encoded into muscle nicotinic acetylcholine receptors (nAChRs) to realize single-molecule imaging in *Xenopus laevis* oocyte (Pantoja, 2009). Photo-crosslinker incorporated G-protein coupled recepters (GPCRs) successfully captured their binding partners (Coin, 2011; Grunbeck, 2011). More interestingly, caged amino acids were encoded to ion channels to control their function externally (England, 1999; Philipson, 2001; Tong, 2001). For example, Philipson *et. al* incorporated caged Cys and Tyr into nAChRs to change its gating kinetics (Philipson, 2001). The caged receptors immediately

recovered their native kinetic pattern after photolysis of caging groups. On the other hand, 2-(nitrophenyl)glycine (Npg) was used to cage the polypeptide backbone to identify the secondary structure of the ion channel (England, 1999). Along with caged neurotransmitters, the temporal and spatial precision of this technology boosted the study of neuronal signal transduction (Riggsbee, 2010).

Uaa technology has especially benefitted the research on ion channels, which has been stagnated by a paucity of three-dimensional structural information (Beene, 2003; Dougherty, 2000). Detailed structural dynamic information such as agonist binding, gating, or voltage sensing been revealed using Uaas incorporated with chemically acylated tRNA injected in *Xenopus laevis* oocytes (Li, 2001; Lummis, 2005; Tao, 2010). However, their expression is circumscribed by injection volume of amino acyl-tRNA, and application of this method into mammalian cells is hampered by technical difficulties. Genetic incorporation of Uaas using orthogonal tRNA/amino acyl synthetase (aaRS) pair was developed and this technique has been successfully transferred to mammalian systems (Wang, 2009). For example, Wang *et. al* genetically incorporated Uaas in potassium channel Kv1.4 to study its fast inactivation mechanism in human embryonic kidney (HEK) cells and rat hippocampal primary neurons (Wang, 2007).

1.2 Ion channel engineering

1.2.1 Ion channels

A living cell has a phospholipid bilayer of membrane that forms a natural barrier for metabolites and chemical signals. Ions and substrates pass through this semi-permeable barrier via multiple ways. Hydrophobic or small polar molecules (oxygen and carbon dioxide for example) pass the membrane with simple diffusion. However, the transport of many large molecules is facilitated by transporters, channels, or carriers. Molecules flow down their electrochemical gradient through ion channels and carriers. On the other hand, ion pumps and co-transporters move molecules against their electrochemical gradient.

Ion channels are far more efficient in permitting the flow of ions than carriers where they have to diffuse with their cargo through the membrane. At the same time, ion channels maintain high specificity for their substrates. Because of these reasons, ion channels were seen as evolutionary developed high performance devices with key functions in sensing, neuronal signal transduction, and muscular control (Grosse, 2011). Therefore, ion channels have been targets for constructing biosensors, interfacing the biological surfaces with semiconductors, or developing therapeutic applications (Grosse, 2011; Halverson, 2005; Millar, 2007).

1.2.2 Engineering ion channels

The study of ion channels opened up possibilities to engineer ion channels with modified or novel functionality. Firstly, many approaches aimed at changing selectivity of ion channels. After resolving high-resolution X-ray crystallographic

structure of the bacterial potassium channel KcsA, MacKinnon and coworkers provided the first structural basis for potassium channel engineering (Doyle, 1998). The selectivity filter of a potassium channel is aligned by the backbone of conserved polypeptide sequence T/S-V/I/L/T-GYG (Macri, 2012). When Muir group engineered a truncated KcsA channel where the amino bond T – G was replaced by an ester bond, cation affinity of this channel was significantly shifted (Valiyaveetil, 2006). For another example, the pore of *α*-hemolysin was engineered to enable stochastic sensing. By attaching a synthetic cyclodextrin adaptor to the pore, a nanopore detecting ribonucleoside- and deoxyribonucleoside 5°-monophosphates was created (Bayley, 2001). Ribonucleoside- and deoxyribonucleoside 5°-monophosphates bind to the ammonium group of cyclodextrin, in order to alter ionic current through the pore in particular ways. Similarly, enantiomers of drug molecules like ibuprofen and thalidomide were separated using a nanopore with a chiral cyclodextrin adaptor (Kang, 2006).

Secondly, many creative methods have been invented to control gating of ion channels. Trauner and Kramer introduced a photo-switchable tethered ligand to open and close ion channels (Banghart, 2004). In their study, the ligand was chemically attached to the extracellular side of Shaker channel to block the pore entrance (*trans*-conformation). The ligand photoisomerized to *cis*-conformation after 380nm light irradiation to release the channel block. Photoisomerable glutamate receptors were developed in a similar way (Volgraf, 2006). On the

other hand, Feringa group studied the pH-dependent opening of the mechanosensitive channel of large conductance (MscL) channel upon protonation of engineered basic functional groups in the constriction zone of the channel (Koçer, 2006).

Lastly, researchers have also designed *de novo* ion channels. For example, Matile and coworkers assembled ion channel active pores by combining rigid rod building blocks in *β*-barrel structure (Sakai, 2005). Selectivity and functionality of these channels could be fine-tuned by modulating the building block structure. In conclusion, above attempts have not only deepened our understanding of ion channels but also expanded the horizon of ion channel application in basic and applied science.

1.3 Controlling neuronal activity

1.3.1 Neuronal excitability regulation

Many brain diseases stem from irregular excitability of the corresponding circuitry. That is, aberrant firing of neurons disturbs normal information flow in brain and can cause neuropsychiatric diseases. For example, exceptional firing of neurons in the subthalamic nucleus has been implicated in Parkinson's disease (Remple, 2011). Likewise, abnormal diminution of neuronal activity is involved in central nervous system (CNS) depression, neuronal conduction disorder, or cognition disorder. Irregularly augmented neuronal activity is related

to CNS hyperexcitability, epilepsy, pain, or neuropsychiatric diseases such as anxiety and schizophrenia (Wulff, 2009).

Activation or silencing of a set of neurons in a time-specific manner allows for the study of neuronal circuitry in developing and adult systems in their native or disturbed states (Callaway, 2005; Tervo, 2007). By manipulating neuronal activity exogenously, researchers can demonstrate a distorted neuronal circuitry in an experimental setup in order to study its mechanism and ultimately to find a way to alleviate its symptom. Deep brain stimulation technology to stimulate disease-implicated neurons has led to powerful therapies in clinical neuroscience (Lozano, 2013). On the other hand, electronic stimulation is often applied to study neuronal circuitry and their functional relationship in basic neuroscience. Selective activation/suppression of the target neurons' activity provides the readout of their functional connectivity and related mechanism.

1.3.2 Approaches to control neuronal activity

Earlier approaches focused on transcriptional regulation of a specific ion channel to regulate neuronal activity. When G-protein gated inwardly rectifying potassium channels (GIRKs) were overexpressed in cultured hippocampal neurons, GIRK activation increased the cell membrane conductance by 1- to 2-fold, hyperpolarized the cell by 11–14 mV, and inhibited action potential firing by increasing the threshold current for firing by 2- to 3-fold (Ehrengruber, 1997). Likewise, voltage-dependent potassium channel Kv1.4 was expressed in primary

cultured rat skeletal muscle cells (Falk, 2001). Increase in K^+ current led to a decrease in membrane resistance and a 10-fold increase in the current threshold for action potential generation in these cells.

Some studies used membrane-tethered toxins to block ion channels and membrane receptors. Heintz and coworkers tethered *α*-bungarotoxin to nAChRs in zebrafish. This targeted elimination of nAChRs silenced synaptic transmission without inhibiting synaptic formation (Ibanez-Tallon, 2004). Glutamatergic neurotransmission was also suppressed in a specific manner using tetanus neurotoxin light chain (TeNT) (Yamamoto, 2003). Along with its expression, TeNT proteolytically cleaved the synaptic vesicle protein VAMP2/Synaptobrevin and reduced glutamate release from granule cells.

More elaborate control over spiking or synaptic transmission was achieved by pharmaceutically based methods. Svoboda group invented a method to control neurotransmitter release reversibly (Karpova, 2005). Chemically induced dimerization of two vesicle proteins VAMP2/Synaptobrevin and Synaptophysin blocked synaptic transmission in about 10 minutes. Reversibly, the block was released after the chemical was washed out. On the other hand, Lester group expressed invertebrate ivermectin (IVM)-sensitive chloride channels (*Caenorhabditis elegans* GluCl *α* and *β*) in HEK cells and then activated these channels with IVM to produce inhibition via a Cl^- conductance (Slimko, 2002). Similarly, using expression of *Drosophila melanogaster* allatostatin receptors in

mammalian neurons, neuronal spiking activity could be rapidly and reversibly silenced *in vivo* (Lechner, 2002; Tan, 2006). Despite handful successes with these approaches, their slow kinetics and potential side effects hindered them to be more broadly adopted.

1.3.3 Optical control of neuronal activity

Since Fork shined his first laser light on Aplysia abdominal ganglian neurons to evoke action potential in 1971 (Fork, 1971), optical stimulation technology over neuronal cells has greatly improved in both the biochemical toolkit and laser optics. Optical approach is extraordinarily powerful in that it can achieve a great temporal/spatial resolution with minimal damage to subjects. It especially fascinates neuroscientists since (1) the speed of light activation can mimic a fast signal transmission between neurons; (2) two-photon excitation can control a single neuron's function in the meshwork of brain circuitry; and (3) *in vivo* recording from a moving animal is possible with a specific light apparatus. Therefore, there have been numerous attempts to devise active chromophore-containing chemical compounds, and channel proteins that can modulate ion channel activity or neurotransmitter distribution in response to light.

Many creative approaches were targeted to use light to stimulate neurons. First, photocaged agoinsts were invented to activate partner ion channels and receptors in a local region of brain tissue in a timely controlled fashion. The earliest innovation was the development of caged glutamate (Callaway, 1993). In

this study, caged glutamate in synaptic cleft was released by laser stimulation to bind to postsynaptic receptors to initiate downstream signaling. This was the first attempt to combine optic stimulation with electronic stimulation from the presynapse. Since then, many caged molecules and their application have been studied (Cambridge, 2009; Yoshimura, 2005). Still, this technique has limitation in that the diffusion of caged neurotransmitters makes it difficult to stimulate specific target neurons.

In another approach, an ion channel or postsynaptic receptor is engineered to operate it by light irrespective of ligand availability. A representative case is photoisomerizable azobenzene compound-tethered potassium channel (Banghart, 2004; Volgraf, 2006). An azobenzene moiety covalently linked to cysteine residue in the extracellular domain of Shaker K^+ channel blocks the pore of channel in its *trans*-configuration. Upon UV absorption, the azobenzene moiety isomerizes to *cis*-form to unblock the pore. This clever invention is based on delicate structural information about the channel protein and is advantageous in that it provides reversible control over channel function. However, exogenously added azobenzene compound can cross-react with other Cys residues in the channel protein, which will complicate the result. In addition, the reaction does not go to completion, resulting in incomplete blockage of membrane-expressed K^+ channels.

The most outstanding approach is the adoption of a natural photoreactive protein, channelrhodopsin. Channelrhodopsin-2 (ChR2), light-sensitive cation channel adopted from green alga *Chlamydomonas reinhardtii*, was delivered to rat hippocampal neurons to show light-driven excitation of the neuron (Boyden, 2005). Soon after, the negative regulation counterpart of ChR2, NpHR was introduced (Zhang, 2007). NpHR is light-driven chloride pump from archea *Natronomonas pharaonis*, which can suppress the neuronal activity when expressed in neuron. ChR2 and NpHR have been applied to neurons to convey bidirectional control (Zhang, 2007). A nice feature of the channelrhodopsin method is that it uses naturally occurring proteins that respond to visible light. *in vivo* application of this technique was quickly realized (Adamantidis, 2007; Aravanis, 2007). At the same time, intensive studies have improved the expression efficiency and photocurrent amplitude of halorhodopsin (NpHR) (Gradinaru, 2010). More recently, a proton pump originated from the halobacterium *Halorubrum sodomense*, Archaeorhodopsin-3 (Arch), was discovered (Chow, 2010). NpHR and Arch are members of the family that are employed to silence neuronal activity. With technical improvement, Arch and Halo both can induce ~250 pA photocurrent with 3.5 mW/mm^2 light exposure (Gradinaru, 2010).

Still, there are still some concerns about these applications. First of all, continuous light stimulation is required to get constant excitation or inhibition of neural activity with channelrhodopsin method, which might cause phototoxicity to

the specimen. Persistent light stimulation is also more difficult in moving animals, so that delayed response of animals to photostimulation/inhibition is hard to be measured with the method. Moreover, this is not ideal for the study such as epilepsy where it is important to maintain membrane hyperpolarization for a long period of time (Kokaia, 2012).

Secondly, blue light, used to activate ChR2, is hard to penetrate deep inside the tissue. On the other hand, overexpression of NpHR may disrupt chloride homeostasis of the cell. Sufficient influx of Cl^- ion caused depolarization to excite GABAergic synapses, leading to excitotoxicity (Raimondo, 2012). Furthermore, high intracellular Cl^- level has been implicated to hamper G-protein signaling pathways. This could be a similar problem for Arch. When Arch is illuminated for the extended time period, intra/extracellular pH disturbance could possibly impact negatively on the cell health (Han, 2012; Okazaki, 2012).

1.4 Inwardly rectifying potassium channels

1.4.1 Inwardly rectifying potassium channel physiology

Novel K^+ currents that flow more readily into the cell than out of the cell was first observed in skeletal muscle and described as ‘anomalous’ rectifier K^+ currents (Katz, 1949). This characteristic was very different from that of voltage-gated potassium currents and later defined as inwardly rectifying K^+ (Kir) currents. Under physiological conditions, Kir channels permit a large K^+ current flow at

potentials negative to E_K but generate less conductance at potentials positive to E_K, thus regulating resting membrane potential. Kir channels can be found in cardiac myocytes, neurons, blood cells, osteoclasts, endothelial cells, glial cells, epithelial cells, and oocytes (Hibino, 2010).

Kir channel comprises four subunits each with two transmembrane domains (M1 and M2 helices) that are linked by pore-forming P domain. Similar with other K^+ channels, the P domain forms a selectivitiy filter with consensus GYG sequence (Dart, 1998; Kubo, 1998). M2 domain lines the ~10 Å wide inner pore in the cytoplasmic side of the membrane, which continues to the wider cytoplasmic pore (Minor, 1999). Inward rectification characteristic of Kir channels was found out to be a result of pore blockage by intracellular Mg^{2+} or polyamines (Lopatin, 1994; Matsuda, 1987). So far, fifteen Kir genes have been identified and classified into seven subfamilies (Kir1 to Kir7).

Kir channels in skeletal and cardiac muscles are categorized as Kir2 subfamily. Kir2.1 is a strong rectifier in this family and responsible for regulating processes including cell excitability, vascular tone, heart rate, renal salt flow and insulin release. In heart for example, Kir2.1 functions to set the resting potential, to permit the plateau phase, and to induce rapid final stages of repolarization (Hibino, 2010).

Earlier prediction of Kir2.1 structure (Kubo, 1993) was followed by a number of studies regarding pore topology and cytoplasmic structure of the protein (Garneau, 2003; Kurata, 2007; Lu, 1999a; Lu, 1999b; Minor, 1999). X-ray crystallographic studies later revealed Kir2.1 structure and confirmed these predictions. For example, characterization of the Kir2.1 cytoplasmic structure (Pegan, 2005) and the structure of bacterial protein KirBac1.1 (~26% sequence homology with rat Kir2.1; Kuo, 2003) helped understand Kir2.1 topology. More recently, high-resolution structure of chicken Kir2.2 (~76% sequence homology with rat Kir2.1) was reported to demonstrate Kir2.1 structure much more clearly (Tao, 2009).

1.4.2 Engineering inwardly rectifying potassium channels

Kir2.1 is a strong inward rectifying potassium channel that is crucial in regulating neuronal excitability, action potential cessation, hormone secretion, heart rate, and salt balance (Bichet, 2003). At resting membrane potential of a neuron, Kir2.1 effuses small K^+ current to keep the membrane potential balance. Once a neuron reaches the action potential threshold however, Kir2.1 current becomes negligible because of its strong inward rectification property. The strong inward rectifying ability of Kir2.1 makes it a good model to engineer in order to silence target neurons. That is, overexpression of Kir2.1 hyperpolarizes the membrane potential of a target neuron, which becomes less excitable. Because of its direct neuronal silencing ability by disturbing K^+ balance, and lack of

obvious side effects, Kir2.1 has been used in a variety of researches to study the effect of neuronal excitability over the last decade (Burrone, 2002; Johns, 1999).

The study of engineering potassium channels flourished after it was revealed that their overexpression could silence the neurons (White, 2001). However, its application was limited since the chronic efflux of potassium led to the cell apoptosis unless counteracted by augmented potassium concentration in the culture medium (Nadeau, 2000). Strongly rectifying potassium channel Kir2.1 was recognized as a preferred target since it does not kill cells due to potassium leak unlike weakly rectifying potassium channels. Genetically inducible Kir2.1 was devised to manipulate excitability at different temporal points in development or different spatial regions in embryonic stem cells, *Drosophila melanogaster*, or transgenic mice (Liao, 2013; Thum, 2006; Yu, 2004).

1.4.3 Developing photo-activatable inwardly rectifying potassium channels

Kir2.1 regulates neuronal excitability with its membrane hyperpolarizing ability. Studies have shown that Kir2.1 overexpression can suppress the targeted neurons' excitability (Johns, 1999; Burrone, 2002). In this study, we created a light inducible version of Kir2.1, referred as PIRK (photo-activatable inwardly rectifying potassium channel). 4,5-Dimethoxy-2-nitrobenzyl group is a photocaging group used to cage agonists or key residues in cellular signaling (Lemke, 2007; Zemelman, 2003). By incorporating 4,5-dimethoxy-2-nitrobenzyl

Cysteine (Cmn) in the inner pore of Kir2.1, we blocked the K^+ current with bulky chromophores of Cmn. With a brief light pulse, 4,5-dimethoxy-2-nitrobenzyl groups are photolysed to render the channel functional again.

Genetic incorporation of a photolysable Uaa in the Kir2.1 pore domain to deliver light-induced activation of the channel is the most promising strategy for the photostimulated suppression of neuronal activity. First, genetic targeting is possible with cell-specific promoter to gain cell-specific stimulation. Second, targeted incorporation of Uaas with a specific tRNA/aaRS pair will avoid cross-reaction of exogenous compounds with non-targeted residues. In addition, failure to incorporate Uaas will result in a truncated protein that will not localize to the membrane and is devoid of normal channel function. This assures the complete control of membrane expressed Kir2.1 by light.

Third, a two-photon excitable uncaging group can be efficiently incorporated in the channel with a specific tRNA/aaRS pair. In spite of the great success, two-photon excitation technology is hard to apply in channelrhodpsin methods. All-*trans*-retinal, the shared chromophore for channelrhodopsins, does not have a two-photon excitable cross-section. In contrast, Uaa technology is not limited by the chromophore availability. With the invention of an uncaging compound with a two-photon cross-section and evolution of corresponding specific tRNA/aaRS pair, two-photon excitation is readily applied to Uaa

technology to attain a single-cell level resolution. A nanosecond to microsecond-scale brief pulse of two-photon stimulation is enough to get the desired outcome.

Lastly, this strategy can be easily applied to other types of channel proteins to modulate their specific function, suggesting a new tool to study other channel proteins or receptor proteins in the synapse. It will shed light on the research of synaptic mechanism to understand neuronal connectivity and can eventually be applied to reveal the mechanisms of many brain diseases.

Chapter 2

DEVELOPING PHOTO-ACTIVATABLE INWARDLY RECTIFYING POTASSIUM CHANNELS (PIRK)

2.1 Abstract

Optical control of protein function provides excellent spatial-temporal resolution for studying proteins *in situ*. Although light-sensitive exogenous proteins have been employed to manipulate neuronal activity, this approach cannot be readily transferred to optically control proteins native to neurons. Here, we describe the genetic incorporation of a photoreactive unnatural amino acid (Uaa) into the pore of an inwardly-rectifying potassium channel Kir2.1 expressed *in vivo*. The Uaa occluded the pore, rendering the channel non-conducting, and upon brief light illumination, was released to permit outward K^+ current. Expression of this photo-inducible inwardly rectifying potassium (PIRK) channel in rat hippocampal neurons created a light-activatable PIRK switch for suppressing neuronal firing. We also expressed PIRK channels in embryonic mouse neocortex *in vivo* and demonstrated a light-activated PIRK current in cortical neurons. The principles applied here to a potassium channel could be generally expanded to other proteins natively expressed in the brain to enable optical regulation.

2.2 Introduction

The ability to control protein function with light provides excellent temporal and spatial resolution for precise investigation *in vitro* and *in vivo*, and thus is having significant impact on neuroscience. For example, naturally light-sensitive opsin channels and pumps have been exploited to excite or inhibit neurons, enabling specific modulation of selected cells and circuits in diverse model

organisms (Bernstein, 2011; Fenno, 2011; Yizhar, 2011). However, this approach relies on the ectopic expression of an exogenous or chimera protein requiring retinal as the chromophore for controlling the behavior of neurons, so that its application to a wide variety of endogenous proteins is difficult. Another elegant method engineers light responsiveness into endogenous receptors and channels by chemically tethering a photo-switchable azobenzene-coupled ligand (Szobota, 2010). The ligand is presented or withdrawn from the binding site of the protein through the photo-isomerization of the azobenzene moiety. This approach cannot address proteins that are expressed but failed to conjugate with azobenzene-coupled ligands, and ligand tethering has been limited to the extracellular side of membrane proteins, excluding the intracellular side and intracellular proteins.

Photo-responsive Uaas provide another flexible avenue for optical control of proteins activities. Microinjection of tRNAs chemically acylated with Uaas allows the incorporation of photocaged Uaas into receptors and ion channels in *Xenopus oocytes*, which have revealed novel insights on their structure and function (England, 1997; Miller, 1998). The requirement of microinjection has mainly limited this approach to large oocytes. Genetically encoding Uaas with orthogonal tRNA/synthetase pairs enables the Uaa to be incorporated into proteins with high protein yields in mammalian cells and organisms (Liu, 2010; Wang, 2001; Wang, 2006; Wang, 2009), providing potential for studying proteins directly in primary neurons and mouse models (Shen, 2011; Wang, 2007). A challenge in the neuroscience field, however, has been the application of Uaa

technology in mammalian neurons *in vitro* and ultimately in the mouse brain *in vivo*. Here we demonstrate the optical control of a native protein expressed in neurons *in vitro* and *in vivo* using a genetically encoded photoreactive Uaa. Kir2.1 is a strong inwardly-rectifying potassium channel that is crucial in regulating neuronal excitability, action potential cessation, hormone secretion, heart rate, and salt balance (Bichet, 2003). We incorporated Cmn into the pore of Kir2.1, generating a photo-activatable inwardly rectifying potassium (which we refer to as 'PIRK') channel. Light activation of PIRK channels expressed in rat hippocampal neurons suppressed neuronal firing. In addition, we expressed PIRK channels in embryonic mouse neocortex and measured light-activated PIRK current in cortical neurons, demonstrating for the first time the successful implementation of the Uaa technology *in vivo*. Genetically encoding Uaas has no limitations on protein type and location (Wang, 2005), and photocaging is compatible with modulating various proteins (Adams, 1993; Fehrentz, 2011). We therefore expect our method can be generally applied to other brain proteins, enabling optical investigation of a range of natively expressed channels, receptors, and signaling proteins in the brain.

2.3 Results

2.3.1 Initial attempt to find a candidate site for Cmn incorporation

Potassium ions flow through the central pore of Kir2.1 channels (Ishii, 1994; Kubo, 1993). We reasoned that incorporation of a Uaa with a bulky side chain might occlude the channel pore and restrict current flow. Photolysis of the

Uaa would enable release of the bulky side chain moiety and restore current flow through the channel, thus creating a photo-activatable inwardly rectifying potassium channel, PIRK (Figure 2.1A). Ideally, a natural amino acid residue can be regenerated after discharging the caging compound, minimizing potential perturbation to protein structure and function. Cmn is a perfect Uaa for incorporation. The dimethoxynitrobenzyl group of Cmn is readily hydrolyzed by UV or blue light, releasing the cage group and becoming Cys (Figure 2.1B) (Rhee, 2008). Compared to the conventional photocaging *o*-nitrobenzyl group, the dimethoxynitrobenzyl group is bulkier and has a higher quantum yield to facilitate photolysis. Previously, 4,5-dimethoxy-2-nitrobenzyl serine was incorporated into the transcription factor Pho4 in *Saccharomyces cerevisiae* to control phosphorylation with light (Lemke, 2007). Based on the similar structure and characteristics between serine and cysteine, we hypothesized that the orthogonal $tRNA^{Leu}_{CUA}$ /synthetase pair evolved in yeast to incorporate 4,5-dimethoxy-2-nitrobenzyl serine might also selectively incorporate Cmn. Indeed, Cmn is efficiently incorporated into proteins in mammalian cells by this pair, which we refer to as $tRNA^{Leu}_{CUA}$/CmnRS for clarity. Like the hydroxyl group of Ser, the sulfhydryl group of Cys also provides a chemically reactive amino acid for possible secondary modifications, thereby expanding scope of photocaged Uaas. Cmn was chosen over 4,5-dimethoxy-2-nitrobenzyl serine because multiple pore lining residues of Kir2.1 are known permissive for the Cys mutation, so that a

functional Kir2.1 is ensured after photolysis (Dart, 1998; Kubo, 1998; Lu, 1999a; Lu, 1999b, Minor, 1999; Xiao, 2003).

To achieve photo-activation of Kir2.1 using Cmn, we considered the following criteria for identifying a target site for incorporation into the channel protein: (1) the residue should be exposed to the channel pore for Cmn incorporation; (2) the side chain of the residue should be heading towards the pore axis so that incorporated Cmn would reside in the pore lumen but not be buried in the hydrophobic core; (3) the size of the pore plane where the residue is located should be large enough to accommodate four Cmn molecules (one from each subunit of Kir2.1 homotetramer) without disrupting protein folding; (4) the size of the pore plane where the residue is located should be small enough that incorporated Cmn molecules would completely block the pore; and (5) that photolysis of Cmn recovers normal Kir2.1 function, i.e., Cys mutation of the residue does not interfere with Kir2.1 function.

Phe147 was first selected as a target residue for several reasons. It is exposed to the channel pore and F147C mutation retains ~70% of wild-type Kir2.1 conductance (Dart, 1998; Kubo, 1998). It is located in the selectivity filter region of the channel next to GYG consensus sequence. It was expected that Uaas would more easily block the pore because the selectivity filter region forms the narrowest part of the entire channel lumen. For the control experiments, inward currents of Kir2.1_F147C and Kir2.1_F147W transfected cells were tested

using whole-cell patch-clamp recordings. Kir2.1_F147W was expected to reduce or even completely block the current flow through Kir2.1 pore because of the size of Trp, thereby mimicking Kir2.1_F147$_{TAG}$Cmn. As previously described, Kir2.1_F147C had large inward currents when voltage-clamped at -100 mV (Dart, 1998). Unexpectedly, Kir2.1_F147W had even greater inward currents. To measure the Kir2.1 specific current, Kir2.1 specific inhibitor Ba^{2+} was added in the bath. Ba^{2+} sensitive current (I_{Kir}), which is the difference between the amplitude of inward currents with and without 1 mM $BaCl_2$ added in bath solution, was 2.15±1.06 nA (n=11) for Kir2.1_F147C transfected cells and 4.66±1.43 nA (n=16) for Kir2.1_F147W cells (holding potential -100 mV). One possible explanation for why Kir2.1_F147W had greater I_{Kir} is that Trp is structurally closer to the wild-type amino acid, Phe, thereby forming more native pore structure. Another possibility is that a disulfide bond among F147C residues might disrupt the pore structure.

To validate the Uaa incorporation system is efficiently working for Kir2.1 in living cells, well-characterized $tRNA^{Leu}_{CUA}$ /leucyl-tRNA synthetase (LeuRS) was tested to incorporate endogenous leucine in the target residue with the amber stop codon. If Leu incorporation makes a functional channel, $tRNA^{Leu}_{CUA}$/CmnRS is also expected to favorably incorporate Cmn in Kir2.1. Kir2.1$_{TAG}$ gene was transfected to Human embryonic kidney (HEK) 293T cell along with $tRNA^{Leu}_{CUA}$ /LeuRS. The gene for green fluorescent protein (GFP) engineered with an amber

stop codon at Tyr182 (GFP_Y182$_{TAG}$) was co-transfected (Wang, 2007). GFP fluorescence indicated the successful suppression of TAG stop codon. Fluorescence activated cell sorting (FACS) analysis showed that ~40% of transfected HEK293T cells had GFP fluorescence, which represents the efficiency of $tRNA^{Leu}_{CUA}$/LeuRS pair to incorporate Leu to TAG. Kir2.1_F147$_{TAG}$/ $tRNA^{Leu}_{CUA}$/LeuRS transfected cells had a smaller but normal inward rectifying current. In the same manner, *o*-methyltyrosine (OMeY) was incorporated to F147$_{TAG}$ with 4 mM OMeY added in the media. The bulkiness of OMeY could interfere with K^+ flow to result in reduced inward currents. Finally, Cmn was incorporated to F147$_{TAG}$ with 4 mM Cmn added in the media. From the FACS analysis, $tRNA^{Leu}_{CUA}$/CmnRS had ~33% efficiency for Cmn incorporation. Without photo-stimulation, Kir2.1_F147$_{TAG}$Cmn had negligible I_{Kir}. Supplemental Figure 2.1A summarizes Ba^{2+} sensitive currents of all the mutant Kir2.1 channels tested.

UV light was introduced to HEK293T cells to evoke photo-uncaging of Cmn. However, whole-cell recording profile of Kir2.1_F147$_{TAG}$Cmn transfected cells didn't show any change in conductance (holding potential -100 mV) upon light excitation (n=9). Optimization of light stimuli by changing pulse duration, frequency, total exposure time or light intensity did not result in any positive data. The only recurring phenomenon was that cells were becoming leaky and the current profile was getting more ohmic as light stimulation continued. To reduce photo-damage, we installed a 365nm filter for the light source to cut down heat

generated by infrared light. Although it took more time for cells to become leaky, there was still no increase of inward currents upon light stimulation (n=11). Both Kir2.1_F147$_{TAG}$-only transfected cells and HEK293T cells exhibited the same phenomenon. This result made us wonder if Kir2.1_F147$_{TAG}$Cmn was ever expressed in the cell membrane. To verify this, mCitirine (mCit), an enhanced yellow fluorescent protein (YFP), was fused in the N-terminal of Kir2.1_F147$_{TAG}$ and this fusion protein was transfected to HEK293T cells. mCit-Kir2.1_F147$_{TAG}$Leu had the normal inward currents profile, indicating that N-terminal fused mCit doesn't disturb normal channel function. Confocal imaging of mCit-Kir2.1_F147$_{TAG}$Cmn demonstrated possible membrane localization of the channel protein.

We returned to the initial question: is F147 a good target residue? To answer this question and to have better understanding of pore-lining residues, crystal structure information was mandatory. Two KirBac1.1 dimers (PDB 1p7b; Kuo, 2003) were dimerized according to the Kir2.1 cytoplasmic tetramer structure (PDB 1u4f; Pegan, 2008) coordinates to rebuilt Kir2.1 mimicking KirBac1.1 tetramer. Surprisingly enough, KirBac1.1 D115, which corresponds to Kir2.1_F147 had its side chain heading toward protein-protein interface (Supplemental Figure 2.1B). This is also the case for KcsA K^+ channel that the backbone of the residues sizes the selectivity filter (Doyle, 1998). If F147 side chain is heading away from the pore, it is less likely that incorporated Cmn would block the pore. Therefore, more thorough target screening was conducted based

on the chicken Kir2.2 tetrameric structure information (Tao, 2009). A total of fifteen residues were selected as candidate sites.

2.3.2 Construction of PIRK channels

Using published data on Kir2.1 pore topology and function (Kubo, 1993; Lu, 1999a; Minor, 1999; Tao, 2009), and on the crystal structure of chicken Kir2.2 (Tao, 2009), we identified fifteen amino acids in the pore of rat Kir2.1 (which has ~76% sequence homology with chicken Kir2.2) with side chains that face the pore lumen (K117, V118, A131, T142, I143, C149, V150, D152, S165, C169, D172, I176, M180, A184, and E224). Previous studies indicated that Cys substitution at T142, I143, D172, I176, A184, or E224 did not interfere with Kir2.1 function (Dart, 1998; Kubo, 1998; Lu, 1999a; Lu, 1999b; Minor, 1999; Xiao, 2003). Therefore, these six amino acids plus C149 and C169 were selected for Cmn incorporation (Figure 2.2A).

The codon for these candidate sites was first mutated to the amber stop codon TAG to generate eight different mutant Kir2.1 ($Kir2.1_{TAG}$) channels. The $Kir2.1_{TAG}$ cDNA was individually coexpressed with the orthogonal $tRNA^{Leu}_{CUA}$ /CmnRS pair in HEK293T cells. Upon exogenous addition of the Uaa Cmn to growth media, the CmnRS aminoacylates Cmn onto the $tRNA^{Leu}_{CUA}$, which in turn recognizes the amber stop codon (UAG) in Kir2.1 mRNA and incorporates Cmn into Kir2.1 protein during translation (Lemke, 2007; Wang, 2009).

Each candidate site was initially tested whether it was permissive for UAG suppression by the orthogonal $tRNA^{Leu}_{CUA}$/LeuRS pair. Each Kir2.1$_{TAG}$ gene was transfected into HEK293T cells along with the $tRNA^{Leu}_{CUA}$/LeuRS (Figure 2.2B). GFP_Y182$_{TAG}$ gene was co-transfected. GFP fluorescence would indicate the successful suppression of the UAG stop codon by the orthogonal tRNA/synthetase. The function of individual Kir2.1$_{TAG}$ channels was then determined by whole-cell patch-clamp recordings from GFP-positive cells. For example, a green-positive HEK293T cell transfected with Kir2.1_C169$_{TAG}$ and the $tRNA^{Leu}_{CUA}$/LeuRS expressed a basally active inwardly rectifying current that was inhibited by extracellular Ba^{2+} (I_{Kir}), similar to wild-type Kir2.1 channels (Figure 2.2C). Of the eight candidate sites, I_{Kir} currents measured at -100 mV from HEK293T cells expressing Kir2.1_I143$_{TAG}$, Kir2.1_C149$_{TAG}$, Kir2.1_C169$_{TAG}$, or Kir2.1_I176$_{TAG}$ were significantly larger than those from untransfected cells (Figure 2.2D), indicating successful suppression and incorporation of Leu.

If a functional Kir2.1 channel could be generated through Leu incorporation at the TAG site, then it seemed likely the same site would be compatible for Cmn since CmnRS was evolved from LeuRS (Lemke, 2007). We therefore tested Kir2.1_I143$_{TAG}$, Kir2.1_C149$_{TAG}$, Kir2.1_C169$_{TAG}$, and Kir2.1_I176$_{TAG}$ for functional incorporation of Cmn (Figure 2.2E–H). HEK293T cells were transfected with cDNAs for the Kir2.1$_{TAG}$ channel, $tRNA^{Leu}_{CUA}$/CmnRS

and the GFP_Y182$_{TAG}$ reporter (Figure 2.2B), and incubated in Cmn (1 mM) for 12–24 hr. Functional incorporation of Cmn was expected to either lead to a basally active I_{Kir} or to I_{Kir} that is revealed upon brief (1 sec) light illumination (385 nm at 10 mW). For HEK293T cells expressing Kir2.1_I143$_{TAG}$ or Kir2.1_I176$_{TAG}$, we could detect no I_{Kir} before or after light illumination, indicating either no amber suppression or a non-functional channel after Cmn incorporation (Figure 2.2E). By contrast, HEK293T cells expressing Kir2.1_C149$_{TAG}$ displayed a large I_{Kir} that was unchanged by light illumination (Figure 2.2F), suggesting incorporation of Cmn at C149 did not significantly occlude the pore. Strikingly, HEK293T cells expressing Kir2.1_C169$_{TAG}$ displayed little I_{Kir} at negative membrane potentials that increased significantly upon light illumination (Figure 2.2G-H). These results suggested that incorporation of Cmn at C169 largely occludes the channel pore and that the blocking particle is released following brief light stimulation, indicating the successful construction of a photo-activatable Kir2.1 channel.

2.3.3 Light-dependent PIRK activation in HEK293T cells

We next examined the light-sensitivity features of Kir2.1_C169$_{TAG}$Cmn (referred to as PIRK) channels expressed in HEK293T cells. To enhance channel expression, we fused the fluorescent protein mCit to the C-terminus of Kir2.1_C169$_{TAG}$ (Figure 2.3A), which reduced the number of plasmids needed for transfection and allowed tracking the location of PIRK channels. Fusion of GFP to the C-terminus of Kir2.1 was shown previously to not affect Kir2.1 channel physiology (Sekar, 2007). Addition of Cmn to the bath resulted in fluorescently

labeled HEK293T cells (Figure 2.3B). A brief (1 sec) pulse of UV light (385 nm LED, 10 mW) led to activation of an inwardly rectifying current that was blocked by Ba^{2+} (Figure 2.3C, D). The activation kinetics had fast and slow components with time constants (τ) of 298 ± 134 ms and 15.0 ± 4.3 sec, respectively (n=7). Note the amplitude of light-activated current is larger than that in Figure 2.2H, indicating that PIRK expression level increased with the two plasmid system. When incorporated with Leu, Kir2.1_C169$_{TAG}$Leu channels showed large I_{Kir} (8.30 ± 1.48 nA, n = 7), which was not affected by light illumination (data not shown). On the other hand, HEK293T cells expressing PIRK (Kir2.1_C169$_{TAG}$Cmn) channels had no or negligible I_{Kir} before UV light (0.14 ± 0.07 nA, n = 10), and marked increase in I_{Kir} after UV light (1.65 ± 0.41 nA, n = 10) (Figure 2.3E). The smaller I_{Kir} for PIRK compared to Kir2.1_C169$_{TAG}$Leu was likely due to the less efficient aminoacylation with CmnRS and therefore less Cmn incorporation.

To investigate the relationship between the light dosage and current activation, we varied the duration and frequency of UV light pulses. Single light pulses with different lengths were applied to cells expressing PIRK channels. Using a 10 mW LED light source, one second and 500 ms light pulses evoked similar amount of current at -100 mV (2.27 ± 0.51 nA, n = 5 for 1 sec; 2.04 ± 0.39 nA, n = 5 for 500 ms). Shorter UV pulses (200 ms, 100 ms, and 50 ms) led to progressively smaller currents (Figure 2.3F). No significant change in current amplitude was measured with a single 20 ms light pulse (n = 6, data not shown).

We next investigated the effect of sequential UV light pulses. 200 ms light pulses delivered sequentially led to stepwise activation of PIRK channels (Figure 2.3G). Fewer UV pulses were required to maximally activate PIRK channels with longer duration UV light pulses (Figure 2.3H). Together, these results illustrate that modulating the duration and number of light pulses can be used to fine-tune the extent of PIRK current activation.

2.3.4 Neuronal expression of PIRK using viral vectors

C169 was selected as the best target site to incorporate Cmn for the photo-activation of mKir2.1. The most interesting next step was to express Kir2.1_C169$_{TAG}$Cmn in neuronal cells to see if neuronal firing was suppressed by light irradiation.

First, rat hippocampal dissociated primary neurons were chosen as experimental subjects. At a single cell level, it would be tested if the neuronal firing could be suppressed solely by light without any input from neighboring cells. Since the efficiency of transient transfection to neurons was very low (<10%) compared to that of HEK293T cells, the viral gene delivery (up to 100% efficiency) was suggested as an alternative to express Kir2.1_C169$_{TAG}$Cmn in neurons. Moreover, these viral vectors make possible other approaches, such as Kir2.1 expression in rat hippocampal acute tissue slices. Lentiviral vector derived from HIV-1 is advantageous as it is capable of infecting a wide variety of dividing and nondividing cells and is stably integrated into the host genome, resulting in

long-term expression of the transgene (Tiscornia, 2006). Therefore, Lentiviral vectors to express Kir2.1_C169$_{TAG}$Cmn were constructed. The first viral vector (LV1) expressed CmnRS and $tRNA^{Leu}_{CUA}$, and the second viral vector (LV2) expressed Kir2.1_C169$_{TAG}$Cmn and $tRNA^{Leu}_{CUA}$. Unfortunately, the titers of these viral vectors were very low: 4.07 x 10^7 Transducing unit (TU/ml) for LV1 and 6.64 x 10^7 TU/ml for LV2. The possibility of the error in viral prep procedure was excluded since the control viral vector expressing GFP had much higher titer, ~10^9 TU/ml. LV1 and LV2 viral vectors were produced again by the Salk Viral Vector Core facility to result in viral vectors with slightly higher titers: 1.22 x 10^8 TU/ml for LV1 and 9.24 x 10^8 TU/ml for LV2. However, when LV1 and LV2 were co-infected to rat hippocampal primary neurons with Mode of infection (MOI) of 2.03 and 15.4 each, no cells expressed Kir2.1-mCit. When similar experiment was performed in HEK293T cells with MOI of 1.84 and 1.4 each, again, there was no Kir2.1-mCit expression. Possible explanations for this result are as follows: (1) The tRNA gene encoded in the viral vector forms a secondary structure, interrupting with the process of lentiviral infection. This could affect the reverse transcription of the infected lentiviral gene, which is in the single-stranded RNA (ssRNA) form, if the secondary structure of tRNA stalled the reverse transcription complex; (2) Uaa-incorporated proteins are less efficiently expressed than native proteins for several reasons (Wang, 2009); (3) two viral vectors should infect the same cell to express Kir2.1-mCit; and (4) a co-infected

cell should still uptake Cmn from the bath solution to incorporate them in Kir2.1-mCit.

To test if tRNA gene indeed hampered the lentiviral infection procedure, a viral vector encoding Tyrosyl RS (TyrRS) without $tRNA_{TAG}^{Tyr}$ was constructed. Without the tRNA gene, we could make viral vector with a much higher titer (4.07 x 10^9 TU/ml). Considering the tRNA expression as the biggest hurdle, adenovirus-associated viral vector (AAV) was proposed as an alternative. There is no reverse transcription step in the AAV infection process, which makes AAV a better viral vector to deliver the $tRNA_{CUA}^{Leu}$ gene. A new strategy was to make AAV encoding only $tRNA_{CUA}^{Leu}$ (either one or two copies), and to make LV expressing both CmnRS and Kir2.1-mCit. LV and AAV are known to have high rates of co-infection (personal discussion with the Salk Viral Vector Core facility) and this assumption was confirmed by a coinfection experiment with LV-mCherry and AAV-GFP in rat hippocampal primary neurons (Supplemental Figure 2.3A). AAV U6promoter- $tRNA_{CUA}^{Leu}$-H1 promoter- $tRNA_{CUA}^{Leu}$ and AAV U6promoter- $tRNA_{CUA}^{Leu}$ were both produced with high titers, 4.32 x 10^{11} genome copies (GC)/ml and 2.64 x 10^{11} GC/ml respectively. When these viral vectors infected HEK293T cells that are expressing CmnRS and Kir2.1_$C169_{TAG}$-mCit, Cmn successfully suppressed TAG codon in Kir2.1_$C169_{TAG}$-mCit to result in mCit fluorescence. LV expressing CmnRS and Kir2.1_$C169_{TAG}$-mCit was also produced by viral vector with high titer, 3.25 x 10^9 TU/ml. When these two viral vectors were delivered in the same

neuron, Kir2.1_C169$_{TAG}$Cmn would be produced and mCit fluorescence would be observed on plasma membrane in neurons.

Different combinations of MOI were tested to deliver two viruses. Serial or simultaneous infection of two viruses was compared. However, no successful co-infection was observed (Supplemental Figure 2.3B). Varying Cmn concentration in growth media didn't make any difference. Cells with fluorescence in cytosol indicated single infection of LV and read-through transcription of mCit. AAV-U6-$tRNA^{Leu}_{CUA}$-H1-$tRNA^{Leu}_{CUA}$ and LV-CmnRS-skip- Kir2.1_C169$_{TAG}$-mCit gene constructs were confirmed by co-transfection into HEK293T cells, which yielded high co-infection and good membrane fluorescence. However, when viruses were produced, their co-infection was unsuccessful both in HEK293T cells and neurons. Hypothetically, this was because the co-infection of LV and AAV was not strong enough. When LV-GFP and AAV-mCherry were tested, GFP and mCherry co-expression was relatively low. At the same time, viruses for my gene constructs could not be produced in high titer enough for chances of co-infection.

To overcome this obstacle, Sindbis virus was chosen as a carrier of my gene constructs. It delivers genes in the single-stranded RNA form and has extreme infection efficiency. Only drawback is that it is toxic to cells and the experiments should be done within three days. Sindbis-CmnRS-skip-Kir2.1_C169$_{TAG}$-mCit would to be constructed to co-infect with AAV-U6-$tRNA^{Leu}_{CUA}$-

H1-$tRNA^{Leu}_{CUA}$. For the first step, AAV-GFP (Viral Vector Core, Salk) and Sindbis-tdTomato (R. Malinow laboratory) were infected in disassociated neurons to test co-infection of two viruses. Among different AAV serotypes, AAV2/1 and AAV2/9 showed the most co-expression of GFP and tdTomato (Supplemental Figure 2.3C). When the same experiment was done on organotypic hippocampal slices, it was not easy to see co-expression (Supplemental Figure 2.3D). It was observed that AAV was not easily delivered into organotypic slices. Possible explanation was that because AAV by Salk Viral Vector Core was prepped in viscous solution, it was hard to be injected into the slices. The next possible step could be: (1) the expression of all genes in Sindbis virus; (2) the expression of all genes in Herpes simplex virus-1 (HSV-1), which delivers genes in the double-stranded DNA form.

2.3.5 Neuronal expression of PIRK using AMAXA electroporation

As the viral vector approach required extensive troubleshooting, other options to express PIRK were concurrently explored. Amaxa neucleofection (Lonza, Swiss) is an enhanced electroporation technology using specific electrical parameters and cell type-specific reagents (Zeitelhofer, 2007). It is recognized to have higher transfection efficiency and lower cell toxicity than Lipofectamine (Invitrogen, CA) transfection method, but it is limited to freshly-isolated neurons. When $tRNA^{Leu}_{CUA}$/LeuRS and GFP_$Y182_{TAG}$ plasmids were introduced in rat hippocampal primary neurons, no GFP-positive cells were

observed. This result indicated that Amaxa strategy was not compatible with the Uaa system.

2.3.6 Neuronal expression of PIRK using biolistics

Gene gun method was also tested to deliver genes to express PIRK. To verify TAG amber codon suppression with biolistics, LeuRS plasmids and GFP_Y182$_{TAG}$ plasmids were combined to make gene gun bullets and introduced to rat hippocampal organotypic slices. Compared to wild-type GFP expression, LeuRS + GFP_Y182$_{TAG}$ yielded ~10% transfection efficiency. When it came to CmnRS and Kir2.1_C169$_{TAG}$-mCit, transfection was not successful. Generally, LeuRS + GFP_Y182$_{TAG}$ expression would be higher than CmnRS + Kir2.1_C169$_{TAG}$-mCit since it doesn't require addition of Uaas. However, unsuccessful transfection of CmnRS + Kir2.1_C169$_{TAG}$-mCit suggested that Cmn was not carried into cells. Both bath addition and drop-wise addition didn't help the expression. Further optimization would be required to pursue this method.

2.3.7 Light-activation of PIRK suppresses neuronal firing

A breakthrough was achieved using Calcium phosphate (Ca-P) transfection method. It is known to be less toxic than lipid-based transfection method. This is great since the healthiness of cells is the top priority to measure action potentials from rat hippocampal primary neurons. Finding optimal condition for Ca-P transfection was tricky. Uaa suppression was at its peak 12−24 hr after transfection. At the same time, primary neurons mature to have

action potentials on and after 9 days *in vitro* (DIV). However, the transfection efficiency in neurons started to drop after 3 DIV. Most favorable timing for successful transfection was on 9 DIV. CmnRS + Kir2.1_C169$_{TAG}$-mCit plasmids were freshly prepped before transfection to increase the transfection efficiency. Cmn was added to the growth media 0.2 mM immediately after transfection and 1 mM more 4−6 hr after transfection. Recording was done 12−24 hr after transfection.

A significant obstacle in using Uaa technology has been the implementation of Uaas in vertebrate neurons. Transfection of rat hippocampal primary neurons with the cDNA for PIRK-mCit and $tRNA^{Leu}_{CUA}$/CmnRS (Figure 2.3A) led to fluorescence in cultures exposed to Cmn for 12–24 hr (Figure 2.4A), indicating the successful incorporation of Cmn into PIRK channels. Whole-cell patch recordings from m-Citrine positive neurons revealed little basal inward current at negative potential. However, UV light stimulant (1 sec; 10 mW) induced large inwardly rectifying current (Figure 2.4B). By contrast, control neurons (-Cmn) showed little or no response to UV light (Figure 2.4B, 2.4C). In PIRK-expressing neurons incubated with Cmn, UV light induced a nearly two-fold increase in inwardly rectifying current, likely due to activation of Kir2.1 channels (Figure 2.4C). .

We next examined the effect of PIRK activation on the excitability of hippocampal neurons. Activation of an inwardly rectifying K^+ current would be expected to significantly reduce neuronal excitability (Burrone, 2002; Yu, 2004). In whole-cell current-clamp recordings, current injection (20 nA) induced firing of action potentials at 5–8 Hz (Figure 2.4D) in both control neurons and PIRK-expressing neurons before UV light exposure. By contrast, action potential firing abruptly stopped in PIRK-expressing neurons following brief UV light stimulation (1 sec; 10 mW). Importantly, addition of Ba^{2+} to the bath restored action potential firing (Figure 2.4D), confirming that the observed suppression of activity was due to activation of Kir2.1 channels. Neither light illumination nor Ba^{2+} addition had effect on the excitability of control neurons (Figure 2.4E). In multiple recordings from different preparations of hippocampal neuronal cultures, we consistently observed a significant decrease in firing frequency in PIRK-expressing neurons (+Cmn) following UV light, which was restored to normal levels of firing in the presence of extracellular Ba^{2+}(Figure 2.4F). In control neurons, we observed no significant change in firing frequency after light activation or Ba^{2+} addition.

Plotting the membrane potential induced by the current step before and the after UV light stimulation showed a clear hyperpolarization in PIRK-expressing (+Cmn) neurons following UV light (Figure 2.4G). Furthermore, extracellular Ba^{2+} reproducibly depolarized the membrane potential (Figure 2.4G). Taken together, these experiments demonstrate that UV light activation of PIRK

channels provides a technique for spatially inhibiting neuronal activity through membrane hyperpolarization.

To explore the dynamic range of PIRKs effect on neuronal firing, we measured the firing frequency over a range of current injections. With small current injections (<40 pA), the firing frequency decreased significantly upon UV light activation of PIRK channels (Figure 2.5A). With larger current injections (40–70 pA) and higher firing frequencies, however, there was no significant change in firing frequency following UV light illumination of PIRK-expressing neurons. This ceiling effect can be explained by the native properties of strong inwardly rectifying Kir2.1 channels, which conduct little outward current at positive membrane potentials (Ishii, 1994; Kubo, 1993). Kir channels are well known for their ability to hyperpolarize membranes and increase the threshold for firing an action potential. To examine this, we measured the minimum amount of current required to evoke an action potential (referred to as rheobase). The rheobase increased in PIRK-expressing neurons following UV light exposure (Figure 2.5C). UV light activation of PIRK also hyperpolarized the resting membrane potential of PIRK-expressing neurons by -17 mV, whereas UV light had no effect on the resting potential of control neurons (Figure 2.5D).

In Figure 2.5D, resting membrane potential of PIRK-expressing neurons was shifted from -70 ± 2 mV (n = 19) to -87 ± 2 mV (n = 19) after light activation.

Light-induced change in K^+ permeability of these neurons can be deduced from the Goldman-Hodgkin-Katz (GHK) equation:

$$V_m = \frac{RT}{F} \ln\left(\frac{p_K[K^+]_o + p_{Na}[Na^+]_o + p_{Cl}[Cl^-]_i}{p_K[K^+]_i + p_{Na}[Na^+]_i + p_{Cl}[Cl^-]_o}\right)$$

where $\boldsymbol{V_m}$ is the membrane potential (in Volt), ***R*** is the universal gas constant (8.314 $J.K^{-1}.mol^{-1}$), ***T*** is the temperature in Kelvin (K = °C + 273.15), ***F*** is the Faraday's constant (96,485 $C.mol^{-1}$), p_K, p_{Na}, and p_{Cl} are the membrane permeabilities for K^+, Na^+, and Cl^-, respectively. For a typical neuron at rest, $p_K : p_{Na} : p_{Cl}$ = 1 : 0.05 : 0.45 (Kew, 2010). $\boldsymbol{[K^+]_o}$, $\boldsymbol{[Na^+]_o}$, and $\boldsymbol{[Cl^-]_o}$ are the extracellular concentration of K^+, Na^+, and Cl^-, respectively. $\boldsymbol{[K^+]_i}$, $\boldsymbol{[Na^+]_i}$, and $\boldsymbol{[Cl^-]_i}$ are the intracellular concentration of K^+, Na^+, and Cl^-, respectively.

In whole-cell patch-clamp recordings of cultured hippocampal neurons for Figure 2.4 and 2.5, K^+, Na^+, and Cl^- concentration in internal and external solutions were as below (See also Materials and Methods section).

	mM		mM
$\boldsymbol{[K^+]_i}$	135	$\boldsymbol{[K^+]_o}$	3
$\boldsymbol{[Na^+]_i}$	10	$\boldsymbol{[Na^+]_o}$	150
$\boldsymbol{[Cl^-]_i}$	14	$\boldsymbol{[Cl^-]_o}$	164

Before light activation (at 25°C),

$$-0.070\ V = \frac{8.314\ J/K \cdot mol\ * 298.15\ K}{96485\ C/mol} \ln\left(\frac{p_K * 3\ mM + 0.05 * 150\ mM + 0.45 * 14\ mM}{p_K * 135\ mM + 0.05 * 10\ mM + 0.45 * 164\ mM}\right)$$

$$p_{K\,(bef)} = 1.5$$

After light activation (at 25°C),

$$-0.087\ V = \frac{8.314\ J/K \cdot mol\ * 298.15\ K}{96485\ C/mol} \ln\left(\frac{p_K * 3\ mM + 0.05 * 150\ mM + 0.45 * 14\ mM}{p_K * 135\ mM + 0.05 * 10\ mM + 0.45 * 164\ mM}\right)$$

$$p_{K\,(aft)} = 7.2$$

Based on the assumption that neither p_{Na} nor p_{Cl} were affected by the light exposure, we concluded that the light activation increased the K^+ permeability by ~4.7 fold in the same buffer condition. That is, based on the Goldman-Hodgkin-Katz equation, the -17 mV shift in membrane potential corresponds to an ~4.7 fold increase in K^+ permeability, consistent with activation of Kir2.1 channels.

2.3.8 In vivo expression of PIRK in the chicken embryos

To test the light activation of PIRK in a more physiological context, chicken embryo was selected as another subject. Chicken embryo spinal cord is

favorable for the current study in that (1) it is easy to introduce the transgene into the spinal cord; (2) electrophysiological recording is feasible, (3) *in vivo* study is possible; and (4) one side of the spinal cord serves as an internal control. In this approach, Kir2.1_C169$_{TAG}$-mCit was introduced in the chicken embryo spinal cord. Upon its expression in motor neurons lining the spinal cord, neuronal activity would be monitored with the patch clamping technique. The circuit connecting motor neurons between forelimb and hindlimb would be disturbed when neurons in the middle are silenced by light activation of PIRK. Interestingly, the limb movement could also be monitored to see if it is affected by suppressing neuronal activity. Initially, tRNA$_{TAG}^{Tyr}$/TyrRS and GFP_Y182$_{TAG}$ were coexpressed in the spinal cord to result in green fluorescence. Again, tRNA$_{TAG}^{Tyr}$/TyrRS and Kir2.1_C169$_{TAG}$-mCit were coexpressed to result in mCit fluorescence. However, this result was not repeatable. To increase the expression level, a single plasmid expressing both tRNA$_{TAG}^{Tyr}$/TyrRS and GFP_Y182$_{TAG}$ was electroporated in the chicken embryo spinal cord, only to have negative results. Considering the need to optimize the Uaa system expression in chicken embryos, the original human H1 promoter and 3'-terminal flanking sequence of the $tRNA_{CUA}^{Leu}$ construct were replaced with chicken H1/U6 promoter and 3'-terminal flanking sequences (Wang, 2007). The new constructs, which worked well in HEK293T cells, did not work in chicken embryos. The chicken embryo approach needs more troubleshooting in the future.

2.3.9 In vivo expression of PIRK in the mouse neocortex

Having successfully expressed PIRK channels in dissociated hippocampal neurons, we next attempted to express PIRK channels *in vivo*. Genetically encoding Uaas using orthogonal tRNA/synthetase has great potential to address challenging biological questions *in vivo*, but this technology has yet to be applied in mammals. There were two main challenges for *in vivo* incorporation of Uaas in mammals: (1) efficient delivery and expression of the genes for the orthogonal tRNA/synthetase and the target protein into specific tissue or cells; and (2) sufficient bioavailability of the Uaa at the target tissue and cells. We chose mouse embryos for genetically incorporating Uaas into the brain because of the ability to introduce cDNA and chemicals *in utero*, and then to prepare brain slice pre- and post-natally (Mulder, 2008; Saito, 2006; Tabata, 2001).

We started addressing the first challenge by attempting to incorporate Leu, an endogenously available amino acid, into GFP through UAG suppression in mouse embryonic brain. The GFP_Y182$_{TAG}$ reporter gene was encoded on the same plasmid with the orthogonal $tRNA^{Leu}_{CUA}$ (Figure 2.6A). Three copies of this tRNA expression cassette driven by the H1 promoter were included to increase the UAG suppression efficiency, as we previously demonstrated in mammalian cells (Coin, 2011). A red fluorescent protein mCherry was coexpressed with the orthogonal LeuRS through IRES on the other plasmid to indicate successful gene delivery *in vivo*. Genes were introduced in the mouse neocortex using *in utero*

electroporation, and four days later the embryonic cortical sections were prepared and fluorescently imaged to check gene expression (Figure 2.6C). Electroporation of the LeuRS-IRES-mCherry plasmid alone showed red fluorescence, indicating mCherry served as a good indicator for gene delivery (Figure 2.6D). Co-delivery of the $tRNA^{Leu}_{CUA}$-GFP_{TAG} plasmid with a separate plasmid encoding mCherry showed mCherry fluorescence but no GFP fluorescence, demonstrating that there was no background read-through of the UAG stop codon in the GFP mRNA. On the other hand, GFP fluorescence was now observed in the neocortices of mice electroporated with $tRNA^{Leu}_{CUA}$, GFP_{TAG}, and LeuRS cDNA. In addition, all green fluorescent cells had red fluorescence, indicating that translation of full-length GFP required both $tRNA^{Leu}_{CUA}$ and the LeuRS to suppress the UAG codon. Therefore, these results suggest the successful *in vivo* incorporation of Leu into GFP through UAG suppression.

Incorporation of a Uaa *in vivo* presented an additional challenge. For the convenience of detection, we initially tried to incorporate Cmn into GFP_{TAG} in the mouse brain. The $tRNA^{Leu}_{CUA}$, CmnRS, and GFP_{TAG} genes (Figure 2.6A) were first electroporated *in utero*, and then after two days, we injected Uaa Cmn directly into the lateral ventricle of the mouse brain (Figure 2.6C). Without injecting Cmn, no green fluorescence was detected in the neocortical plates (Figure 2.6E, top row). After injecting Cmn, weak green fluorescence could be detected (not shown). Previously we discovered that preparation of Uaas in the dipeptide form

increased the efficiency of Uaa incorporation in *C. elegans*, possibly because the dipeptide was transported into cells more efficiently than the single Uaa via oligopeptide trasporter PEPT1 and PEPT2 (Parrish, 2012). Intracellular dipeptide would then be hydrolyzed by cellular peptidases to generate free Uaas for incorporation. Since PEPT2 is highly expressed in rodent brain (Lu, 2006), Cmn-Ala was adopted to improve Cmn bioavailability. We thus synthesized the Cmn-Ala dipeptide and injected it in the lateral ventricle of the mouse brain. Indeed, with this adjustment we could observe a dramatic improvement, with strong green fluorescence in the nerocortex (Figure 2.6E, bottom row), indicating the successful incorporation of Cmn into GFP_{TAG} *in vivo*.

After overcoming both challenges we proceeded to incorporate Cmn into Kir2.1_$C169_{TAG}$ to express PIRK channels directly in the mouse brain. The Kir2.1_$C169_{TAG}$ gene was encoded with the $tRNA^{Leu}_{CUA}$ in one plasmid, and another plasmid encoded the CmnRS together with mCherry as a reporter for gene delivery (Figure 2.6B). A third plasmid encoding GFP_$Y182_{TAG}$ was also co-electroporated *in utero*. Detection of GFP fluorescence would indicate the successful delivery of all three plasmids, since UAG suppression in GFP would require both $tRNA^{Leu}_{CUA}$ and the CmnRS; Cmn incorporation in GFP_{TAG} would suggest Cmn incorporation in $Kir2.1_{TAG}$ as well, because both genes were present in the same cell. As expected, only when all three gene constructs were present and Cmn-Ala was introduced to the brain, green fluorescent cells were

observed (Figure 2.6F). Cells with both red and green fluorescence should have Cmn incorporated into $Kir2.1_{TAG}$ to make PIRK channels.

To verify if functional PIRK channels were expressed in these neurons, whole-cell recordings were conducted on acute slices prepared from the mouse neocortical plates. Indeed, the green/red fluorescent neurons had no inward current at negative holding potential, but a brief pulse of light rapidly activated the inward current (Figure 2.6G). The current was completely blocked by adding Ba^{2+}, confirming it was generated by PIRK. I_{kir} measured from these PIRK-expressing neurons in the mice neocortical slices was significantly increased upon light activation (Figure 2.6H). The light-dependent activation of PIRK channels further confirmed the successful incorporation of Cmn into $Kir2.1_{TAG}$ in the mouse brain. In short, these data demonstrated the successful expression of a functional PIRK *in vivo*.

2.3.10 Expanding the PIRK strategy to AMPAR

Ligand-gated ion channels open in response to chemical signals such as neurotransmitters in synapse. Therefore, they have important roles in synaptic transmission and its regulation. *α*-Amino-3-hydroxy-5-methyl-4-isoxazolepropionic acid receptor (AMPAR), N-methyl-D-aspartic acid receptor (NMDAR), γ-Aminobutyric acid receptor ($GABA_AR$), and serotonin receptor ($5\text{-}HT_3R$) were carefully studied and AMPAR was selected for the next target protein.

AMPAR forms a functional homotetramer so that Uaa-incorporated tetramers can be produced efficiently.

The crystal structure of AMPAR has revealed that transmembrane regions of AMPAR have a common architecture with the structure of Kir2.1 (Sobolevsky, 2009). Therefore, a similar strategy could be applied to incorporate Uaas to block the pore of AMPAR. Unlike Kir2.1 however, AMPAR changes its conformation in the presence of its ligand like glutamate, kainite, and AMPA. Thus, it is crucial to pick a residue in the AMPAR pore to incorporate Cmn where the channel is not functional with or without ligands but it can be reactivated by UV irradiation. In the structure of rat GluR2 homotetrameric receptor, M3 helix aligns the pore of transmembrane region (Sobolevsky, 2009). Eleven candidate residues were picked based on the direction of amino acid side chain: R599, G602, G603, W606, T609, L610, I613, S614, T617, A621, and T625 (Supplemental Figure 2.4A). However, the structure shows only closed conformation with antagonist. The structure of M2 loop, which aligns the pore lumen, is also missing. The substituted cysteine accessibility method in a previous study showed that I600, G603, W605, W606, F607, S614, N619, and A621 residues are pore accessible in the presence of glutamate (Sobolevsky, 2009). L610, I613, T617, L610, and F613 residues are accessible with or without glutamate. At the same time, I600, V601, G602, G603, V604, F607, T609, L610, I611, I612, I613, S614, S615, T617, N619, A621, F623, L624, and T625 can be mutated to cysteine to have functional receptors.

After combining all the information, G603, F607, L610, I613, S614, T617, N619, A621, and F623 were chosen to experiment Cmn incorporation. GFP-GluR2 (Q, flop, gifted from R. Malinow laboratory) gene, where a single residue is mutated to TAG amber codon, was expressed with CmnRS and $tRNA^{Leu}_{CUA}$ to express GFP-GluR2$_{TAG}$Cmn homotetramer in HEK293T cells. Each GFP-GluR2$_{TAG}$ gene was transfected into HEK293T cells along with the $tRNA^{Leu}_{CUA}$ /CmnRS. mCherry_Y182$_{TAG}$ gene was co-transfected. Cmn was added in the media for 12−24 hr after transfection. GFP and mCherry fluorescence would indicate the successful suppression of the UAG stop codon by the orthogonal tRNA/synthetase. The function of individual GFP-GluR2$_{TAG}$ channels was then determined by whole-cell patch-clamp recordings from GFP/mCherry-positive cells. When whole-cell recording was done from the cell expressing wild-type GFP-GluR2 as the positive control, glutamatergic currents were recorded repeatedly in response to 1 mM glutamate puff in the presence of 0.1 mM cyclothiazide (blocking rapid desensitization of AMPAR; Yamada, 1993) (Supplemental Figure 2.4B). However, none of GFP-GluR2$_{TAG}$ channels responded to glutamates. To test if UAG stop codons in GFP-GluR2$_{TAG}$ channels were suppressed properly with the Uaa system, each GFP-GluR2$_{TAG}$ gene was transfected into HEK293T cells along with the $tRNA^{Leu}_{CUA}$/LeuRS. Again, no GFP-GluR2$_{TAG}$ channels acted like wild-type GluR2 channels. To test if any GluR2 full proteins were ever made, HEK293T cells transfected with GFP-GluR2_L610$_{TAG}$ +

$tRNA^{Leu}_{CUA}$/LeuRS was harvested for western blotting (Supplemental Figure 2.4C). Full-length GFP-GluR2 proteins were observed but a lot of truncated GFP-$GluR2_{TAG}$ proteins were also detected. Now we suspect if truncated GFP-$GluR2_{TAG}$ has any dominant-negative effect to GluR2 function. Or, it is possible that candidate sites in GluR2 are not efficiently permissive enough for Uaa suppression. Targeting different region such as ligand binding region is recommended for future studies.

2.4 Discussion

Genetically encoding Uaas with orthogonal tRNA/synthetase was initially developed in E. *coli* and later extended to various cells and organisms (Liu and Schultz, 2010; Wang, 2001; Wang, 2009). For neuroscience research, Uaa incorporation in primary neurons (Wang, 2007), neural stem cells (Shen, 2011), and animals would permit the use of Uaas to directly address neurobiological processes in the native environment. Previously, Uaas have been incorporated into ion channels and receptors expressed in *Xenopus* oocytes (Beene Darren, 2003) and mammalian cells *in vitro* (Wang, 2007). Although sufficient for probing the structure and function of a single target protein, heterologous expression systems are not suitable for investigating neuronal signaling and circuits involving a cascade of neuronal proteins or multiple cells. In this study we describe the methodology for manipulating a neuronal protein directly in primary neurons using genetically encoded Uaas. Moreover, we report the successful

incorporation of Uaas into the brain of mouse embryos, which represents to the best of our knowledge the first report on Uaa incorporation in mammals. The ability to genetically incorporate Uaas into neuronal proteins in mammal brains provides a novel toolbox for innovative neuroscience research.

The development of optically controlled channels and pumps is a powerful method for analyzing the function of specific neurons in neural circuits (Yizhar, 2011). However, the photoresponsiveness of opsin, which depends on the retinal chromophore and its modulation protein domain, cannot be simply transplanted into other proteins without dramatically altering the target protein. Therefore, this approach is not suitable for optical control of proteins natively expressed in neurons. Alternatively, natively expressed channels and receptors can be modified to be controlled by an optically switched ligand. For example, a photoisomerizable azobenzene-containing ligand can be chemically attached to the glutamate receptor sGluR0 or the potassium channel TREK1 for light gating (Janovjak, 2010; Sandoz, 2012). A limitation with this technique is that application of the chemical photoswitch is limited to extracellular regions of the membrane protein, making intracellular proteins inaccessible to this labeling method. In contrast, genetically encoding photo-reactive Uaas should provide a general methodology for manipulating native proteins with light in neurons. Since genetic incorporation of Uaas using orthogonal tRNA/synthetase pairs imposes no restrictions on target protein type, cellular location or the site for Uaa incorporation (Wang and Schultz, 2005), with methods reported herein we expect

that various proteins native to neurons can be generally modified with photo-reactive Uaas at appropriate site to enable optical control. This flexibility should significantly expand the scope of proteins and neuronal processes subject to light regulation.

Photoactivation of PIRK channels rapidly suppress neuronal firing. Unique features of PIRK may complement existing methods for neuronal silencing and enable new research. Arch and NpHR originated from halobacteria are members of the opsin family employed to silence neuronal activity (Chow, 2010; Zhang, 2007). Illumination of Arch, a proton pump, for extended period of time results in intra- and extracellular pH disturbance, which could negatively impact on cell health (Han, 2012; Okazaki, 2012). Activation of the chloride pump NpHR leads to accumulation of intracellular chloride ions and can compromise $GABA_A$-receptor-mediated inhibition (Raimondo, 2012). In addition, continuous activation of Arch or NpHR is limited by its inactivation and potential photo damage, which is not ideal for studies such as epilepsy where it is important to maintain membrane hyperpolarization for a long period of time (Kokaia, 2012). In contrast, PIRK is based on Kir2.1, an inward rectifying potassium channel whose native function is to regulate neuronal excitability. Kir2.1 conducts K^+ ions to directly silence neurons, and has been used in a variety of studies to investigate the effect of neuronal excitability over the last decade (Burrone, 2002; Johns, 1999; Nadeau, 2000; Yu, 2004). We now endow Kir2.1 with photo-responsiveness in PIRK, which provides temporal control through light precision to these and future

studies. Another feature of PIRK is its binary switch, i.e., a single light pulse can induce the lasting silencing effect on target neurons. Without the need to continuously deliver light through the optical fiber, this feature is convenient for animal studies to mitigate potential interference of light or light devices to animal behavior, and may find use in studying or treating intractable epilepsy, intractable pain, or muscle spasms. Moreover, Kir2.1 is involved in a variety of physiological processes and diseases. For instance, Kir2.1 interacts with PDZ-domain proteins or protein kinases such as PKA and PKC (Hibino, 2010). Kir2.1 is also associated with diseases such as Andersen syndrome and short Q-T syndrome (Ma, 2011; Priori, 2005), and is required for osteoblastogenesis (Zaddam, 2012). PIRK can provide new means with temporal resolution to investigate the functional consequences of Kir2.1-protein interactions and the mechanisms of pathogenesis.

The pore “block-and-release” strategy we devised to photo-activate Kir2.1 may be generally applicable to other channels and receptors. For instance, G protein-gated Kir channels (Kir3 family), AMPARs, and NMDARs share similar pore topology with Kir2.1. By incorporating Cmn into pore residues in these proteins, one should be able to similarly install light-responsiveness to them for highly disciplined study of channel/receptor physiology. On a broader perspective, it is also possible to expand the Uaa-based optical control to the function of other proteins beyond ion channels and receptors. Multiple amino acids such as tyrosine, serine, lysine, glutamate, aspartate, and glycine have

been protected with different photo-releasable groups (Beene Darren, 2003), and some of them can be genetically encoded in E. *coli*, yeast, and mammalian cells (Liu and Schultz, 2010; Wang, 2009). Using methods in this study, these amino acids can be similarly photocaged in neurons for optical control of various protein functions. For instance, by photocaging appropriate amino acids it should be possible to block-and-release protein-protein interaction, protein-nucleic acid interaction, access of an active site, or access of posttranslational modification sites in neurons. In addition, *in vivo* Uaa incorporation, as demonstrated in the embryonic mouse neocortex here, has the potential to be extended to other regions of the brain, adult animals and more mammals. Genetic knockin or viral delivery (Shen, 2011) can be used to express the orthogonal tRNA/synthetase and target protein in transgenic and adult animals, respectively. Some Uaas may be bioavailable through food or water feeding; others can be prepared in the dipeptide format shown here and injected directly into the brain ventricles. Moreover, optical control via Uaa can be made compatible with two-photon activation. Protecting groups efficient for two-photon photolysis have been developed for caging amino acids (Matsuzaki, 2001). We are evolving new tRNA/synthetase pairs to genetically incorporate Uaas containing such photo-releasable groups, so that light control can be performed with two-photon excitation to increase tissue penetration and acquire spatial resolution in the Z-axis. In sum, we expect that the method presented in this report will serve as a solid basis to enable optical control and study of a variety of proteins and neurobiological processes in neurons and brains.

2.5 Acknowledgements

Chapter 2, in part, has been submitted for publication of the material as it may appear in Kang, J.Y., Kawaguchi, D., Coin, I., Xiang, Z., O'Leary, D.D.M., Slesinger, P.A., and Wang, L. (2013) Neuron. The dissertation author was the first author of this paper. We acknowledge P. A. Slesinger lab for valuable discussion, and support of electrophysiological recording facility and Kir2.1 gene construct. We appreciate D. Kawaguchi's work (D. D. M. O'Leary lab) on *in utero* electroporation and *in utero* injection of Uaa. We acknowledge I. Coin and Z. Xiang for synthesizing Cmn and Cmn-Ala. We thank E. D. Callaway lab for the help with viral vectors and biolistic experiments. We appreciate the contribution of R. Malinow lab by supplying Sindbis virus, GluR2 gene construct, and laboratory facilities. We thank S. Pfaff lab for helping with chicken embryo experiment. We acknowledge Salk animal facility for taking care of rodents. We thank Salk Viral Vector Core (now Gene Transfer Targeting and Therapeutics Core) for constructing LV and AAV viral vectors. We appreciate I. M. Verma lab for supplying viral vectors and viral prep facility. We thank P. S. Schultz lab for granting us with CmnRS gene construct. We also thank Y. Gotoh for providing us with pCAG vector. Financial support from California Institute for Regenerative Medicine (RN1-00577-1) and US National Institutes of Health (1DP2OD004744-01) is much appreciated.

2.6 Materials and methods

2.6.1 Animals

Sprague Dawley rats were purchased from Harlan laboratories. CD-1 (ICR) mice were purchased from Harlan laboratories and Charles River laboratories, or bred in-house. Animals were housed under constant temperature and humidity on a 12 hr light-dark cycle (light 6 am – 6 pm) with free access to food and water. All procedures were performed using IACUC approved protocols for animal handling at the Salk Institute.

2.6.2 Unnatural amino acids

Cmn (4,5-dimethoxy-2-nitrobenzyl-Cysteine) was synthesized as a single amino acid or a dipeptide with alanine, Cmn-Ala. Cmn was added in the HEK293T cell culture, and Cmn-Ala dipeptide was delivered to the neuronal culture and the mouse neocortex *in vivo* to improve the bioavailability of Cmn.

Cmn was synthesized by following a published procedure (Pedersen, 1998) with minor modifications (Supplemental Figure 2.5): we used Boc-Cys-OH instead of Cys as the starting material.

Boc-Cys(DMNB)-OH. To a stirred solution of 4,5-dimethoxy-2-nitrobenzyl bromide (DMNB-Br, 276 mg, 1 mmol) and Boc-Cys-OH (165 mg, 0.75 mmol) in 50 ml Ethanol/water 9/1, N,N-diisopropylethylamine (DIPEA) was added (260 µl, 1.5 mmol) to reach pH ~9. After one hour, an excess Boc-Cys-OH (165 mg, 0.75

mmol) was added, and DIPEA (260 µl, 1.5 mmol) to reach pH~9. Two hours later, the solution was acidified with acetic acid (171 µl, 3 mmol) and the solvent evaporated. Residual water was co-evaporated with toluene (3 times), and the residue recovered with ethyl ether three times. The residue was dissolved in DCM and purified on a flash chromatography column using a linear gradient of 2% → 5% MeOH in DCM (v/v) added of 0.1% HAc. Fractions containing the product were pooled and evaporated to dryness. Residual HAc was co-evaporated with toluene (3 times), the residue recovered with ethyl ether 3 times, and evaporated to dryness. The product gives a single spot in TLC. Yield: 85%.

H-Cys(DMNB)-OH. Boc-Cys(DMNB)-OH (190 mg, 0.45 mmol) was dissolved in 10 ml of a DCM/TFA solution 1/1 containing 5% of water. The mixture was stirred at room temperature until the spot of the starting material disappeared (~1 hr). The solution was concentrated to a small volume (~0.5 ml) and the product precipitated with diethyl ether, filtered, washed thoroughly with ether, and air dried. Yield: 95%. NMR and ms data are identical to what have been reported.

Boc-Cys(DMNB)-Ala-OtBu. To a stirred suspension of Boc-Cys(DMNB)-OH (416 mg, 1.0 mmol) and HOBt (168 mg, 1.1. mmol) in DCM, 210 mg of EDC·HCl (1.1 mmol) was added. After two minutes, a solution containing H-Ala-OtBu·HCl (200 mg, 1.1 mmol) and NMM (121 µl, 1.1 mmol) in DCM was added

slowly, and the mixture was let react at room temperature for one hour. The pH was adjusted to ~7 with NMM and the reaction stirred for further two hours. The solvent was evaporated and the residue recovered in AcOEt, then washed with 10% citric acid (3x), brine, 5% $NaHCO_3$ (3x), and brine. The organic phase was dried on Na_2SO_4, filtered and evaporated to dryness. The product was purified using a flash chromatography and 2% MeOH in DCM as eluent. Fractions containing the pure product were pooled and evaporated to dryness, yielding 60% of the maximum obtainable product amount.

H-Cys(DMNB)-Ala-OH. Boc-Cys(DMNB)-Ala-OtBu (160 mg, 0.3 mmol) was dissolved in 10 ml of a DCM/TFA solution 1/1 containing 5% of water. The mixture was stirred at room temperature until the spot of the starting material disappeared (~1 hr). The solution was concentrated to a small volume (~0.5 ml) and the product precipitated with diethyl ether, filtered, washed thoroughly with ether, re-precipitated with ether from methanol and air dried. Yield: 95%. LC-MS (Single peak), ESI-TOF: $[M+H]^+_{expected}$: 388.12, found: 388.1.

2.6.3 Plasmid construction

All constructs were assembled by standard cloning methods and confirmed by DNA sequencing. pEYCUA-H1-$tRNA^{Leu}_{CUA}$/PGK-LeuRS and pCLHF-CMV-GFP_$Y182_{TAG}$ were constructed as described previously (Wang, 2007). To make the CmnRS expression plasmid, CmnRS gene (obtained from the Schultz

lab) was cloned into the XhoI/NheI sites of the plasmid pEYCUA-H1-$tRNA^{Leu}_{CUA}$ /PGK-LeuRS using primers 5'-GCCTCGAGGAAGAGCAATACCGCCC-3' and 5'-GCGCTAGCTTAGCCAACGACCAGATT-3'. Rat Kir2.1 (rKir2.1) plasmid was gifted from P. Slesinger lab. rKir2.1 was amplified using primers 5'-CGAAGCTTATGGGCAGTGTGAGAACCAAC-3' and 5'-CGGGATCCTTATATCTCCGATTCTCGCC-3' and cloned into the HindIII/BamHI sites of pCDNA3 plasmid (Invitrogen, CA). An amber stop codon TAG was introduced into the rKir2.1 gene at different sites (T142, I143, C149, C169, D172, I176, A184, or E224) through site-directed mutagenesis. mCitirine was fused to the C-terminus of rKir2.1 gene with the linker sequence 5'-GGCAGCGGCAGCGGCAGC-3'.

To construct the expression plasmids for *in vivo* experiments, the backbone plasmid pCAG-IRES-GFP was kindly provided by Y. Gotoh. LeuRS was cloned into the EcoRI/NotI sites using primers 5'-GGCGGCGAATTCCGCCACCATGGAACTCG-3' and 5'-GCGCGCGCGGCCGCTTAGCCAACGACCAGATTGAGGAG-3', whereas CmnRS was inserted to the EcoRI/NotI sites using primers 5'-GGCGGCGAATTCCGCCACCATGGAAGAGC-3' and 5'-GCGCGCGCGGCCGCTTAGCCAACGACCAGATTGAGGAG-3'. mCherry gene substituted each GFP in LeuRS and CmnRS plasmids. rKir2.1_C169tag gene was amplified using primers 5'-GGCGGCCTCGAGCGCCACCATGGGCAGTG-3'

and 5'-GCGCGCTGTACACTTATATCTCCGATTCTCGCCTTAAG-3', and cloned into the XhoI/BsrGI sites of the backbone plasmid. Three copies of H1-$tRNA^{Leu}_{CUA}$ cassettes were inserted into the SpeI/SalI sites using primers 5'-GGCGGCACTAGTGAATTCGAACGCTGACGTCATC-3' and 5'-GCGCGCGTCGACGGGGCGGGATGGGC-3'. GFP_$Y182_{TAG}$ gene was cloned into the XhoI/BsrGI sites of the backbone plasmid pCAG-IRES-GFP using primers 5'- GCGCGCCTCGAGCGCCACCATGGTGAGCAAGGGCGAGG-3' and 5'- GGCGGCTGTACAGCTCGTCCATGCCG-3'.

2.6.4 HEK293T cell culture and transfection

HEK293T cells were continuously cultured at 37°C in a 5% CO_2 : 95% air humidified incubator with Dulbecco's modified Eagle's medium (DMEM; Mediatech, VA) supplemented with 10% fetal bovine serum (FBS; Mediatech). For electrophysiological recording and imaging, HEK293T cells were transiently transfected using Lipofectamine 2000 (Invitrogen). After 6 hr, the cells were reseeded onto 12 mm round cover glasses (Carolina Biologicals, NC) coated with poly-D-lysine (10 μg/ml; Fisher Scientific, PA) in 24-well plates at 5–10% confluency. Cmn was added to the culture medium and cells were incubated for 12–24 hr more before recording or imaging.

2.6.5 Neuronal culture and transfection

Hippocampi from postnatal day 1–3 Sprague Dawley rats were dissected in warm saline (10 mM HEPES and 20 mM D-glucose added in Hank's balanced salt solution, HBSS; Invitrogen). After trypsin treatment, the tissue was thoroughly rinsed with saline and triturated. Dissociated neurons were plated onto coverslips in 24-well plates at 1.0–1.5 x 10^5 cells/well density after filtered through 40 μm nylon mesh (BD Bioscience, CA). Glass coverslips were coated with 0.5 mg/ml poly-D-lysine for over 10 hours in advance. The cells were cultured at 35°C in a 5% CO_2 : 95% air humidified incubator with Minimum Essential Medium (MEM; Invitrogen) supplemented with 5% FBS, D-glucose, B-27 (Invitrogen), GlutaMAX (Invitrogen), and serum extender (BD Biosciences, CA). For electrophysiological recording and imaging, neurons were transiently transfected with 0.7 μg of DNA per coverslip using calcium phosphate method. After 4–6 hr, Cmn-Ala was added to the medium at 1 mM final concentration, and cells were incubated for 12–24 hr more before recording or imaging.

2.6.6 Viral vector preparation and infection

Lentiviral vectors were prepared in the lab or by the Salk Viral Vector Core facility. All AAVs were prepared by Salk Viral Vector Core. Lentiviral vectors were titrated by Salk Viral Vector Core using Q-PCR method (Tiscornia, 2006). AAVs were also titrated by Salk Viral Vector Core by extracting DNA from the purified viral supernatants and checking the physical titer by Q-PCR. HEK293T cells were grown to 70−90% confluency on 10−30 10 cm-culture dishes. Lentiviral transfer vector and third-generation packaging vectors (pMDL, pREV, and

pVSVG, gifts from Inder Verma's lab) were isolated by endotoxin-free maxi-prep kits (Macherey-Nagel, Germany) and trasnsfected to HEK293T cells using polyethylenimine (PEI) MAX (Polysciences, PA). 4−6 hr after transfection, normal growth media replaced (or was added to) the transfection solution. ~72 hr later, the supernatant was collected and cleared by centrifugation at 2,000 rpm for 2−3 mins, passed through a 0.45 μm filter. Lentiviral vector in the media was concentrated using ultra-centrifuge (Beckman, Verma lab). The supernatant was centrifuged for 2 hr at 19,400 rpm in SW28 rotor at 18°C. The pellet was re-suspended in HBSS (Invitrogen) and centrifuged again for 2 hr at 21,000 rpm in SW55 rotor at 18°C. 20% sucrose solution in HBSS was used as a cushion for the second centrifugation. The pellet was resuspended in HBSS and shaken at 150 rpm for 1−2 hr. Concentrated lentiviral vectors were aliquoted and stored at -80°C. To infect HEK293T cells, cells were grown to number ~2 x 10^5 cell/well in a 24-well dish on the day of infection. The growth media was replaced with the fresh growth media containing 8 μg/ml polybrene just to cover the cells and the cells were incubated for 30 min. Diluted viral vectors were added to the cells to incubate for 3−5 hr and the growth media was added in the culture. Imaging was performed 48−72 hr post-infection. 5 DIV neurons were infected in the similar way but they were incubated for 7−10 days before imaging.

2.6.7 Amaxa neucleofection

Neucleofection to rat hippocampal primary neurons was performed as previously reported (Zeitelhofer, 2007).

2.6.8 Chicken embryo electroporation

Eggs (SPAFAS, McIntyre Farms) were incubated in a humidified chamber for 52−60 hr at 37°C until they reached Hamburger and Hamilton (HH) stage 14−16. Glass capillary with mouth-pipette was used to inject the mixture of the highly concentrated plasmids (1−3 μg/μl) with Fast Green dye into the chicken embryo spinal cord. Upon injection, the electrodes were immediately placed on both sides of the embryo, parallel to the spinal cord, and pulses were given 5 times at 25−30 volts for 50 ms at 1 sec intervals using a square wave electroporator (BTX). Eggs were sealed and put back into the incubator for 12−24 hr before imaging.

2.6.9 In utero electroporation and in utero injection of unnatural amino acids

Introduction of plasmid DNA into the neuroepithelial cells of mouse embryonic neocortex *in utero* was performed as described previously (Tabata, 2001), with minor modifications. In brief, the uterine horns were exposed at embryonic day 14.5 (E14.5), and ~1 μl DNA solution (0.2–5 μg/μl of each plasmid, depending on the construct) was injected into the lateral ventricle of each littermate. Embryos were then electroporated with the use of an electroporator CUY21EDIT (BEX, 0.5 cm puddle type electrode, 33–35 V, 50 ms duration, 4–8 pulses). After electroporation, the uterine horns were returned to the abdominal cavity to allow the embryos to continue development. For Leu incorporation

experiment (Figure 2.6D), the embryos were harvested four days after electroporation, and the brains were then subjected to the imaging analysis. For Cmn incorporation experiment (Figure 2.6E–H), the uterine horns were exposed again at E16.5, and Cmn (100–500 mM) was injected to the electroporated side or both sides of the lateral ventricle. The uterine horns were placed back into the abdominal cavity again. 12–24 hr after Cmn injection, the embryos were harvested, and the brains were then subjected to the imaging analysis or electrophysiology as described below. For imaging analysis, the brains were fixed with 4% paraformaldehyde in PBS at 4°C for 2–4 hr. After equilibration with 30% (w/v) sucrose in PBS, the fixed brains were embedded in OCT compound (Sakura) and frozen. Coronal sections (10 μm thick) were prepared by cutting the frozen brains with a cryostat CM3050S (Leica), and the fluorescence of GFP and mCherry was detected using microscopies described below. DAPI (Sigma) was used to counterstain nuclei.

2.6.10 Electrophysiology and light activation in culture

Whole-cell patch clamp was used to record macroscopic currents. For HEK293T cells, borosilicate glass electrodes (Warner Instruments, CT) had 5–10 MΩ resistance and were filled with internal solution (in mM: 150 KCl, 5.46 $MgCl_2$, 10 HEPES, 5 EGTA, 2.56 K_2ATP, and 0.3 Li_2GTP, pH 7.4). Extracellular solution contained (in mM) 140 NaCl, 20 KCl, 2 $MgCl_2$, 0.5 $CaCl_2$, and 10 HEPES (pH 7.4). 1 mM $BaCl_2$ was diluted into the extracellular solution and applied directly to the cell with a rapid, valve-controlled perfusion system (Warner Instruments, VC6,

MM-6 manifold). For cultured hippocampal neurons, glass electrodes had 3–6 MΩ resistance and were filled with internal solution containing (in mM) 135 potassium gluconate, 10 NaCl, 2 $MgCl_2$, 10 HEPES, 1 EGTA, 2.56 K_2ATP, and 0.3 Li_2GTP at pH 7.4. The extracellular recording solution contained (in mM) 150 NaCl, 3 KCl, 5 $MgCl_2$, 0.5 $CaCl_2$, 5 glucose, and 10 HEPES at pH 7.4. 0.5 mM $BaCl_2$ was diluted into the extracellular solution and applied directly to the cell. All of the chemicals were purchased from Sigma-Aldrich (St. Louis, MO).

Patch-clamp currents were recorded using an Axopatch 200B (Molecular Devices, Axon Instruments) amplifier. Currents were adjusted electronically for cell capacitance and series resistance (80–100%), filtered at 1 kHz with an 8-pole Bessel filter and digitized at 5 kHz with a Digidata 1200 interface (Molecular Devices, Axon Instruments). Cells were current-clamped at 0 nA with step current injection, or voltage-clamped at -100 mV. For some recordings, currents were elicited with voltage ramp protocol, from -100 mV to +40 mV, delivered at 0.5 Hz. For Cmn photolysis, LED with 385 nm filter (maximum ~40 mW; Prizmatix, Israel) was externally installed at the microscope to deliver light to the cell from 1 cm away at 45° angle. Light pulse was signaled from the amplifier through the digitizer when the membrane potential was held at -100 mV. Data are expressed as mean ± s.e.m. and statistical significance ($p < 0.05$) were determined by one-way analysis of variance (ANOVA) with Newman-Keuls test or Student's t test. All measurements were made at room temperature.

2.6.11 Electrophysiology and light activation in acute slices

After *in utero* electroporation and Cmn delivery, E17.5 mice embryos were harvested, and sagittal slices (200 μm) from their neocortices were prepared in ice-cold artificial cerebral spinal fluid or ACSF (in mM: 119 NaCl, 2.5 KCl, 1.3 $MgCl_2$, 2.5 $CaCl_2$, 1 NaH_2PO_4, 26.2 $NaHCO_3$, and 11 glucose, pH 7.3) continuously bubbled with 95/5% O_2/CO_2. Vibratome slices were warmed to 33°C and incubated for 42 mins in ACSF supplemented with 3 mM *myo*-inositol, 0.4 mM ascorbic acid and 2 mM sodium pyruvate, and then transferred to the recording chamber superfused with ACSF (2 ml/min).

Neurons were visualized with Hamamatsu digital camera (Model C8484) on Olympus microscope (BX51WI), and whole-cell patch-clamp recordings (Axopatch 200B) were made from neurons in the neocortex. PIRK-expressing neurons were identified by GFP and mCherry fluorescence. The internal solution contained (in mM) 130 potassium gluconate, 4 $MgCl_2$, 5 HEPES, 1.1 EGTA, 3.4 Na_2ATP, 10 sodium creatine phosphate, and 0.1 Na_3GTP at pH 7.3 with KOH. 0.5 mM $BaCl_2$ was diluted into ACSF and applied directly onto the slice. Currents were elicited with voltage ramp protocol, from -100 mV to +40 mV. For Cmn photolysis, 385 nm LED (light source ≥190 mW; Prizmatix) was installed at the microscope to deliver light through the objective. Electrophysiological chemicals were purchased from Sigma-Aldrich or Tocris Bioscience (Minneapolis, MN). Data are expressed as mean ± s.e.m. and statistical significance ($p < 0.05$) were determined by Student's t test. All measurements were made at ~33°C.

2.6.12 Microscopy

The images of HEK293T cells and cultured neurons were taken with Olympus IX81 microscope and Hamamatsu EM-CCD (Model C9100-02) camera. The light source was a xenon lamp from Sutter Instruments and filters were from Chroma (GFP Exc: 480/30 nm, Emi: 535/40 nm; mCitrine Exc: 495/10 nm, Emi: 525/25 nm; mCherry Exc: 580/20 nm Emi: 675/130 nm). The images of coronal sections of embryonic neocortices were taken with the use of Olympus BX61 microscope or Zeiss LSM700 confocal microscope.

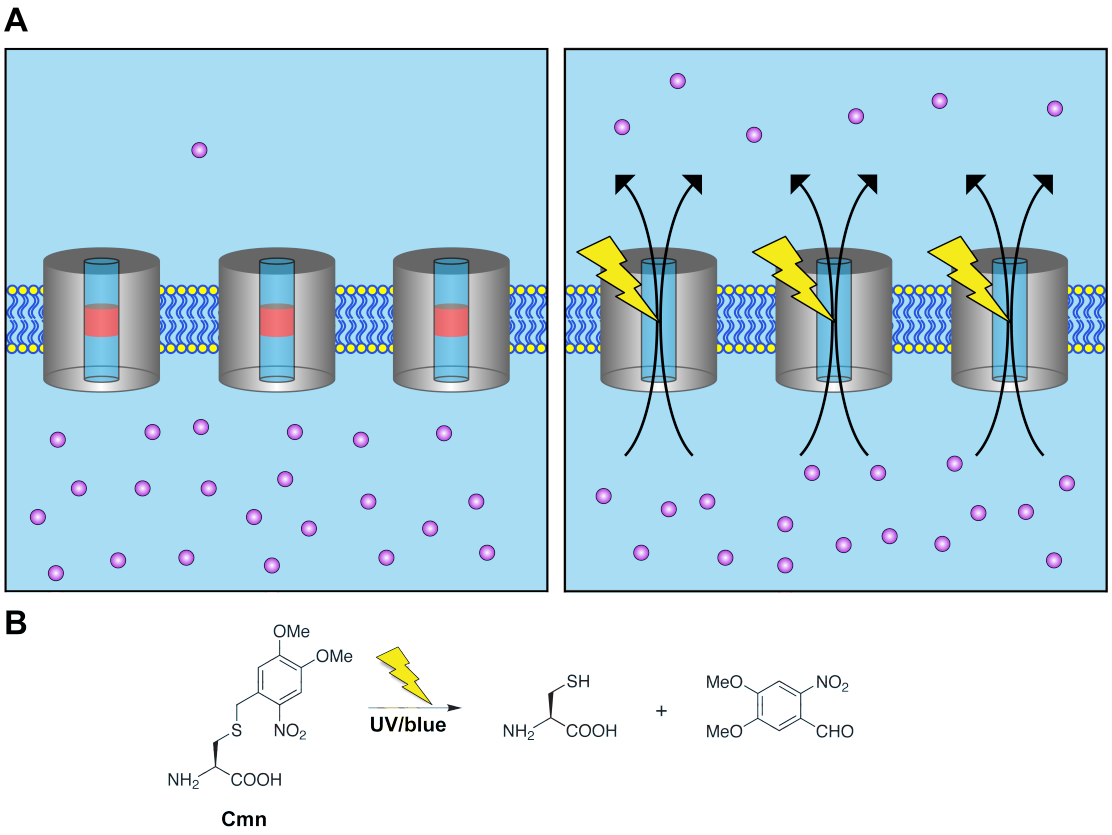

Figure 2.1: Photo-activatable Inwardly Rectifying Potassium channel (PIRK) using genetic incorporation of photocaged unnatural amino acids.

(**A**) A model illustrating photo-activation of PIRK channels (grey cylinder with pore) expressed on the plasma membrane. Left panel, incorporating 4,5-dimethoxy-2-nitrobenzyl-cysteine (Cmn) residues (in red) in the pore of Kir2.1 channels renders the channel non-conducting. Right panel, UV or blue light exposure irreversibly removes dimethoxy-nitrobenzyl group to allow permeation through the Kir2.1 channel, restoring outward K^+ (in purple) current and reducing membrane excitability. (**B**) Chemical pathway for photolysis of Cmn. UV/blue light cleaves S – C bond, releasing dimethoxy-nitrobenzyl group from Cys.

Figure 2.2: Identification of a critical site in Kir2.1 for Cmn incorporation that enables photo-activation.

(**A**) Side view of the crystal structure of chicken Kir2.2 channel (PDB ID: 3JYC) showing positions of candidate sites for incorporating Cmn. Two of four subunits are shown for clarity. Eight residues that potentially contribute to ion permeation are highlighted: T142 (red), I143 (orange), C149 (yellow), C169 (green), D172 (light blue), I176 (navy), A184 (purple), and E224 (black). Molecular drawings were prepared using UCSF Chimera 1.6.2. (**B**) Design of expression plasmids for Uaa mutagenesis. A plasmid for Leu incorporation, the amber suppressing orthogonal $tRNA^{Leu}_{CUA}$ driven by the H1 promoter and the aminoacyl-tRNA synthetase LeuRS driven by the mPGK promoter. A plasmid for Cmn incorporation, $tRNA^{Leu}_{CUA}$ driven by the H1 promoter and the aminoacyl-tRNA synthetase CmnRS driven by the mPGK promoter. A plasmid encoding Kir2.1 with the amber stop codon TAG and driven by the CMV promoter. A plasmid for the GFP reporter gene (GFP_$Y182_{TAG}$) driven by the CMV promoter. (**C**) I-V plot of currents recorded from HEK293T cells expressing wild-type Kir2.1 ('WT'; black), expressing Kir2.1_$C169_{TAG}$Leu with $tRNA^{Leu}_{CUA}$/LeuRS ('$C169_{TAG}$Leu'; green), or were untransfected ('HEK'; grey). (**D**) Mean Ba^{2+} sensitive currents (I_{Kir}) for eight amber stop codon (TAG) mutations. Four sites in Kir2.1 were permissive for UAG suppression with Leu (I143, C149, C169 and I176). Ba^{2+}-sensitive currents at -100 mV (mean ± s.e.m.) were: WT Kir2.1 (-5.92 ± 1.95 nA, n = 4), untransfected HEK293T cells (-0.04 ± 0.02 nA, n = 4), $T142_{TAG}$Leu (-0.03 ± 0.02 nA, n = 5), $I143_{TAG}$Leu (-1.62 ± 0.30 nA, n = 5), $C149_{TAG}$Leu (-0.92 ± 0.20 nA, n = 6), $C169_{TAG}$Leu (-1.03 ± 0.29 nA, n = 5), $D172_{TAG}$Leu (-0.10 ± 0.05 nA, n = 5), $I176_{TAG}$Leu (-2.46 ± 0.47 nA, n = 4), $A184_{TAG}$Leu (-0.05 ± 0.04 nA, n = 4), and $E224_{TAG}$Leu (-0.04 ± 0.04 nA, n = 4). *P < 0.05 and ***P < 0.001, one-way ANOVA. WT Kir2.1 was excluded from statistical analysis. (**E-G**) Examples of I-V plots for three different PIRK channels before (black) and after blue light (385 nm) illumination. Cmn was incorporated at the indicated sites by the orthogonal $tRNA^{Leu}_{CUA}$/CmnRS. (**H**) Ba^{2+} sensitive current (I_{Kir}) measured at -100 mV before (open column) and after (solid column) light exposure from HEK293T cells expressing different PIRK channels. Only incorporation of Cmn at C169 site led to a channel where light exposure increased the current above background levels. Mean Ba^{2+}-sensitive currents (mean ± s.e.m.) were: $I143_{TAG}$Cmn (before: -0.03 ± 0.01 nA, after: -0.07 ± 0.07 nA, n = 4), $C149_{TAG}$Cmn (before: -0.72 ± 0.21 nA, after: -0.71 ± 0.21 nA, n = 3), $C169_{TAG}$Cmn (before: -0.02 ± 0.02 nA, after: -0.17 ± 0.05 nA, n = 7), and $I176_{TAG}$Cmn (before: -0.14 ± 0.05 nA, after: -0.16 ± 0.11 nA, n = 8). **P < 0.01, paired t-test.

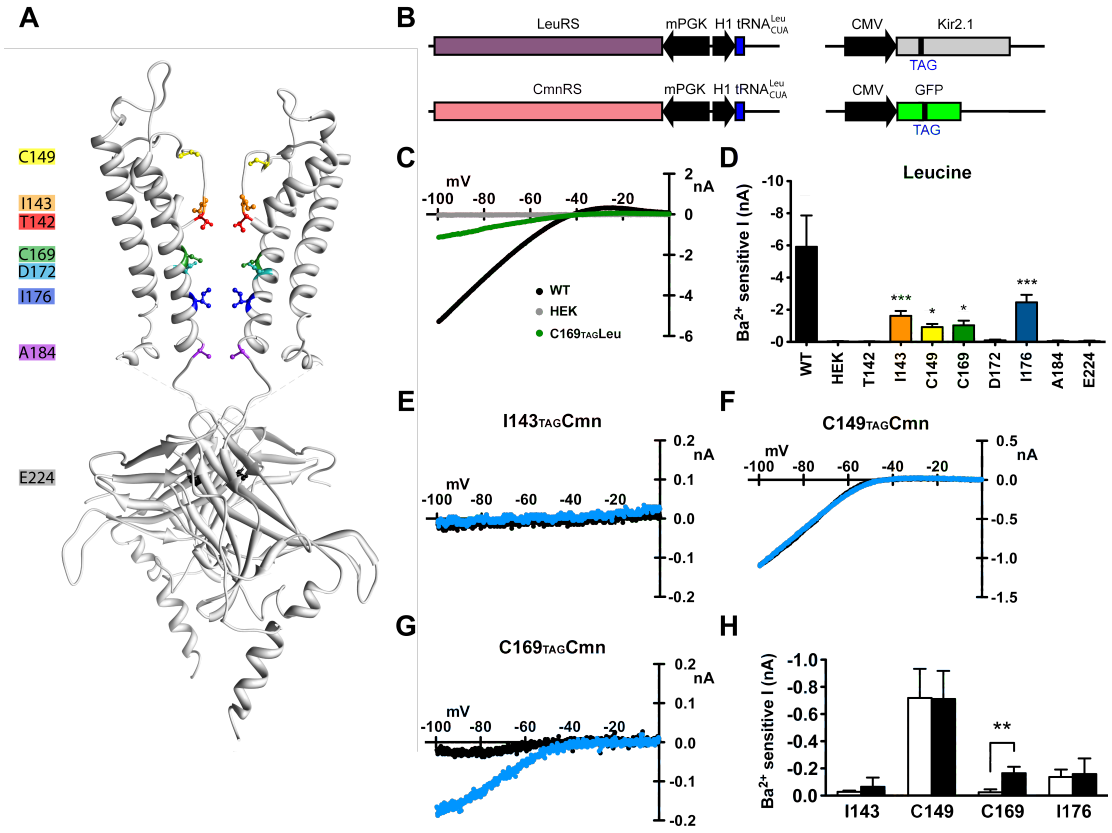
A
C149
I143
T142
C169
D172
I176
A184
E224
B
LeuRS
mPGK H1 tRNA$^{Leu}_{CUA}$
CMV Kir2.1
TAG
CmnRS
mPGK H1 tRNA$^{Leu}_{CUA}$
CMV GFP
TAG
C
mV
-100 -80 -60 -40 -20
2 nA
0
-2
-4
-6
WT
HEK
C169$_{TAG}$Leu
D
Leucine
Ba^{2+} sensitive I (nA)
-10 -8 -6 -4 -2 -0
***
*
*
***
WT HEK T142 I143 C149 C169 D172 I176 A184 E224
E
I143$_{TAG}$Cmn
mV
-100 -80 -60 -40 -20
0.2 nA
0.1
0.0
-0.1
-0.2
F
C149$_{TAG}$Cmn
mV
-100 -80 -60 -40 -20
0.5 nA
0.0
-0.5
-1.0
-1.5
G
C169$_{TAG}$Cmn
mV
-100 -80 -60 -40 -20
0.2 nA
0.1
0.0
-0.1
-0.2
H
Ba^{2+} sensitive I (nA)
-1.0 -0.8 -0.6 -0.4 -0.2 0.0
**
I143 C149 C169 I176

Figure 2.3: Light-dependent activation of PIRK (Kir2.1_C169$_{TAG}$Cmn) expressed in HEK293T cells.

(**A**) A model illustrating photo-activation of PIRK channels (grey (**A**) Plasmids for PIRK expression and detection in HEK293T cells and hippocampal neurons. One plasmid encoded Kir2.1_C169$_{TAG}$ with C-terminal fusion of mCitrine (mCit) for fluorescent detection of PIRK expression, and the other plasmid encoded $tRNA^{Leu}_{CUA}$ and CmnRS. (**B**) Localization of PIRK channels at cell membrane. Images show PIRK expression for HEK293T cells transfected with two plasmids in (A) in the absence or presence of Cmn (1 mM) in the growth media. DIC and fluorescence images are shown. Note green fluorescence in +Cmn indicating incorporation of Cmn. (**C**) Continuous current recording at -100 mV from HEK293T cells expressing PIRK. One second pulse of 385 nm light activated an inward current that was inhibited by extracellular $BaCl_2$ (1 mM). (**D**) Photo-activated PIRK currents. The I-V plot shows the currents recorded from HEK293T cells expressing Kir2.1_C169$_{TAG}$Leu (black), and PIRK before (grey) and after (blue) light activation (385 nm). (**E**) Ba^{2+} sensitive current (I_{Kir}) measured from HEK293T cells expressing Kir2.1_C169$_{TAG}$Leu (-8.30 ± 1.48 nA, n = 7), PIRK before light activation (-0.14 ± 0.07 nA, n = 10), and PIRK after light activation (-1.65 ± 0.41 nA, n = 10). *P < 0.05, paired t-test. (**F**) PIRK activation was dependent on duration of light exposure. Ba^{2+}-sensitive photo-activated current was measured at -100 mV from HEK293T cells expressing PIRK after the indicated duration of 385 nm light exposure. Mean (± s.e.m.) currents were: 1,000 ms (-2.27 ± 0.51 nA, n = 5), 500 ms (-2.04 ± 0.39 nA, n = 5), 200 ms (-0.79 ± 0.22 nA, n = 8), 100 ms (-0.65 ± 0.18 nA, n = 8), and 50 ms (-0.20 ± 0.12 nA, n = 6). **P < 0.01 and ***P < 0.001, one-way ANOVA. (**G**) Stepwise activation of PIRK following multiple light pulses. Representative current trace at -100 mV shows effect of three 385 nm light pulses (200 ms each) applied sequentially. Extracellular $BaCl_2$ (1 mM) inhibits light-activated current confirming Kir2.1 specific current. (**H**) Frequency dependence of light activation for PIRK channels. Mean Ba^{2+}-sensitive current measured at -100 mV is plotted as a function of number of light pulses of different durations. 1,000 ms (n = 5), 500 ms (n = 5), 200 ms (n = 8), 100 ms (n = 8), and 50 ms (n = 6). Error bars represent s.e.m.

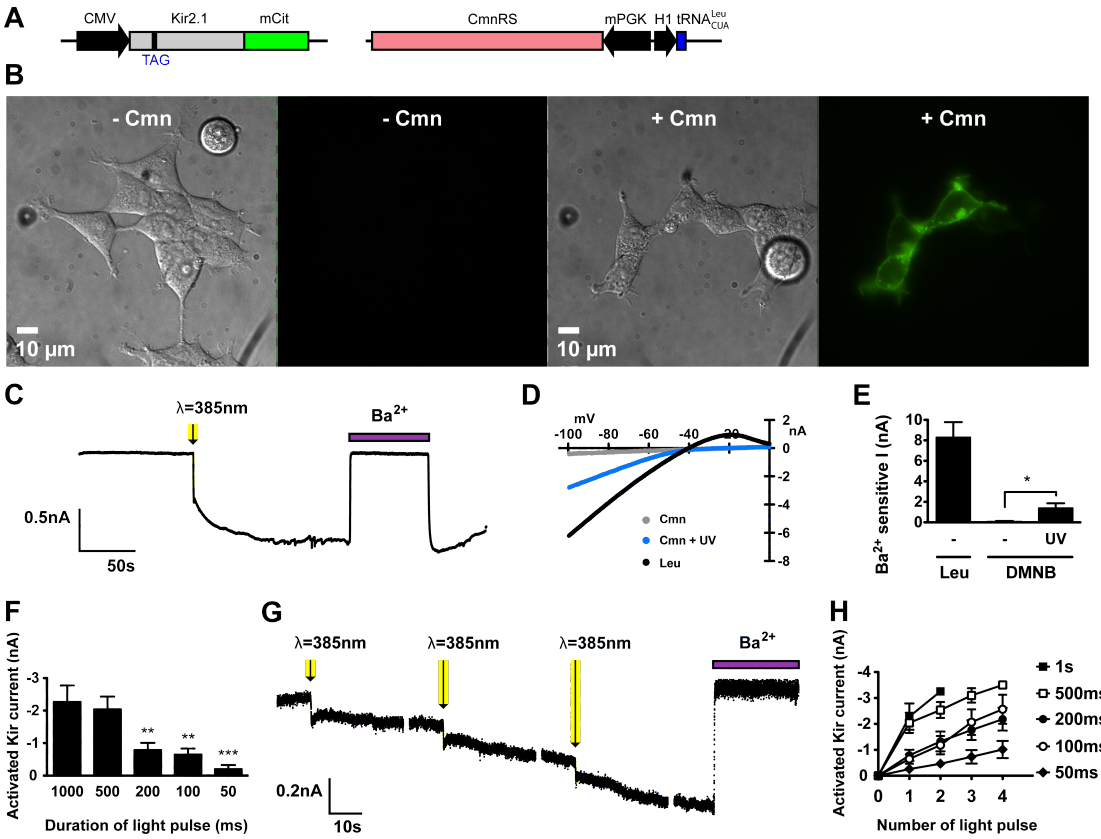
A
CMV
Kir2.1
mCit
TAG
CmnRS
mPGK
H1 tRNA$^{Leu}_{CUA}$
B
- Cmn
- Cmn
+ Cmn
+ Cmn
10 µm
10 µm
C
λ=385nm
Ba2+
0.5nA
50s
D
mV
-100 -80 -60 -40
2 nA
0 -2 -4 -6 -8
Cmn
Cmn + UV
Leu
E
Ba2+ sensitive I (nA)
10 8 6 4 2 0
*
- - UV
Leu
DMNB
F
Activated Kir current (nA)
-3 -2 -1 0
** ** ***
1000 500 200 100 50
Duration of light pulse (ms)
G
λ=385nm
λ=385nm
λ=385nm
Ba2+
0.2nA
10s
H
Activated Kir current (nA)
-4 -3 -2 -1 0
0 1 2 3 4
Number of light pulse
1s
500ms
200ms
100ms
50ms

Figure 2.4: Light-activation of PIRK suppresses firing of rat hippocampal primary neurons.

(**A**) DIC and fluorescence images of rat hippocampal primary neurons transfected with PIRK fused to mCitrine (mCit) and $tRNA^{Leu}_{CUA}$/CmnRS (plasmids shown in Figure 2.3A) in the absence or presence of Cmn (1 mM) in the growth media. Note green fluorescence in +Cmn indicating incorporation of Cmn. (**B**) PIRK-expressing neurons showed photo-activated inward current. I-V plots produced with a voltage-ramp protocol for a control neuron and a neuron expressing PIRK before (black) and after (blue) illumination (385 nm). Note inwardly rectifying current negative to -70 mV. Rapid downward deflections likely reflect action potentials. (**C**) Mean photo-activated currents for PIRK-expressing neurons. Currents were measured at -100 mV before (open column) and after (solid column) illumination: control neurons (before, -0.21 ± 0.06 nA; after, -0.19 ± 0.07 nA, n = 6), PIRK-expressing neurons (before, -0.43 ± 0.09 nA; after, -0.89 ± 0.25 nA, n = 6). *P < 0.05, paired t-test. (**D**) A single light pulse suppressed firing a hippocampal neuron expressing PIRK. Representative current traces recorded continuously. Action potentials were evoked in the neuron by current injection (green trace). Light exposure (385 nm for 1 sec, arrow) completely and rapidly suppressed neuronal firing. Firing was restored with extracellular 500 μM $BaCl_2$ which selectively inhibits Kir2.1 channels. (**E**) Neither UV illumination alone nor $BaCl_2$ (500 μM) altered excitability of control neurons. (**F**) Plot of action potential frequency of PIRK-expressing neurons before, after light activation and following application of Ba^{2+}. Action potentials measured in current-clamp and elicited by single current pulse (45 ± 4 pA, n = 56). Mean firing frequencies (± s.e.m.) for PIRK-expressing neurons were: before UV (7.4 ± 0.5 Hz, n = 28), after UV (0.4 ± 0.2 Hz, n = 28), and after Ba^{2+} addition (7.9 ± 1.0 Hz, n = 7). ***P < 0.001, one-way ANOVA; values for control neurons were: before UV (5.6 ± 0.6 Hz, n = 28), after UV (4.9 ± 0.6 Hz, n = 28), after Ba^{2+} addition (7.4 ± 1.2 Hz, n = 11). (**G**) Light activation significantly hyperpolarized PIRK-expressing neurons. Membrane potential was measured at the evoked state (as in "**D**") after current injection (25.6 ± 1.75 pA, n = 28). Left panel, the membrane potential after light activation is plotted as a function of membrane potential before light activation for each cell (PIRK-expression neurons: solid circle, n = 28; control neurons: open circle, n = 28). Right panel, membrane potential measured under different conditions was plotted. Mean (± s.e.m.) values for control neurons were: before UV (-57 ± 1 mV, n = 28), after UV (-56 ± 1 mV, n = 28), and after 500 μM $BaCl_2$ addition (-56 ± 2 mV, n = 8); for PIRK-expressing neurons: before UV (-54 ± 1 mV, n = 28), after UV (-84 ± 2 mV, n = 28), and after 500 μM $BaCl_2$ (-53 ± 3 mV, n = 7). ***P < 0.001, one-way ANOVA.

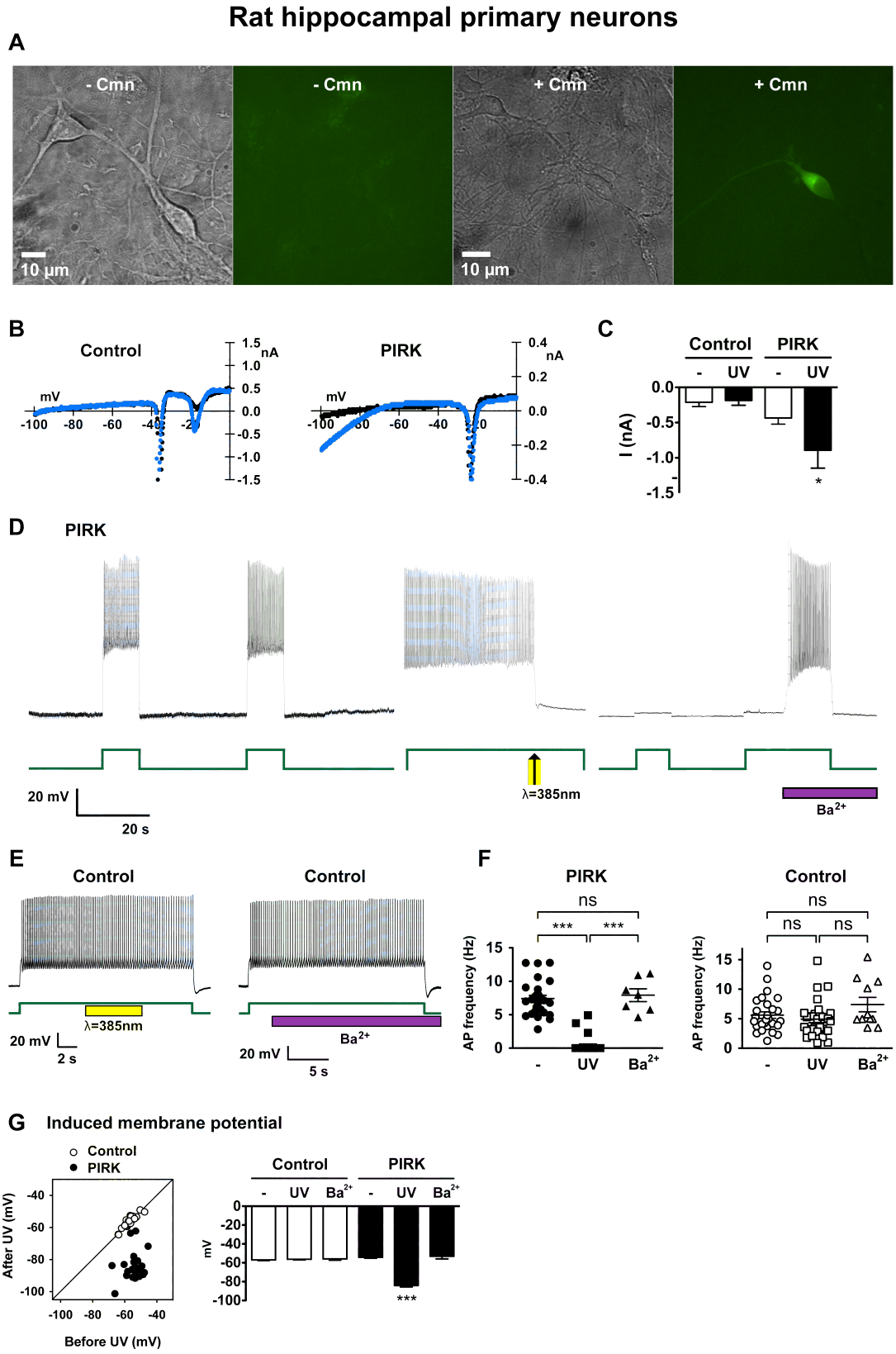
Rat hippocampal primary neurons
A
- Cmn
- Cmn
+ Cmn
+ Cmn
10 µm
10 µm
B
Control
PIRK
mV
nA
C
Control
PIRK
- UV - UV
I (nA)
*
D
PIRK
20 mV
20 s
λ=385nm
Ba2+
E
Control
Control
λ=385nm
20 mV
2 s
Ba2+
20 mV
5 s
F
PIRK
Control
ns
***
AP frequency (Hz)
- UV Ba2+
G
Induced membrane potential
Control
PIRK
After UV (mV)
Before UV (mV)
mV
***

Figure 2.5: Dynamic range of PIRK suppression of neuronal firing.

(**A**) In PIRK-expressing neurons, photo-activation of PIRK significantly decreased action potential firing frequency with different current injections. Representative whole-cell current-clamp traces show voltage response with three step-current injections (10 (black), 30 (red), and 50 (blue) pA) before (left) and after 385 nm light exposure. Graph shows mean action potential frequency plotted as a function of current injection. $^{**}P < 0.01$, paired t-test. Error bars represent s.e.m. (**B**) In control neurons, light exposure had no effect on action potential frequency. Representative whole-cell current-clamp traces show voltage response with three step-current injections (10 (black), 30 (red), and 50 (blue) pA) before (left) and after light exposure. Graph shows mean action potential frequency plotted as a function of current injection. Error bars represent s.e.m. (**C**) Rheobase, the minimum injected current required to fire an action potential, significantly increased in PIRK-expressing neurons upon light activation. Mean rheobase values (mean ± s.e.m.) for control neurons were: before UV, 31 ± 5 pA; after UV, 28 ± 6 pA, n = 12; for PIRK-expressing neurons were: before UV, 24 ± 3 pA; after UV, 35 ± 4 pA, n = 13. $^{*}P < 0.05$, paired t-test. (**D**) Resting membrane potential of PIRK-expressing neurons was negatively shifted upon light activation. Left panel, the resting potential after light activation is plotted as a function of the resting potential before light activation for each cell (PIRK-expressing neurons: solid circle, n = 19; control neurons: open circle, n = 19). Right panel, bar graph shows light-induced shift in resting potential. Specific values (mean ± s.e.m.) were: control neurons (1 ± 1 mV, n = 19); PIRK-expressing neurons (-17 ± 3 mV, n = 19). $^{***}P < 0.001$, unpaired t test.

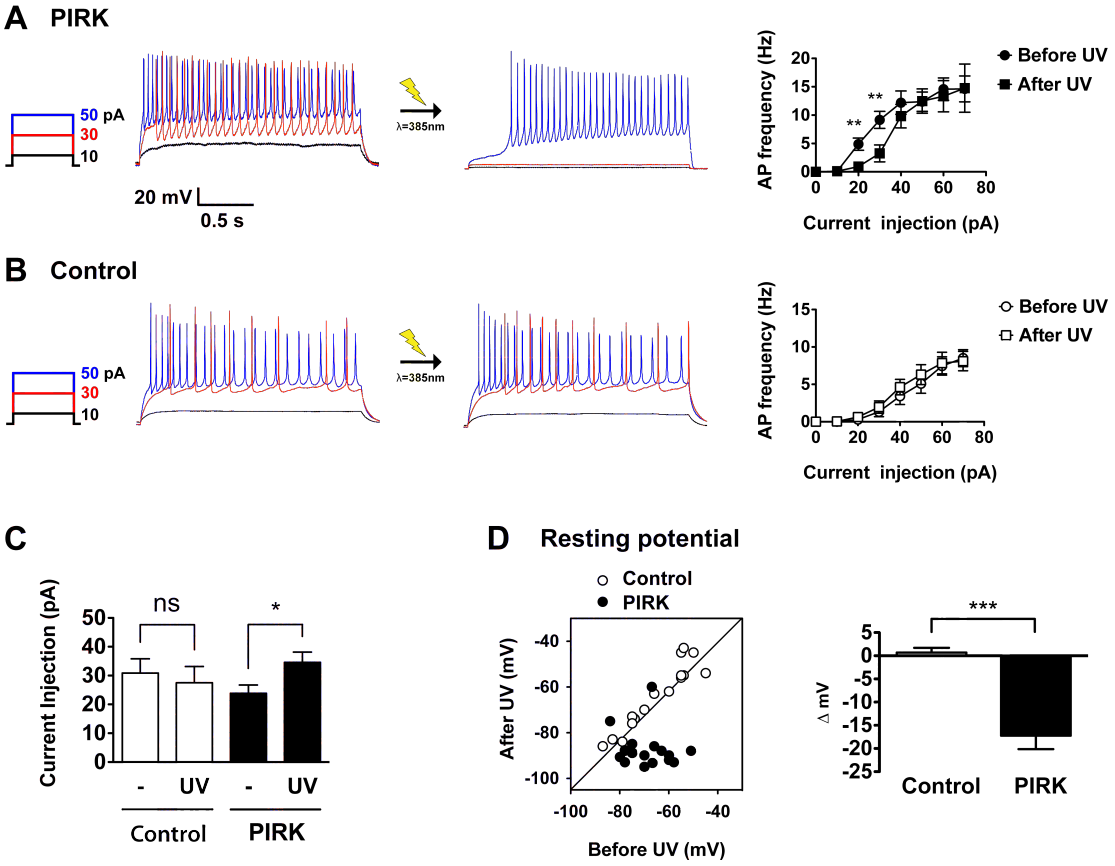
A PIRK
50 pA
30
10
20 mV
0.5 s
λ=385nm
AP frequency (Hz)
Current injection (pA)
Before UV
After UV
B Control
C
Current Injection (pA)
ns
*
- UV - UV
Control
PIRK
D Resting potential
Control
PIRK
After UV (mV)
Before UV (mV)
***
Δ mV
Control
PIRK

Figure 2.6: In vivo expression of PIRK channels in the mouse neocortex.

(**A**) Validation plasmid set: one plasmid for LeuRS or for CmnRS, under the control of CAG promoter and coexpressed with mCherry via IRES sequence; one plasmid encoding GFP_Y182$_{TAG}$ under the control of the CAG promoter. Three copies of $tRNA^{Leu}_{CUA}$ driven by the H1 promoter were combined with the GFP_Y182$_{TAG}$ to increase incorporation efficiency. Green fluorescence indicates suppression of amber codon by Leu or Cmn. Red fluorescence indicates successful gene delivery of synthetase *in vivo*. (**B**) PIRK expression plasmid set: one plasmid for CmnRS, under the control of CAG promoter and coexpressed with mCherry via IRES sequence; one plasmid for Kir2.1_C169$_{TAG}$ coupled with three copies of $tRNA^{Leu}_{CUA}$; one plasmid for GFP_Y182$_{TAG}$. Green and red fluorescence indicates successful expression of all three plasmids and Cmn incorporation. (**C**) Cartoon shows experimental procedure for PIRK expression *in vivo*. Gene constructs in (**B**) were injected into the mouse neocortex (E14.5) and electroporated *in utero*. Two days later, Cmn was injected to the brain. Slice imaging and electrophysiological assay were performed on E17.5. (**D**) Fluorescence images of mice embryonic cortical plates showing the successful incorporation of Leu into GFP$_{TAG}$ *in vivo*. Top row: CAG-LeuRS-IRES-mCherry only. Middle row: 3x(H1 $tRNA^{Leu}_{CUA}$)-CAG-GFP$_{TAG}$, with CAG-mCherry as an injection marker. Bottom row: CAG-LeuRS-IRES-mCherry and 3x(H1 $tRNA^{Leu}_{CUA}$)-CAG-GFP$_{TAG}$. Fluorescence of mCherry and GFP was imaged in separate channels, shown with DAPI staining of DNA, and merged in the right column. GFP fluorescence was detected only when the $tRNA^{Leu}_{CUA}$, LeuRS, and GFP_Y182$_{TAG}$ were all present. Leu is present *in vivo* all the time.

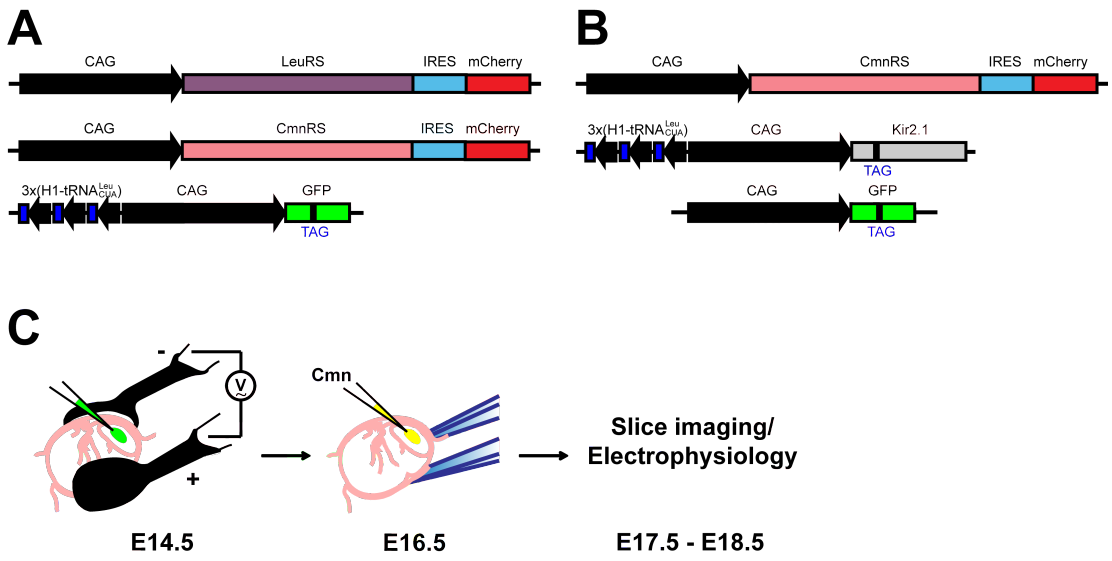
A
CAG
LeuRS
IRES
mCherry
CAG
CmnRS
IRES
mCherry
3x(H1-tRNA$^{Leu}_{CUA}$)
CAG
GFP
TAG
B
CAG
CmnRS
IRES
mCherry
3x(H1-tRNA$^{Leu}_{CUA}$)
CAG
Kir2.1
TAG
CAG
GFP
TAG
C
-
+
Cmn
Slice imaging/
Electrophysiology
E14.5
E16.5
E17.5 - E18.5
D
mCherry/DAPI
GFP/DAPI
merge
LeuRS-IRES-mCherry
10 µm
tRNA$^{Leu}_{CUA}$-GFP$_{TAG}$
mCherry
LeuRS-IRES-mCherry
tRNA$^{Leu}_{CUA}$-GFP$_{TAG}$

Figure 2.6: In vivo expression of PIRK channels in the mouse neocortex, Continued.

(**E**) Fluorescence images of mice embryonic cortical plates showing the successful incorporation of Cmn into GFP_{TAG} *in vivo*. CAG-CmnRS-IRES-mCherry and 3x(H1 $tRNA^{Leu}_{CUA}$)-CAG-GFP_{TAG} were electroporated *in utero* in both rows. The unnatural amino acid Cmn was injected *in utero* in the bottom row but not in the top row. GFP fluorescence was detected in neurons only when the $tRNA^{Leu}_{CUA}$, CmnRS, GFP_$Y182_{TAG}$, and Cmn were all present. (**F**) Fluorescence images of mice embryonic cortical neurons showing the incorporation of Cmn into GFP_{TAG} and $Kir2.1_{TAG}$ *in vivo*. The three gene constructs in (**B**) were electroporated *in utero*. GFP fluorescence was detected only with Cmn injection (bottom row), indicating Cmn incorporation in GFP_{TAG} and likely Cmn incorporation in the $Kir2.1_{TAG}$. (**G**) I-V plot of currents recorded from mice neocortical neurons showing light dependent activation of PIRK. Two days after gene constructs in (**B**) were electroporated and Cmn injected *in utero*, neocortical acute slices were prepared from embryos, as in (**C**). PIRK-expressing neurons in the slices (detected by both red and green fluorescence) were recorded before (black) and after (blue) 385 nm light exposure. $BaCl_2$ (500 μM) was added to verify I_{Kir} after photo-activation (orange). (**H**) Ba^{2+} sensitive current (I_{Kir}) measured from PIRK-expressing neurons in mice neocortical slices showed significant increase upon photo-activation. I_{Kir} (mean ± s.e.m.) at -100 mV was; before (-16.69 ± 13.25 pA) and after (-317.0 ± 72.85 pA) light exposure. n = 15, ***P < 0.001, paired t-test.

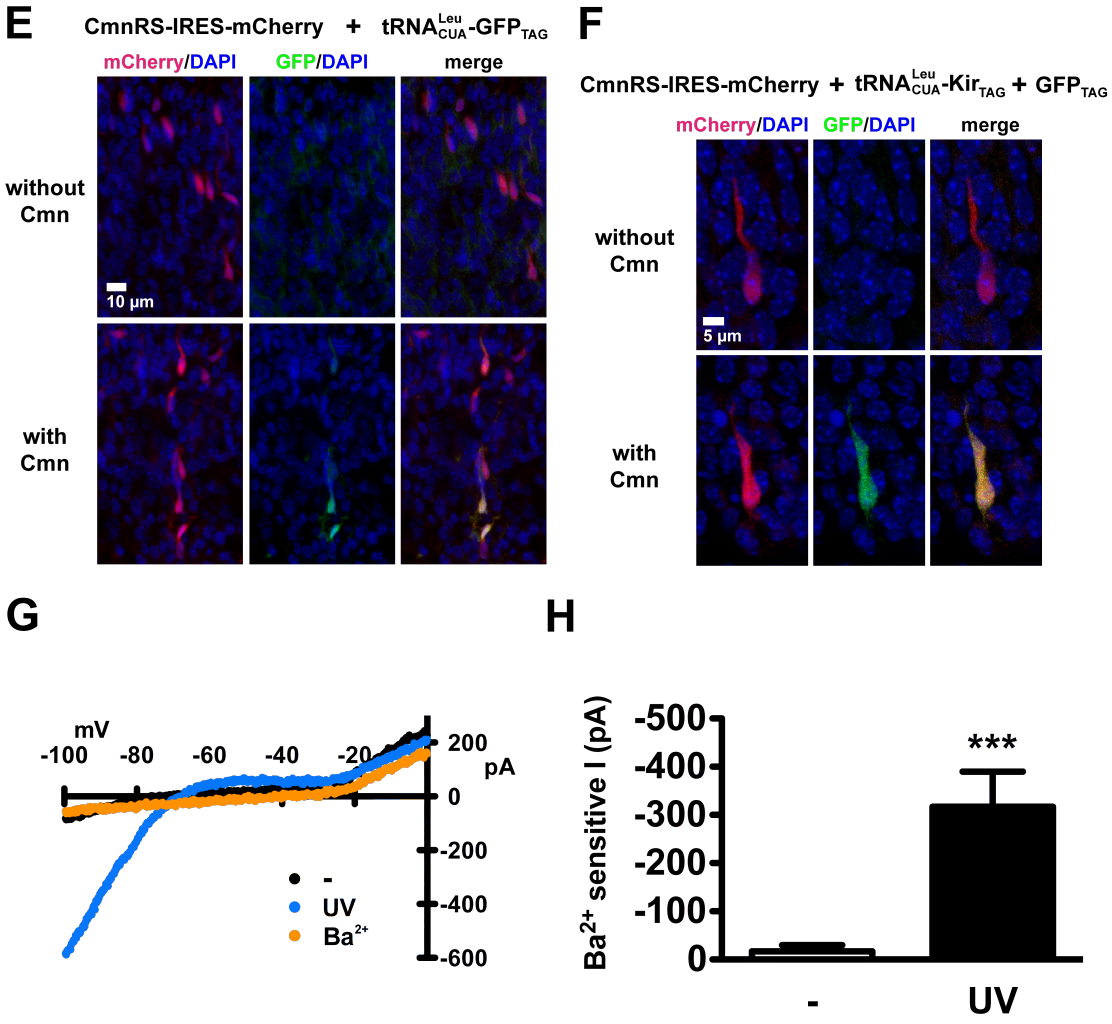
E
CmnRS-IRES-mCherry + tRNA$^{Leu}_{CUA}$-GFP$_{TAG}$
mCherry/DAPI
GFP/DAPI
merge
without Cmn
with Cmn
10 μm
F
CmnRS-IRES-mCherry + tRNA$^{Leu}_{CUA}$-Kir$_{TAG}$ + GFP$_{TAG}$
mCherry/DAPI
GFP/DAPI
merge
without Cmn
with Cmn
5 μm
G
mV
-100
-80
-60
-40
-20
200
pA
0
-200
-400
-600
-
UV
Ba^{2+}
H
Ba^{2+} sensitive I (pA)
-500
-400
-300
-200
-100
0
***
-
UV

A

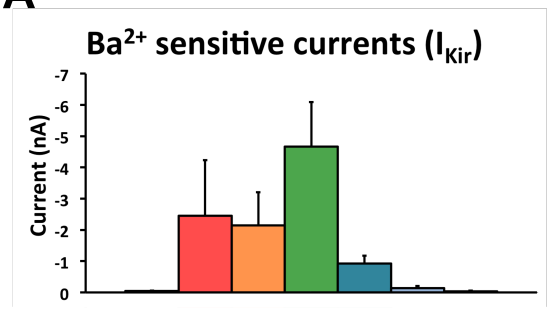

	HEK 293T	WT	F147C	F147W	$F147_{TAG}$ /LeuRS	$F147_{TAG}$ /OMeYRS + OMeY	$F147_{TAG}$ /CmnRS + Cmn
Avg. I (nA)	-0.05	-2.45	-2.15	-4.66	-0.93	-0.14	-0.03
n	4	3	11	16	17	13	6

B

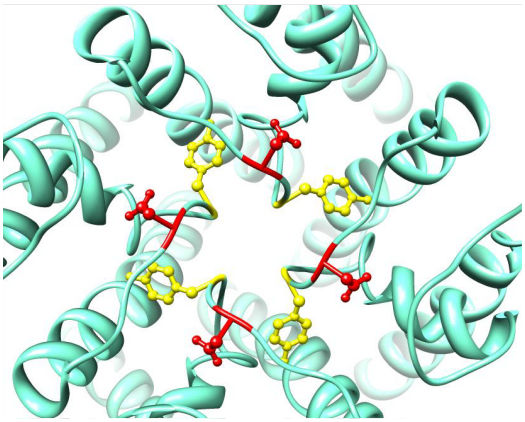

Supplemental Figure 2.1: Test of Kir2.1 F147 site for unnatural amino acids incorporation.

(**A**) Mean Ba^{2+} sensitive currents (I_{Kir}) for wild-type and different mutant Kir2.1_F147 channels. The current was measured by whole-cell recording in a voltage-clamped HEK293T cells held at -100 mV. Extracellular solution contains 20 mM [K+], whereas intracellular solution contains 140 mM [K+]. (**B**) Extracellular view of KirBac1.1 structure. D115 (red) corresponds to Kir2.1_F147 and Y113 (yellow) shows GYG location.

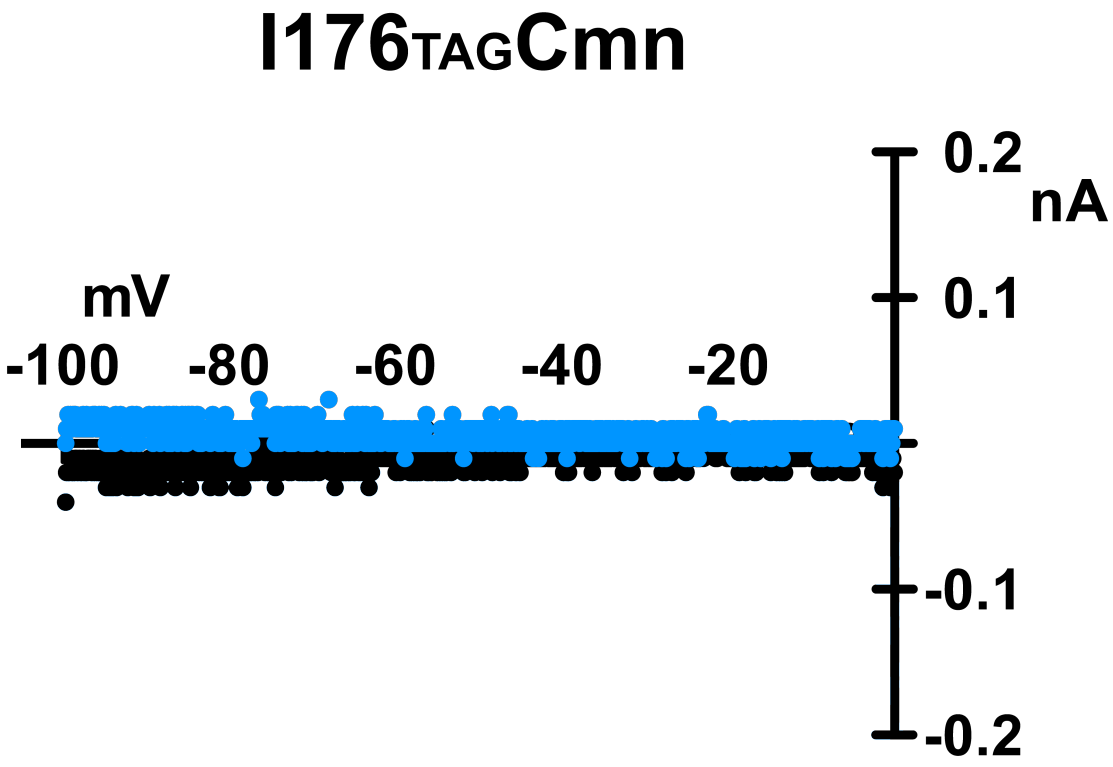

Supplemental Figure 2.2: Cmn incorporation into the I176 site in Kir2.1 did not generate a photo-activatable channel.

Exemplary I-V plot for Kir2.1_I176$_{TAG}$Cmn channels before (black) and after (blue) light (385 nm) illumination. Cmn was incorporated by the orthogonal $tRNA^{Leu}_{CUA}$/CmnRS.

Supplemental Figure 2.3: Attempts to express PIRK in neurons using viral vectors

(**A**) LV and AAV co-infection in neurons. Top left: neurons on 12 days *in vitro* (DIV), top right: neurons infected with LV-GFP, bottom left: neurons infected with AAV-mCherry, and bottom right: neurons co-infected with both LV and AAV. (**B**) Infection of LV Kir2.1_C169$_{TAG}$-mCit and AAV-U6-$tRNA^{Leu}_{CUA}$-H1-$tRNA^{Leu}_{CUA}$ in rat hippocampal primary neurons. (**C**) Coinfection of Sindbis-tdTomato with AAV-GFP in different serotypes. (a) Sindbis-tdTomato infection. (b) Coinfection of Sindbis-tdTomato and AAV2/1-GFP. (c) Coinfection of SindbistdTomato and AAV2/2-GFP. (d) Coinfection of Sindbis-tdTomato and AAV2/8-GFP. (e) Coinfection of Sindbis-tdTomato and AAV2/9-GFP. (f) Magnification of inset in (e). (**D**) Coinfection of Sindbis-tdTomato with AAV-GFP for two days in rat hippocampal organotypic slices. (a) Sindbis-tdTomato, (b) AAV2/9-GFP.

A

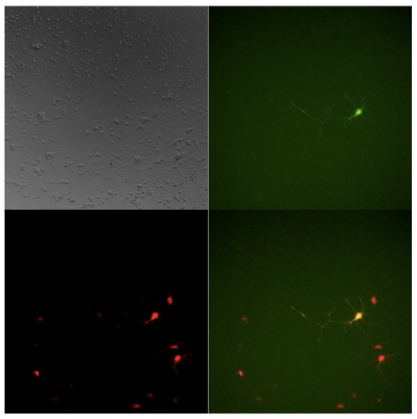

B

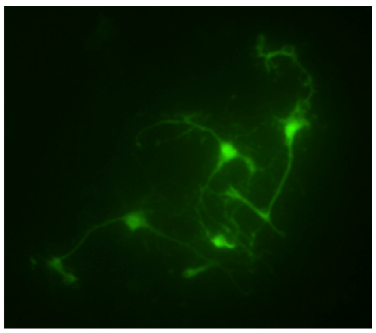

C

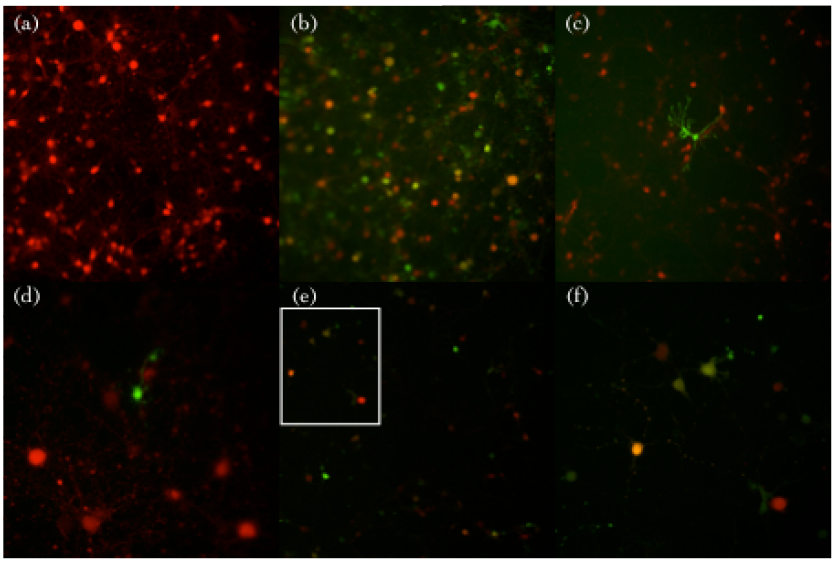

D

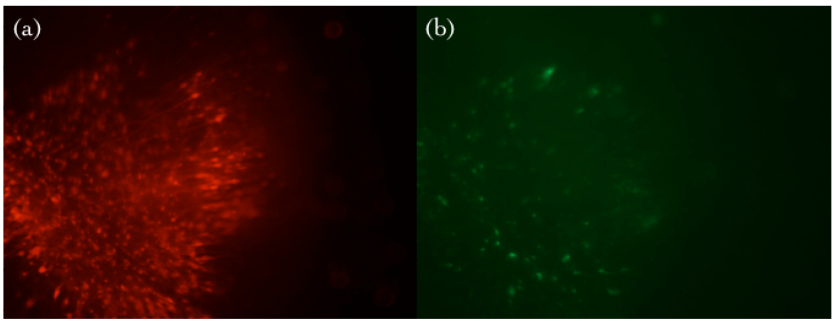

Supplemental Figure 2.4: Cmn incorporation in AMPAR

(**A**) Crystal structure of the transmembrane region in rat GluR2 homotetramer (top-down view; Sobolevsky, 2009). Highlighted residues have side chains heading to the pore, which make them better candidates to incorporate unnatural amino acids. Molecular drawings were prepared using UCSF Chimera 1.6.2. (**B**) Whole-cell recording from HEK293T cells transfected with wild-type GFP-GluR2. The cells were clamped either at +40 mV or -60 mV. Glutamatergic currents were recorded in response to 1 mM glutamate puff in the presence of 0.1 mM cyclothiazide. (**C**) Western blotting from HEK293T cells transfected with LeuRS, GFP, GFP-GluR2_L610$_{TAG}$, or GFP-GluR2_L610$_{TAG}$ + LeuRS. Proteins were detected using anti-GFP monoclonal antibodies. 24, 76, and 102 kDa correspond with the molecular weight of GFP, GFP-GluR2$_{TAG}$ truncated protein, and GFP-GluR2 full protein, respectively.

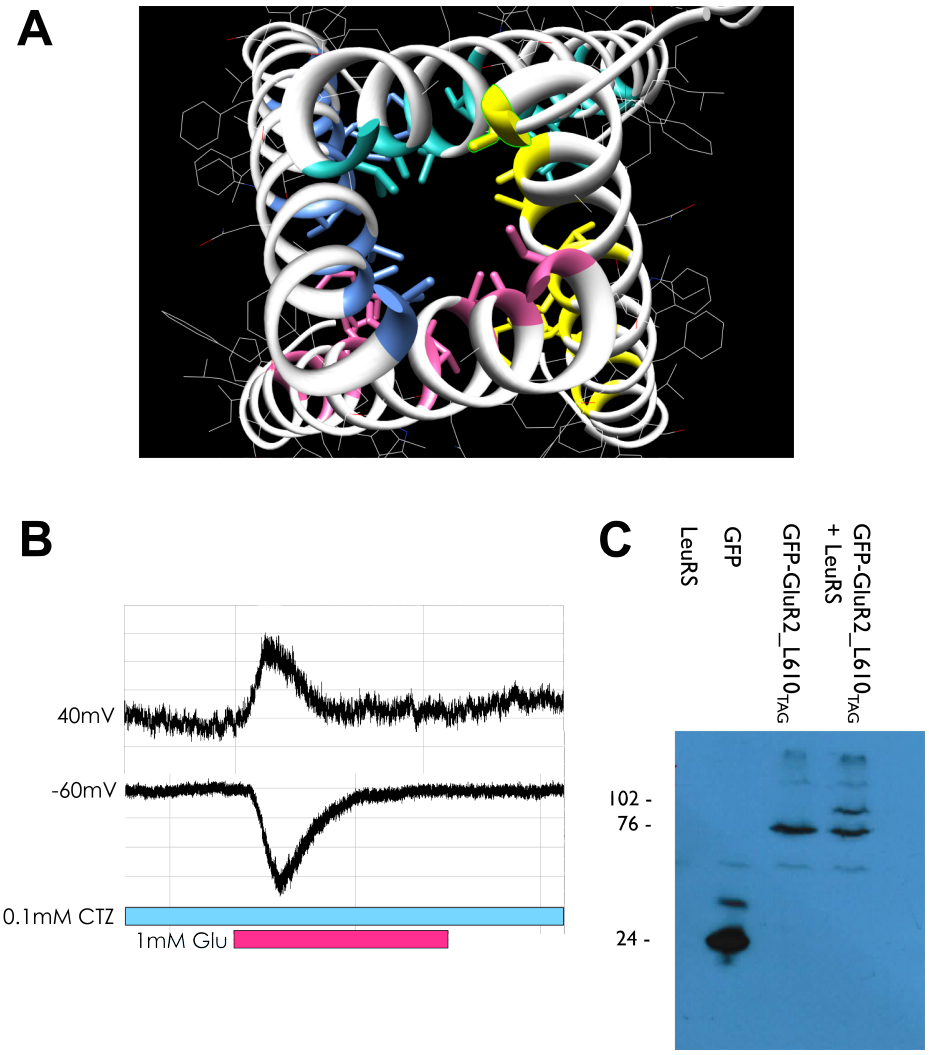
A
B
40mV
-60mV
0.1mM CTZ
1mM Glu
C
LeuRS
GFP
GFP-GluR2_L610TAG
GFP-GluR2_L610TAG + LeuRS
102 -
76 -
24 -

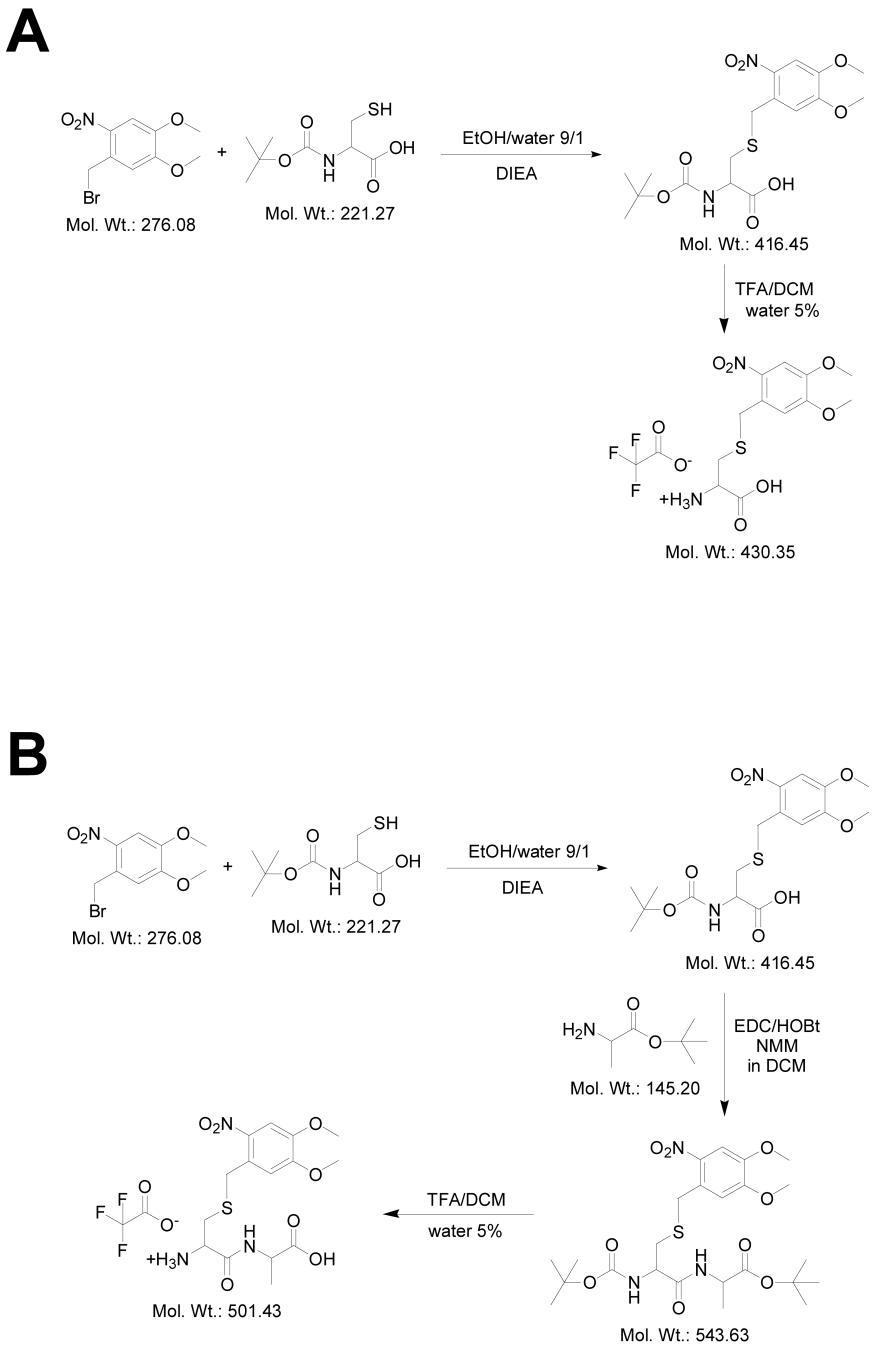

Supplemental Figure 2.5: Synthesis of Cmn and Cmn-Ala

(**A**) Schematic illustration of Cmn systhesis. (**B**) Schematic illustration of Cmn-Ala systhesis.

Chapter 3

ESTERIFICATION OF AN UNNATURAL AMINO ACID TO IMPROVE ITS UPTAKE AND INCORPORATION INTO PROTEINS IN MAMMALIAN CELLS

3.1 Abstract

Unnatural amino acids (Uaas) with noncanonical side chains can be efficiently transported into mammalian cells when the carboxyl group of the Uaa is masked with selected ester groups. This greatly increases the Uaa uptake rate and intracellular concentration, thus reducing the amount of Uaas required.

3.2 Introduction

Genetically encoded Uaas enable novel chemical and physical properties to be selectively introduced into proteins directly in live cells; this provides great potential for addressing biological questions at the molecular and cellular level in native settings (Wang, 2001; Wang, 2005; Wang, 2009). Uaas have been genetically incorporated into proteins in mammalian cells by using orthogonal tRNA-codon–synthetase sets (Liu, 2007; Sakamoto, 2002; Wang, 2007), yet the current low incorporation efficiency hinders their effective application. Efforts to improve efficiency have focused on optimizing the expression and activity of the orthogonal tRNA and synthetase (Liu, 2007; Takimoto, 2009; Wang, 2007), whereas the bioavailability of the Uaa inside mammalian cells, a prerequisite for incorporation, has not been addressed. In addition, there are many Uaas, such as glycosylated and phosphorylated amino acids that have not been genetically incorporated into proteins successfully. These amino acids can be invaluable for studying the contribution of posttranslational modifications of protein function and the role of a target protein in cellular signal transduction. Among many reasons, the inability of the Uaa to enter cells prevents the evolution of a mutant

synthetase specific for the Uaa by using cell-based selections or screens (Wang, 2005). Here, we show that a Uaa that deviates structurally from the canonical amino acids in side chain could not be efficiently transported into mammalian cells, but that masking the carboxyl group of the Uaa as an ester greatly increased the rate of cellular uptake and intracellular concentration of the Uaa. This resulted in a significant increase in the incorporation of this Uaa into proteins in mammalian cells. Among three esters tested, acetoxymethyl ester (AME) yielded the highest Uaa incorporation efficiency, with a concomitant reduction in the Uaa required in the growth medium.

Uaas with side chains similar to canonical amino acids can be transported into cells by endogenous amino acid transporters (Wang, 2006; Wang, 2009), which are relatively nonspecific for substrates (Malandro, 1996). However, Uaas that deviate significantly from canonical amino acids in side chain structure might not be recognized by these transporters. Cell membranes are more permeable to neutral than charged molecules. As zwitterions, Uaas have only a very small proportion present in the neutral form at physiological pH, thereby making it difficult for them to cross the cell membrane. Esters have been widely used in prodrugs to derivatize carboxyl, hydroxyl, and thio functionalities so as to make the parent drugs more membrane permeable (Rautio, 2008). In particular, Tsien *et al.* pioneered the use of AME to enhance the cellular uptake of various charged molecules, such as carboxylate-containing Ca^{2+} chelators and phosphate-containing second messengers (Schultz, 1993; Tsien, 1981). We

reasoned that masking the carboxyl group of the Uaa with an ester would convert the Uaa into a protonated weak base, which has a higher percentage of neutral form and increased lipophilicity for crossing the membrane. Once inside the cell, intracellular esterases can cleave the ester to regenerate the original Uaa for incorporation.

3.3 Results

We demonstrated this strategy with the Uaa 2-amino-3-(5-(dimethylamino)naphthalene-1-sulfonamide)propanoic acid (DanAla, **1**), which does not resemble and is bulkier in size than any canonical amino acid. Its fluorescence property also makes it an attractive candidate to develop optical reporters for imaging protein activities in live cells. We synthesized the methyl, ethyl, and acetoxymethyl esters of DanAla by using the methods shown in Figure 3.1B. Compound **5** was synthesized from Boc-Dap-OH and dansyl chloride according to the known procedure (Summerer, 2006). Alkylation of **5** with iodomethane and iodoethane gave intermediates **6** and **7**, which afforded DanAla-OMe (**2**) and DanAla-OEt (**3**), respectively, after deprotection. However, in the presence of bromomethyl acetate and N,N-diisopropylethylamine (DIPEA), compound **5** was transformed to the undesired cyclization product **8**, instead of Boc-DanAla-OAM. Therefore, the carboxyl group and the sulfonamide group were protected with the benzyl group and the Boc group (Neustadt, 1994), respectively. After debenzylation, carboxylic acid **10** was transformed into

acetoxymethyl ester **11** (Meijler, 2002), which furnished DanAla-OAM (**4**) after removal of the Boc groups.

To determine if the DanAla esters could enhance the incorporation of DanAla into proteins in mammalian cells, we used an in cellulo fluorescence assay to evaluate the incorporation efficiency of DanAla (Takimoto, 2009; Wang, 2007). The incorporation of DanAla into green fluorescent protein (GFP) was measured by using a stable clonal HeLa cell line, into which a GFP gene containing a premature UAG stop codon at a permissive site (Tyr182) was integrated. The cells were transfected with the orthogonal tRNA–synthetase pair specific for DanAla (Summerer, 2006), and the DanAla or DanAla ester was added to the growth medium. The incorporation of DanAla at the UAG182 position results in full-length, fluorescent GFP, whereas no incorporation results in a truncated, non-fluorescent protein. The total fluorescence intensity of cells was measured by flow cytometry analysis. As shown in Figure 3.2A, the cell fluorescence intensity increased when more DanAla was added to the growth medium, but reached a plateau from 0.25 to 1.00 mm. The plateau suggests that either the concentration of DanAla inside the cells has saturated the synthetase or that the cellular availability of DanAla is limiting. When DanAla-OMe was used, the cell fluorescence intensity doubled in comparison to that of cells incubated with the same concentrations of DanAla; this indicates that the cellular availability of DanAla was the limiting factor. Similar results were also obtained for DanAla-OEt. There was no significant increase in cell fluorescence intensity when the

concentration of DanAla-OMe or DanAla-OEt was increased from 0.10 to 0.25 mm. In contrast, DanAla-OAM doubled the fluorescence intensity at 0.10 mm and quadrupled it at 0.25 mm. In comparison to 1.00 mm of DanAla, the amount often used in Uaa incorporation, DanAla-OAM increased the cell fluorescence intensity fourfold in addition to requiring 75% less compound in the growth medium (0.25 mm). Western blot analysis of the cell lysates confirmed the increase in the amount of GFP produced by the AME modification (Figure 3.2B). These results suggest that all three ester modifications were able to increase DanAla incorporation into proteins with a concomitant reduction in the extracellular supply of Uaas. Furthermore, we identified DanAla-OAM as the most effective out of the three esters tested.

To understand how DanAla-OAM increases DanAla incorporation, we first monitored the uptake of DanAla and DanAla-OAM into cells by using fluorescence microscopy. We added 0.10 mm of DanAla or DanAla-OAM to the media of HEK293T cells, and measured the cytosolic fluorescence intensity of cells at sequential time points by using confocal microscopy (Figure 3.3A). For cells incubated with DanAla, the cytosolic fluorescence intensity was almost flat in the range of 620–750 AU. A striking difference was observed in the DanAla-OAM incubated sample. Within 5 min, the intracellular fluorescence intensity rapidly rose to 1100 AU, a 48% increase from that of the DanAla sample. The intensity increased for 3 hr peaking at 1613 AU, which was twice the DanAla peak intensity. The intensity of DanAla-OAM treated cells then gradually

dropped, possibly due to the depletion of the extracellular DanAla-OAM in combination with the equilibration of converted DanAla in and outside of cells. The AME modification thus significantly accelerates the cellular uptake rate of the compound.

Next, we quantified the intracellular concentrations of DanAla and DanAla-OAM by using HPLC. HEK293T cells were incubated with 0.10 mm of the compounds for 1 hr, and cell contents were extracted. Small molecules in the cell extracts were separated by HPLC, and peaks corresponding to DanAla and DanAla-OAM were verified by using pure compounds and mass spectrometry. Surprisingly, after only 1 hr of incubation, cells incubated with DanAla-OAM showed no peak for DanAla-OAM but a large peak for DanAla (Figure 3.3B); this indicates that all intracellular DanAla-OAM had been hydrolyzed into DanAla. The peak area for DanAla was used to determine its intracellular concentration. Cells incubated with DanAla and DanAla-OAM had 0.28 and 8.9 mm intracellular concentration of DanAla, respectively. The AME modification dramatically increased the intracellular concentration of DanAla by 31-fold.

When the concentration of DanAla-OAM was further increased to 0.50 mm, the cell fluorescence intensity decreased unexpectedly (Figure 3.2A). We used propidium iodide (PI) staining to assess the health of cells incubated with DanAla or DanAla-OAM (Figure 3.3C). For cells treated with 0.10 to 0.50 mm DanAla, the percentage of PI-positive cells was similar to that of cells without

Uaas. A slight increase of PI-positive cells was observed at 1.00 mm of DanAla. In contrast, cells treated with DanAla-OAM showed a significantly higher percentage of PI-positive cells, especially at the concentration of 0.50 mm. DanAla-OAM hydrolysis releases formaldehyde, which will negatively affect cell health at high concentration (Tsien, 1981). High intracellular concentration of DanAla could be toxic to cells as well. Therefore, an optimal concentration of the AME ester should be used to achieve highest Uaa incorporation efficiency with minimal negative effect to cell health.

3.4 Discussion

We have demonstrated that masking the carboxyl group of DanAla with AME increased the uptake rate and intracellular concentration of the Uaa in mammalian cells. This resulted in a higher DanAla incorporation efficiency accompanied by the added benefit of reducing the amount of Uaas in the growth medium. Efficient Uaa incorporation could prove valuable for the effective application of genetically encoded Uaas to studying various biological processes in mammalian cells. Modification of Uaas with AME could be generally applicable to other Uaas that have trouble entering mammalian cells. To test this hypothesis, more Uaas need to be modified, and their incorporation efficiency determined. However, there is currently no orthogonal tRNA–synthetase available for the incorporation of these candidate Uaas because a synthetase cannot be evolved for a Uaa that cannot readily enter the cell. We are applying the esterification strategy to highly polar amino acids, such as glycosylated and

phosphorylated amino acids, so as to overcome this problem with the final goal of genetically incorporating these biologically important amino acids into proteins.

3.5 Acknowledgements

Chapter 3, in part, is a reprint of the material as it appears in Takimoto, J. K., Xiang, Z., Kang, J. Y., and Wang, L. (2010) Chembiochem. The dissertation author was the third author of this publication. I appreciate all the hard work by Takimoto, J. K., Xiang, Z., and Wang, L. We thank Dr. Michael Burkart for help with the HRMS. This work was supported by the Ray Thomas Edwards Foundation, Beckman Young Investigator Program, March of Dimes Foundation (5-FY08-110), California Institute for Regenerative Medicine (RN1-00577-1, and National Institutes of Health (1DP2OD004744-01).

3.6 Materials and Methods

3.6.1 Synthesis of DanAla and DanAla esters

Synthesis of DanAla and DanAla esters: All reactions were carried out under nitrogen with dry solvents in anhydrous conditions, unless otherwise noted. Dry N,N-dimethylformamide (DMF), methanol, methylene chloride, and acetonitrile were obtained by passing commercially available pre-dried, oxygen-free formulations through activated alumina columns. Yields refer to chromatographically homogeneous materials. Reagents were purchased from Sigma–Aldrich and used without further purification. Reactions were monitored by TLC, and carried out on 0.25 mm Silicycle silica gel plates (60F-254) by using

UV light for visualization and an ethanolic solution of phosphomolybdic acid and cerium sulfate for developing under heat. Silicycle silica gel (60, particle size 0.040–0.063 mm) was used for flash column chromatography (FCC). NMR spectra were recorded on a Varian Oxford AS500 instrument and calibrated by using residual undeuterated solvent or tetramethylsilane as an internal reference. LCMS experiments were performed on an Agilent1100 Series LC/MSD instrument with a Phenomenex Synergi 4u Fusion-RP 80 A column (150 x 4.6 mm). DanAla was synthesized as described (Summerer, 2006).

NMR (1H and 13C) and HRMS data for compounds are given in the Supporting Information.

Compound **5**: Boc-Dap-OH (2.0 g, 9.8 mmol) was added in one portion to a stirring solution of dansyl chloride (2.4 g, 8.9 mmol) and Et_3N (2.6 mL) in CH_2Cl_2 (50 mL) at 0°C. The reaction mixture was allowed to warm to room temperature. After being stirred for 12 hr, the reaction mixture was concentrated under reduced pressure. The residue was purified by FCC (MeOH/CH_2Cl_2 7:93, v/v) to give compound **5** (3.675 g, 94%) as a yellow solid. Rf=0.22 (SiO_2, MeOH/$CHCl_3$ 1:8, v/v).

Compound **6**: Compound **5** (218.8 mg, 0.50 mmol) was dissolved in DMF (2 mL), and the mixture was cooled to 0°C. DIPEA (0.096 mL, 0.55 mmol) and MeI (0.062 mL, 1.00 mmol) were added drop-wise to the solution. The reaction

mixture was allowed to warm to room temperature and stirred for 12 hr. Water (20 mL) was added, and the solution was extracted with ethyl acetate (3 x 20 mL). The organic phase was washed with brine, dried with sodium sulfate, and concentrated under reduced pressure. The residue was purified by FCC (ethyl acetate/hexanes 3:7, v/v) to give compound **6** (197.4 mg, 87%) as a yellow solid.

Compound **7**: Compound **5** (218.8 mg, 0.50 mmol) was dissolved in DMF (2 mL), and the mixture was cooled to 0°C. DIPEA (0.096 mL, 0.55 mmol) and EtI (0.080 mL, 1.00 mmol) were added drop-wise to the solution. The reaction mixture was allowed to warm to room temperature and stirred for 12 hr. Water (20 mL) was added, and the solution was extracted with ethyl acetate (3 x 20 mL). The organic phase was washed with brine, dried with sodium sulfate, and concentrated under reduced pressure. The residue was purified by FCC (ethyl acetate/hexanes 3:7, v/v) to give compound **7** (174.1 mg, 75%) as a yellow solid.

Compound **2**: Compound **6** (45.2 mg, 0.10 mmol) was dissolved in CH_2Cl_2 (0.9 mL), and the mixture was cooled to 0°C. Trifluoroacetic acid (TFA; 0.3 mL) was added drop-wise to the solution. The reaction mixture was allowed to warm to room temperature and stirred for 4 hr, then concentrated under reduced pressure. After being under vacuum for 48 hr, the residue was dissolved in dimethyl sulfoxide (DMSO; 1.0 mL) for use.

Compound **3**: Compound **7** (46.6 mg, 0.10 mmol) was dissolved in CH_2Cl_2 (0.9 mL), and the mixture was cooled to 0°C. TFA (0.3 mL) was added drop-wise to the solution. The reaction mixture was allowed to warm to room temperature and stirred for 4 hr, then concentrated under reduced pressure. After being under vacuum for 48 hr, the residue was dissolved in DMSO (1.0 mL) for use.

Compound **9**: Compound **5** (569.4 mg, 1.30 mmol) was dissolved in DMF (10 mL), and the mixture was cooled to 0°C. DIPEA (0.25 mL, 1.43 mmol) and benzyl bromide (0.31 mL, 2.60 mmol) were added drop-wise to the solution. The reaction mixture was allowed to warm to room temperature and stirred for 24 hr. Water (70 mL) was added and the solution was extracted with ethyl acetate (50 mL). The organic phase was washed with brine, dried with sodium sulfate, and concentrated under reduced pressure. The residue was purified by FCC (ethyl acetate/hexanes 1:3–1:2, v/v) to give Boc-DanAla-OBn (522.1 mg, 76%) as a yellow solid. Rf=0.25 (SiO_2, ethyl acetate/hexanes 1:2, v/v). Boc-DanAla-OBn (466.7 mg, 0.885 mmol) and 4-dimethylaminopyridine (DMAP; 21.6 mg, 0.177 mmol) were dissolved in CH_2Cl_2 (4 mL), and the mixture was cooled to 0°C. Et_3N (0.136 mL, 0.974 mmol) and Boc_2O (289.8 mg, 1.328 mmol) in CH_2Cl_2 (2 mL) were added drop-wise to this stirring mixture. The reaction mixture was allowed to warm to room temperature and stirred for 4 hr. Saturated aqueous NH_4Cl solution was added to the mixture. The aqueous phase was separated and washed with CH_2Cl_2 (3 x 10 mL). The combined organic phase was washed with brine, dried with sodium sulfate, and concentrated under reduced pressure. The

residue was purified by FCC (ethyl acetate/hexanes 1:3, v/v) to give compound **9** (538.6 mg, 97%). Rf=0.34 (SiO_2, ethyl acetate/hexanes 1:2, v/v).

Compound **10**: Pd/C (87.3 mg) was added to a solution of compound **9** (515.0 mg, 0.82 mmol) in methanol. The reaction mixture was stirred under hydrogen for 2 hr at room temperature. The reaction mixture was passed through a short plug of celite and eluted with ethyl acetate. The filtrate was concentrated to give compound **10** (467.3 mg) as a yellow-green solid. Rf=0.22 (SiO_2, MeOH/$CHCl_3$ 1:10, v/v).

Compound **11**: Compound **10** (434.9 mg, 0.809 mmol) was dissolved in CH_3CN, and the mixture was cooled to 0°C. DIPEA (0.56 mL, 3.236 mmol) and bromomethyl acetate (0.24 mL, 2.427 mmol) were added drop-wise to the solution. The reaction mixture was allowed to warm to room temperature and stirred for 12 hr, then concentrated under reduced pressure. The residue was purified by FCC (ethyl acetate/hexanes 1:2, v/v) to give compound **11** (389.5 mg, 84% over 2 steps) as yellow-green solid. Rf= 0.31 (SiO_2, ethyl acetate/hexanes 1:2, v/v).

Compound **4**: Compound **11** (61.0 mg, 0.10 mmol) was dissolved in CH_2Cl_2 (0.9 mL), and the mixture was cooled to 0°C. TFA (0.3 mL) was added drop-wise to the solution. The reaction mixture was allowed to warm to room temperature and stirred for 6 hr, then concentrated under reduced pressure. After

being under vacuum for 48 hr, the residue was dissolved in DMSO (1.0 mL) for use.

3.6.2 Cell lines and culture conditions

HEK293T cells were used for determining the Uaa intracellular concentration and imaging experiments. A stable clonal HeLa cell line containing the GFP gene with $Tyr182_{TAG}$ mutation was previously established in this lab and was used here for assaying Uaa incorporation efficiency (Wang, 2007). HEK293T and HeLa-GFP_$Tyr182_{TAG}$ cells were cultured in Dulbecco's modified Eagle's medium (DMEM, Mediatech) supplemented with 10% fetal bovine serum (FBS).

3.6.3 Fluorescence imaging

HEK293T cells (3×10^5) were seeded into an imaging dish supplemented with DMEM with 10% FBS, but without phenol red. After 18–24 hr, DanAla or DanAla-OAM was added to the medium to a final concentration of 0.10 mm. Cells were immediately imaged with an Olympus IX81 spinning disc microscope with a Hamamatsu EM-CCD under the same conditions, lex=360 x 30 nm, lem=535 x 20 nm. After each time point, cells were placed back into the incubator. Images were analyzed in Slidebook 4.2 by using the masking tool and average intensity function. Cells not treated with any compound were used as control to determine background fluorescence, which was subtracted from the measured intensities of samples to yield the final net intensities.

3.6.4 HPLC analysis of intracellular concentration

HEK293T cells (8.5 x 10^6) were seeded into a 10 cm tissue culture dish supplemented with DMEM containing 10% FBS. After 18–24 hr, DanAla or DanAla-OAM was added to the medium to a final concentration of 0.1 mm. The compounds were incubated with cells for 1 hr. Cells were then washed with phosphate-buffered saline (PBS; 1 mL) several times. After trypsinization with trypsin (1 mL, 0.05%; Mediatech), cells were centrifuged, and the medium was removed. Cells were washed again with water (1 mL) and centrifuged. The supernatant was removed, and cells were resuspended in water (250 mL). Toluene (50 mL) was added, and the cells were placed in a shaking incubator at 37°C for 30 mins. Cells were centrifuged at 20,000 relative centrifugal force (RCF) for 10 mins. The aqueous layer was placed into a Microcon Ultracel YM10 column (Millipore) and spun for 30 mins at 12,000 RCF. The flow-through was analyzed by HPLC-MS (Agilent 1100 Series LC/MSD instrument): and aliquot (5 mL) of the aqueous layer was separated on a Phenomenex Synergi 4u Fusion-RP 80 A column (150 x 4.6 mm) with a gradient of aqueous acetonitrile/0.1% formic acid (75:25 to 25:75) over 10 min. DanAla and DanAla-OAM were identified by extracting their MW (+1) from the total ion mass spectrum. Pure DanAla and DanAla-OAM were also added into the flow-though prepared from cells not treated with compounds so as to verify the peak positions of DanAla (3.3 mins) and DanAla-OAM (3.7 mins). Calculation of DanAla concentrations in each sample was based on the extracted ion area of DanAla and a standard

curve. The standard curve was made by extracting the area of DanAla in solutions with different concentrations (0.10, 0.20, 0.30, 0.40, 0.50, 0.60, 0.70, 0.80, 0.90, and 1.00 mm). Cells not treated with any compound were used to measure the background area at 3.3 and 3.7 min. The intracellular concentration was given by the total molar amount of DanAla divided by the total volume of cells, by using the volume of a single cell as in (Thomas, 2005).

3.6.5 Flow cytometry

Stable HeLa–GFP_Tyr182$_{TAG}$ clonal cells were seeded in a 3.5 cm culture dish and transfected with pELcua-LeuRS or pELcua-DanAlaRS (5 mg) plasmid DNA by using Lipofectamine 2000 (Wang, 2007). HeLa– GFP_Tyr182$_{TAG}$ cells that were not transfected with a tRNA–synthetase pair were used as a negative control. DanAla and DanAla-OAM were added 24 hr post transfection, and flow cytometry was carried out 24 hr after the addition of the compounds. Cells were trypsinized and washed with PBS twice. Samples were centrifuged and resuspended in PBS (1.0 mL) and PI (5 mL). Samples were analyzed with a FACScan (Becton, Dickinson and Company, Franklin Lakes, USA). The excitation wavelength was 488 nm, and the emission filter was 530/30 nm. The excitation light (488 nm) excites GFP but not DanAla. For each sample, the total fluorescence intensity of 30,000 cells was recorded, and was normalized to the total fluorescence intensity of cells transfected with pELcua-LeuRS. PI (5 mgmL^{-1}, Sigma–Aldrich) was used to determine cell viability by flow cytometry. Cells

were trypsinized and incubated with PI for 15 mins at room temperature, and then analyzed by using FACScan (Becton, Dickinson and Company).

3.6.6 Western blot

HeLa–GFP_Tyr182$_{TAG}$ clonal cells were transfected and incubated with the appropriate DanAla or DanAla ester, as previously described for flow cytometry analysis. Cells were trypsinized and washed with PBS, and cell number was counted by using a hemocytometer. Samples were centrifuged and resuspended with PBS (20 mL) containing ethylendiaminetetraacetate-free protease inhibitor cocktail (Roche) and DNase I (Roche). These samples were lysed by flash freezing in liquid nitrogen, and thawed by sonication. The lysis procedure was repeated three times to ensure complete lysis. Loading buffer was added, and the samples were boiled. Prepared samples were loaded onto a 12% SDS-PAGE gel. For the pELcua-LeuRS sample, 10^4 cells were loaded, while 7.5 x 10^4 cells were loaded for all other samples. The primary antibody (Anti-GFP Monoclonal Antibody 7G9, BioPioneer, San Diego, USA) and horseradish peroxidase (HRP) conjugated secondary antibody (Goat Anti-Mouse IgG-HRP Conjugate, Santa Cruz Biotechnology) were used to detect GFP proteins.

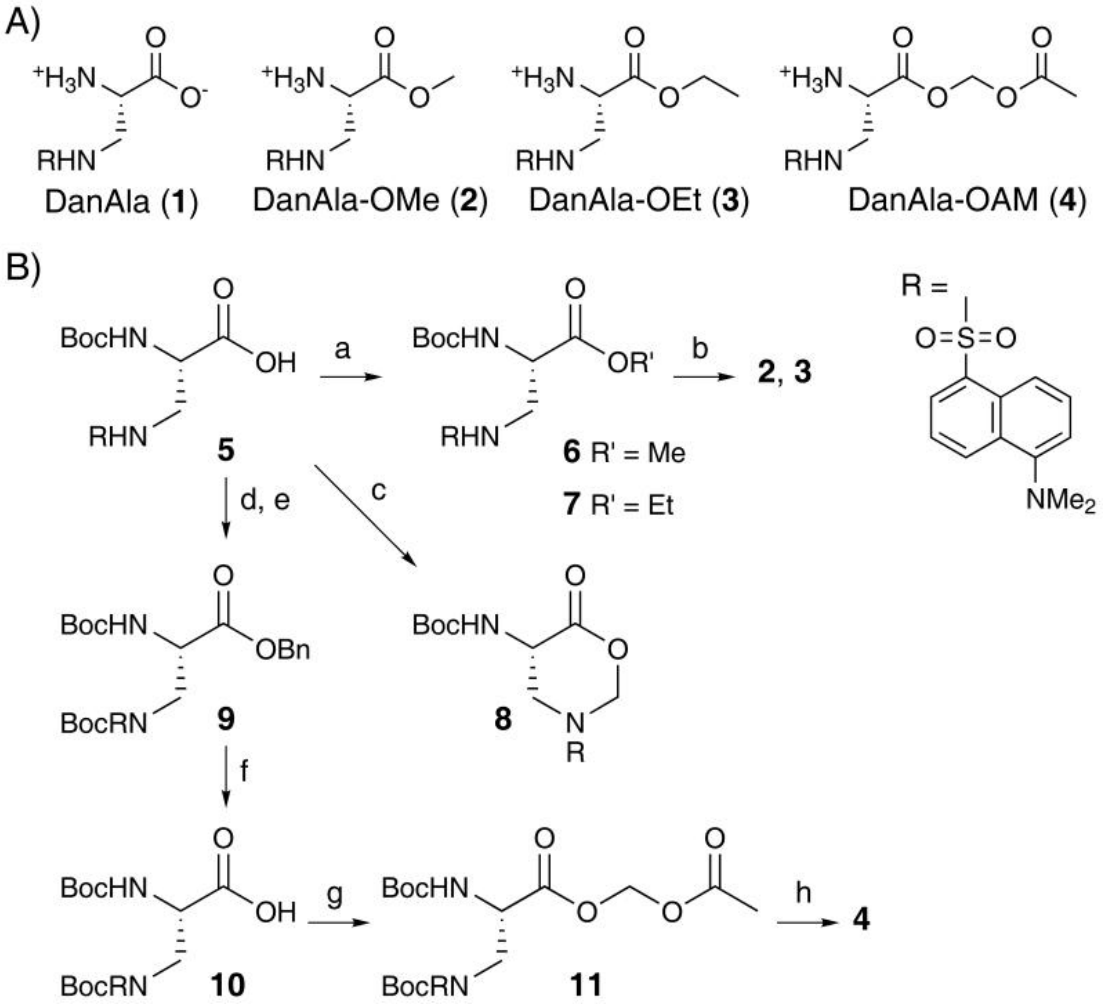

Figure 3.1: Structure and synthesis of DanAla and DanAla esters.

(A) Structures of DanAla and DanAla esters. (**B**) Synthetic approach to DanAla esters. Reagents and conditions: a) MeI, DIPEA, DMF, 12 hr, 87% for **6**; EtI, DIPEA, DMF, 12 hr, 75% for **7**; b) TFA, CH_2Cl_2, 100%; c) bromomethyl acetate, DIPEA, CH_3CN, 81%; d) BnBr, DIPEA, DMF, 0°C to RT, 76%; e) Boc_2O, DMAP, Et_3N, CH_2Cl_2, 97%; f) Pd/C, H_2, MeOH; g) bromomethyl acetate, DIPEA, CH_3CN, 84% over two steps; h) TFA, CH_2Cl_2, 100%.

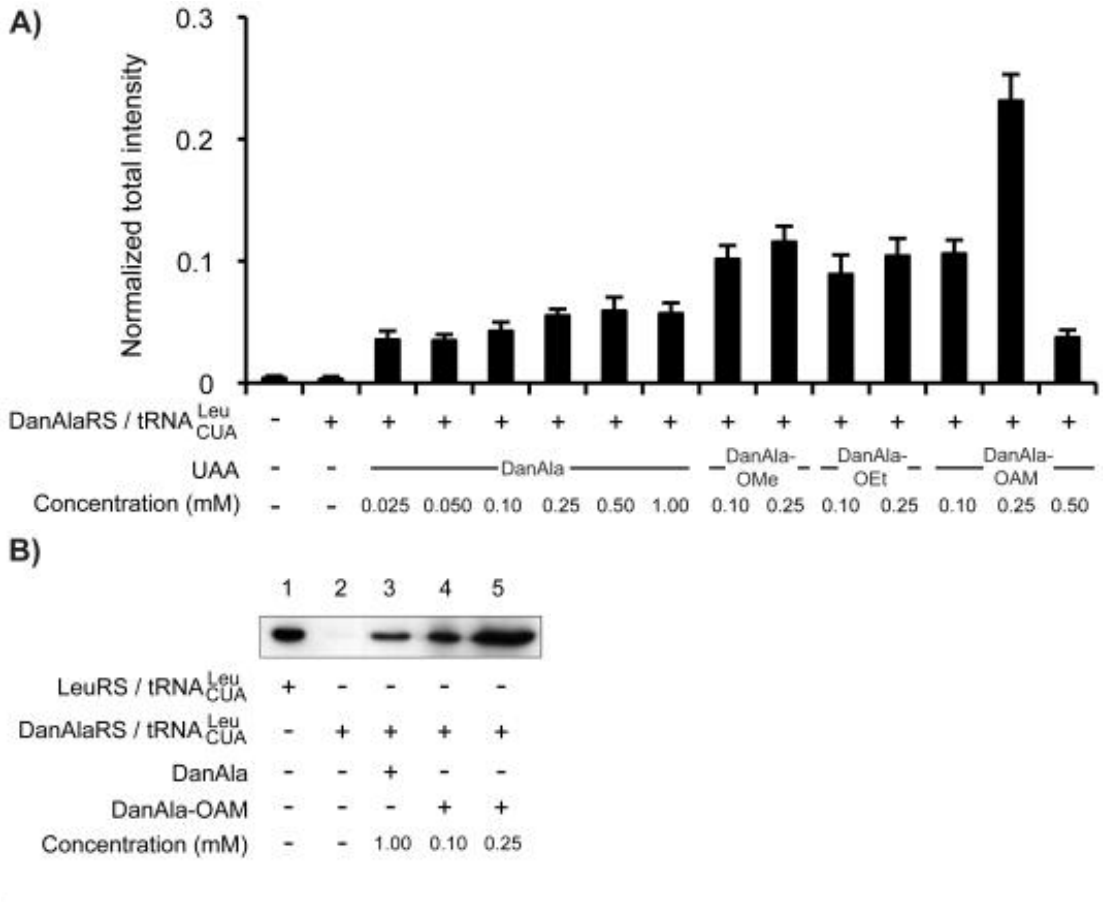

Figure 3.2: Incorporation efficiency of DanAla and DanAla esters

(**A**) Flow cytometric analysis of the incorporation efficiency of DanAla into GFP with different compounds added in the growth media. Reporter cells transfected with the orthogonal suppressor tRNA and the wild-type LeuRS were used as the positive control to normalize the total fluorescence intensity. Error bars represent s.e.m., n = 3. (**B**) Western blot analysis of the GFP protein with a GFP-specific antibody. The same number of cells were used in lane 2−5.

Figure 3.3: DanAla-OAM improves uptake and incorporation of DanAla into proteins.

(**A**) Cytosolic fluorescence intensity of cells incubated with 0.10 mM DanAla or DanAla-OAM. Error bars represent s.d. (**B**) HPLC analysis of cell extracts from cells incubated with 0.10 mM DanAla or DanAla-OAM. Arrows indicate the peak positions for DanAla and DanAla-OAM determined using pure compounds. (**C**) PI staining analysis of cell health at indicated conditions. Error bars represent s.e.m., n = 3.

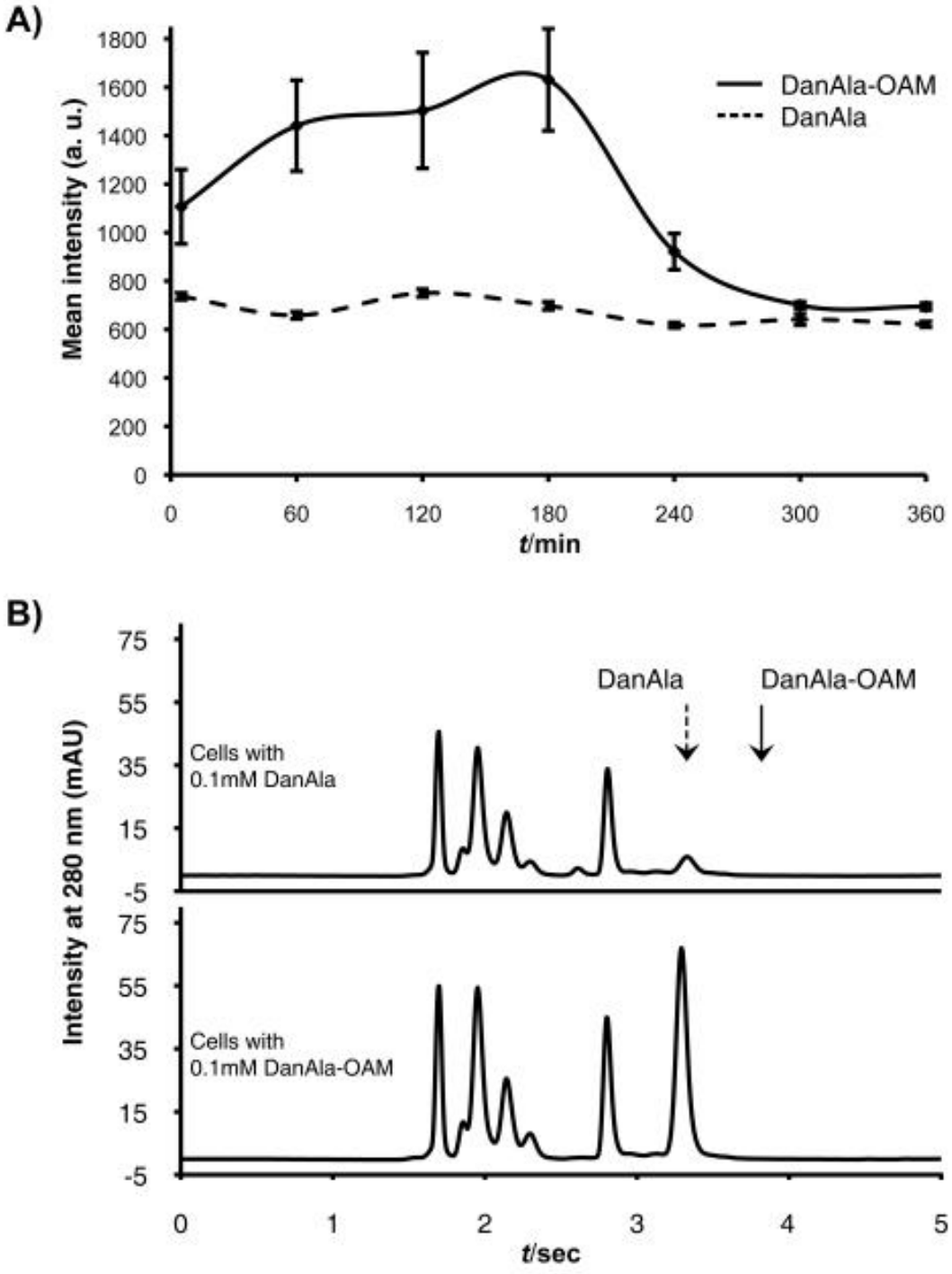
A)
Mean intensity (a. u.)
1800
1600
1400
1200
1000
800
600
400
200
0
0
60
120
180
240
300
360
t/min
DanAla-OAM
DanAla
B)
Intensity at 280 nm (mAU)
75
55
35
15
-5
DanAla
DanAla-OAM
Cells with
0.1mM DanAla
Cells with
0.1mM DanAla-OAM
0
1
2
3
4
5
t/sec

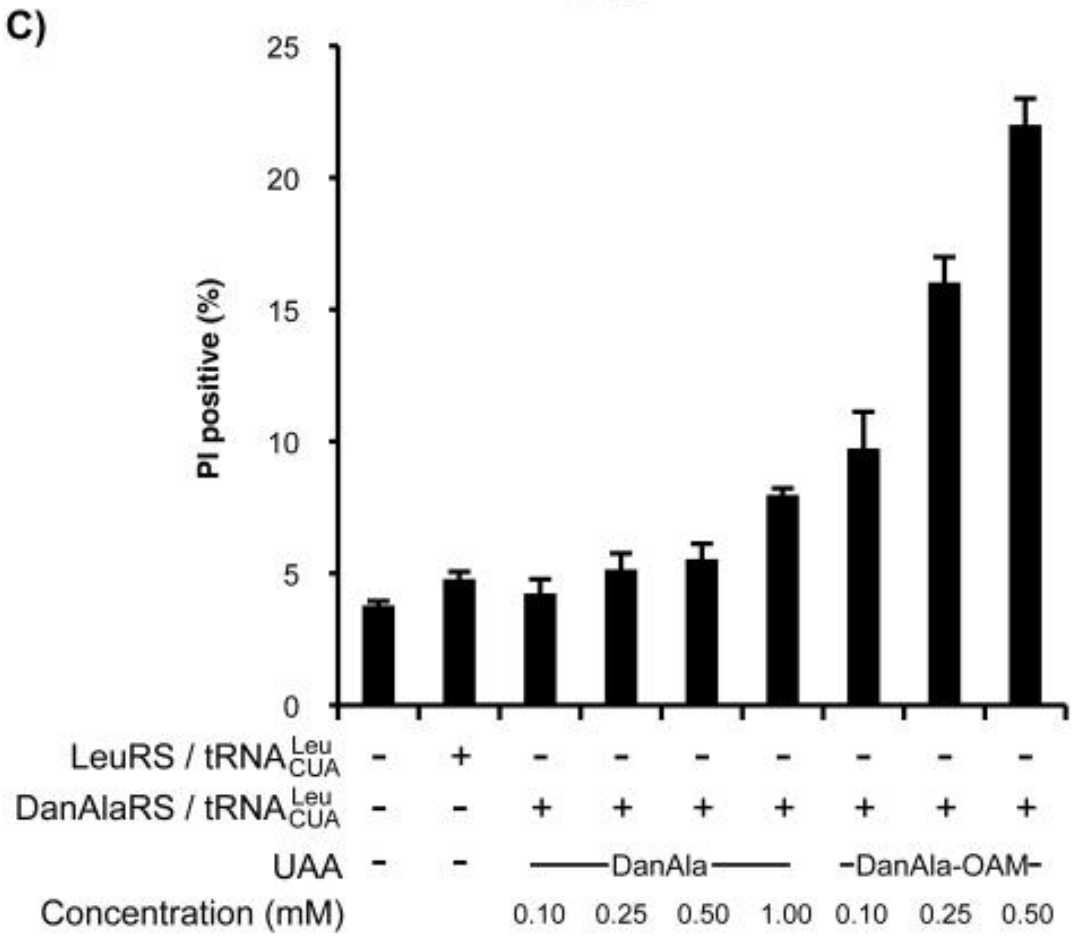

Figure 3.3: DanAla-OAM improves uptake and incorporation of DanAla into proteins, Continued.

Chapter 4

DISCUSSION

4.1 Insight into PIRK activation mechanism

The mechanism of PIRK activation can be deduced from the structural information of other inwardly rectifying potassium channels. In the tetrameric structure of chicken Kir2.2, corresponding pore-lining residues from each monomer surround a circular plane of space. Cmn incorporation capacity of each residue can be inferred from the size of each pore plane (Figure 4.1, 4.2). T142, I143, and I176 are creating pore planes too small to fit four Cmn molecules, where 4,5-dimethoxy-2-nitrobenzyl side chain is ~9Å long. C149 is located in the extracellular entryway where there is open space to adjust incorporated Cmn (Figure 4.2). This explains why Cmn incorporated at this residue did not interfere with normal function of the channel. Similarly, A184 is on the less structured loop region near the inner surface of the membrane (Figure 4.2). Incorporated Cmn would have not tightly block the pore. D172 and E224 have been uncovered to be involved in inward rectification and gating of the channel, thus their mutation could have been detrimental to regular channel function (Hibino, 2010). On the other hand, C169 outlined a pore plane big enough to suit Cmn residues and they would successfully block the current flow in the inner cavity. Neighboring Gly168 would help ease 4,5-dimethoxy-2-nitrobenzyl arm movement inside the cavity. Upon irradiation, this barricade would simply be removed and natural K^+ flow be resumed through the channel. Kir2.1 has two transmembrane regions, the simplest structure among potassium channels. Thus, architectural information of PIRK excitation will be beneficial in expanding the methodology to sister channels and receptors.

4.2 PIRK in the studies of diseases

Silencing neurons in a time- and space-specific manner is valuable for several reasons. The significance of neuronal communication in a specific stage of developing or adult system can be revealed by selectively silencing pathways or populations of neurons (White, 2001). In the treatment of intractable epilepsy, targeted lesion is still the only possible method. Suppressing target neuronal activity without affecting neighboring neurons would be crucial in the study and the treatment of the disease. On the similar note, it could be possible to induce genetic analgesia for the treatment of intractable pain, or muscle spasms in patients with cerebral palsy and spinal cord injuries (Al-Khodairy, 1998; Flett, 1999; Liu, 1997). Moreover, it may be applicable in controlling neurological damage after ischemic injury or neurodegenerative diseases (Rodriguez, 1998). Among the technology in suppressing neuronal excitability, PIRK is especially effective since it can be used as a binary switch, i.e., a single light pulse can induce the lasting significant effect on target neurons.

PIRK methodology also has a huge potential in the study of ion channels and membrane receptors. Kir2.1 interacts with PDZ-domain proteins or protein kinases such as PKA and PKC (Hibino, 2010). The functional consequence of these interactions can be studied using PIRK methodology. Kir2.1 is also associated with diseases such as Andersen syndrome or short Q-T syndrome

(Ma, 2011; Priori, 2005). PIRK can be utilized to study the disease mechanism. Recently, studies showed that Kir2.1 is required for osteoblastogenesis (Zaddam, 2012). PIRK can be introduced to reveal the detailed mechanism of this regulation.

4.3 Application of PIRK technology into other proteins

The beauty of the current study is that PIRK strategy can be easily applied to other types of channel proteins to modulate their specific functions, suggesting a new tool to study other channel proteins or receptor proteins in synapse. For example, G protein-gated Kir channels (Kir3 family), AMPARs, and NMDARs share similar pore topology with Kir2.1. 5-HT_3R or $GABA_A$Rs have different transmembrane structure than Kir2.1 and would require experiments to screen pore-lining residues. Interestingly, ligand-binding sites of these channels/receptors are well studied, and blocking ligand-binding pocket would be another good strategy to modulate functionality of these channels/receptors. Especially, ligand-gated ion channels (LGIC) hold huge potential for engineering. By incorporating Cmn into the pore region or the ligand-binding region in these proteins, one can generate light-responsive ion channels and receptors. Expression of the light responsible LGIC in a certain region in brain and subsequent light activation of the LGIC in a single or multiple neurons would facilitate the understanding of a specific LGIC mechanism in neuronal circuitry. It would shed light on the research of synaptic physiology to study neuronal

connectivity and can eventually be applied to reveal the mechanisms of many brain diseases.

4.4 Summary

The current study demonstrated a new methodology for controlling neuronal excitability using light inducible Kir2.1. Structural information of other inwardly rectifying potassium channels allowed us to determine eight candidate residues placed in the pore lumen of the channel. These eight residues had different permissiveness to UAG suppression and Uaa incorporation, and only C169 was chosen appropriate for Cmn incorporation. Mutant channel Kir2.1_C169$_{TAG}$Cmn was activated only after a brief UV pulse. Engineered PIRK was successfully expressed in rat hippocampal primary neurons. Action potential firing in these neurons was completely aborted or dramatically decreased after UV irradiation and the effect lasted until Ba^{2+} was added to block PIRK channels again. PIRK was also expressed in mouse neocortical neurons showing its successful *in vivo* application.

In the light of Uaa research, the current study presented a huge achievement. It demonstrated that Uaas could be incorporated into each monomer to make a fully functional tetramer. It also showed that Uaa-incorporated ion channels could have a functional consequence in neuronal

system. Most importantly, this study proved that Uaa system could be successfully introduced to rodent brains *in vivo* for the first time. The completion of this study demonstrated an ample potential of Uaa system in neuroscience and protein engineering.

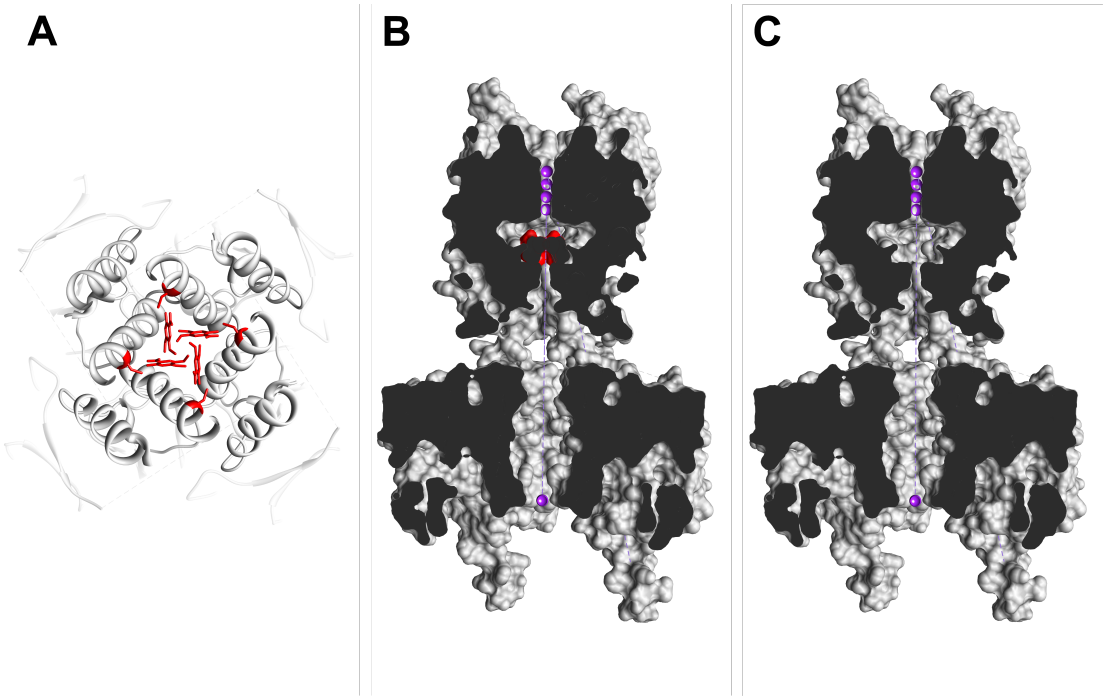

Figure 4.1: Structure model of PIRK mechanism.

(**A**) A model view of the tetrameric structure of the PIRK channel from the extracellular side. Cmn is colored red. Model is generated based on the chicken Kir2.2 structure. (**B & C**) Side views of the PIRK structure showing the pore lumen before (**B**) or after (**C**) photo-activation. Purple spheres represent K^+ ions in the selectivity filter and the cytoplasmic cavity. Red spheres represent Cmn side chains in the inner cavity. Molecular drawings were prepared using UCSF Chimera 1.6.2.

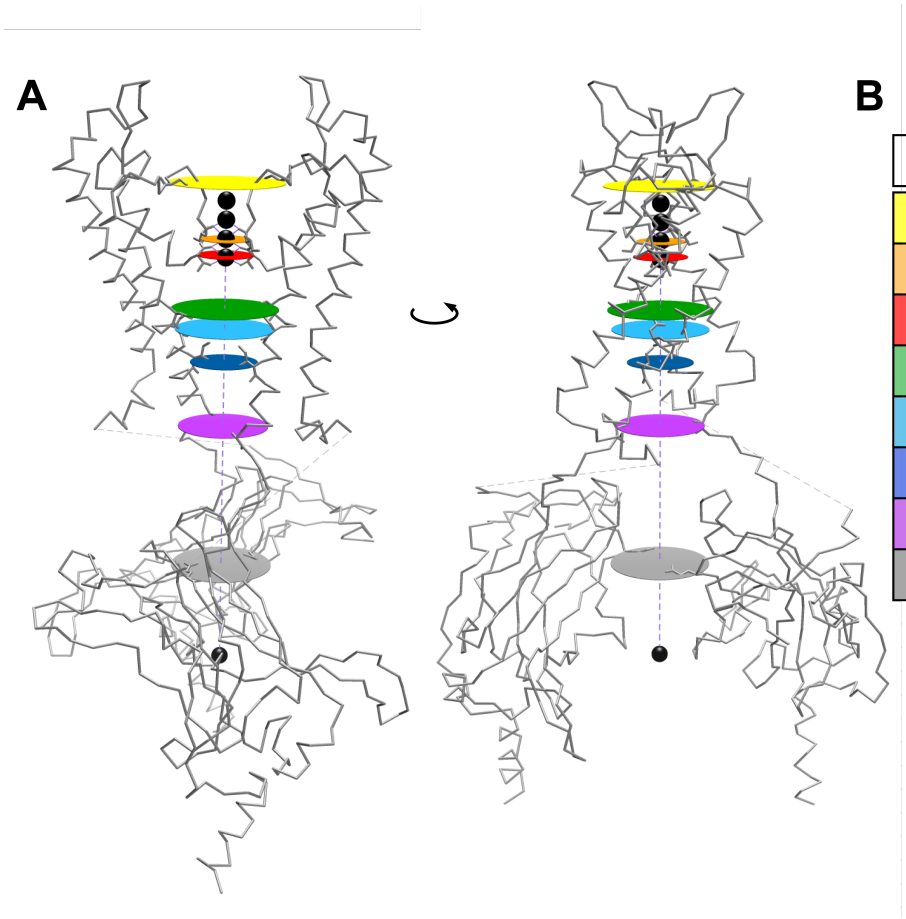

residue	radius (Å)
C149	8.943
I143	3.867
T142	4.306
C169	8.396
D172	7.769
I176	5.321
A184	7.178
E224	8.133

Figure 4.2: Measurement of the pore plane at each candidate site helps predict Cmn incorporation feasibility at the site.

(**A**) Side views of the crystal structure of chicken Kir2.2 channel (PDB ID: 3JYC) showing pore planes at candidate sites for incorporating Cmn. A pore plane was created by connecting four alpha carbons in each candidate site of Kir2.2 tetrameric structure. Two of four subunits are shown for clarity. Rotated views are shown to reveal all pore planes. Eight pore planes of corresponding candidate sites are highlighted: T142 (red), I143 (orange), C149 (yellow), C169 (green), D172 (light blue), I176 (navy), A184 (purple), and E224 (grey). Black spheres represent K^+ ions in the selectivity filter and the cytoplasmic cavity. Molecular drawings were prepared using UCSF Chimera 1.6.2. (**B**) Table showing the radius of each pore plane and its corresponding candidate site.

REFERENCES

Adamantidis, A. R., Zhang, F., Aravanis, A. M., Deisseroth, K., and de Lecea, L. (2007). Neural substrates of awakening probed with optogenetic control of hypocretin neurons. Nature *450*, 420-424.

Adams, S. R., and Tsien, R. Y. (1993). Controlling cell chemistry with caged compounds. Annu. Rev. Physiol. *55*, 755-784.

Al-Khodairy, A. T., Gobelet, C., and Rossier, A. B. (1998). Has botulinum toxin type A a place in the treatment of spasticity in spinal cord injury patients? Spinal cord *36*, 854-858.

Aravanis, A. M., Wang, L. P., Zhang, F., Meltzer, L. A., Mogri, M. Z., Schneider, M. B. & Deisseroth, K. (2007). An optical neural interface: in vivo control of rodent motor cortex with integrated fiberoptic and optogenetic technology. J. Neural. Eng. *4*, 143-156.

Banghart, M., Borges, K., Isacoff, E., Trauner, D., and Kramer, R. H. (2004). Light-activated ion channels for remote control of neuronal firing. Nat. Neurosci. *7*, 1381-1386.

Bayley, H. and Cremer, P. S. (2001). Stochastic sensors inspired by biology. Nature. *413*, 226-230.

Beene, D. L., Dougherty, D. A., and Lester, H. A. (2003). Unnatural amino acid mutagenesis in mapping ion channel function. Curr. Opin. Neurobiol. *13*, 264-270.

Bernstein, J. G., and Boyden, E. S. (2011). Optogenetic tools for analyzing the neural circuits of behavior. Trends Cogn. Sci. *15*, 592-600.

Bichet, D., Haass, F. A., and Jan, L. Y. (2003). Merging functional studies with structures of inward-rectifier K(+) channels. Nat. Rev. Neurosci. *4*, 957-967.

Boyden, E. S., Zhang, F., Bamberg, E., Nagel, G., and Deisseroth, K. (2005). Millisecond-timescale, genetically targeted optical control of neural activity. Nat. Neurosci. *8*, 1263-1268.

Burrone, J., O'Byrne, M., and Murthy, V. N. (2002). Multiple forms of synaptic plasticity triggered by selective suppression of activity in individual neurons. Nature *420*, 414-418.

Callaway, E. M. and Katz, L. C. (1993). Photostimulation using caged glutamate reveals functional circuitry in living brain slices. Proc. Natl. Acad. Sci. USA *90*, 7661-7665.

Callaway, E. M. (2005). A molecular and genetic arsenal for systems neuroscience. Trends Neurosci. *28*, 196-201.

Cambridge, S. B., Geissler, D., Calegari, F., Anastassiadis, K., Hasan, M. T., Stewart, A. F., Huttner, W. B., Hagen, V., and Bonhoeffer, T. (2009). Doxycycline-dependent photoactivated gene expression in eukaryotic systems. Nat. Methods 6, 527-531.

Cellitti, S., E., Jones, D. H., Lagpacan, L., Hao, X., Zhang, Q., Hu, H., Brittain, S. M., Brinker, A., Caldwell, J., Bursulaya, B., Spraggon, G., Brock, A., Ryu, Y., Uno, T., Schultz, P. G., and Geierstanger, B. H. (2008). In vivo incorporation of unnatural amino acids to probe structure, dynamics, and ligand binding in a large protein by nuclear magnetic resonance spectroscopy. J. Am. Chem. Soc. *130*, 9268-9281.

Chow, B. Y., Han, X., Dobry, A. S., Qian, X., Chuong, A. S., Li, M., Henninger, M. A., Belfort, G. M., Lin, Y., Monahan, P. E., and Boyden, E. S. (2010). High-performance genetically targetable optical neural silencing by light-driven proton pumps. Nature *463*, 98-102.

Coin, I., Perrin, M. H., Vale, W. W., and Wang, L. (2011). Photo-cross-linkers incorporated into G-protein-coupled receptors in mammalian cells: a ligand comparison. Angew. Chem. Int. Ed. Engl. *50*, 8077-8081.

Dart, C., Leyland, M. L., Spencer, P. J., Stanfield, P. R., and Sutcliffe, M. J. (1998). The selectivity filter of a potassium channel, murine kir2.1, investigated using scanning cysteine mutagenesis. J. Physiol. *511*, 25-32.

Deiters, A., Cropp, T. A., Summerer, D., Mukherji, M., and Schultz, P. G. (2004). Site-specific PEGylation of proteins containing unnatural amino acids. Bioorg. Med. Chem. Lett. *14*, 5743-5745.

Dougherty, D. A. (2000). Unnatural amino acids as probes of protein structure and function. Curr. Opin. Chem. Biol. *4*, 645-652.

Doyle, D. A., Morais Cabral, J., Pfuetzner, R. A., Kuo, A., Gulbis, J. M., Cohen, S. L., Chait, B. T., and MacKinnon, R. (1998). The structure of the potassium channel: molecular basis of K+ conduction and selectivity. Science *280*, 69-77.

Ehrengruber, M. U., Doupnik, C. A., Xu, Y., Garvey, J., Jasek, M. C., Lester, H. A., and Davidson, N. (1997). Activation of heteromeric G protein-gated inward rectifier K+ channels overexpressed by adenovirus gene transfer inhibits the excitability of hippocampal neurons. Proc. Natl. Acad. Sci. USA *94*, 7070-7075.

England, P. M., Lester, H. A., Davidson, N., and Dougherty, D. A. (1997). Site-specific, photochemical proteolysis applied to ion channels in vivo. Proc. Natl. Acad. Sci. USA *94*, 11025-11030.

England, P. M., Lester, H. A., and Dougherty, D. A. (1999). Mapping disulfide connectivity using backbone ester hydrolysis. Biochemistry *38*, 14409-14415.

Essen, L.-O. and Koert, U. (2008). Ion-channel engineering. Annual Reports Section "C" (Physical Chemistry) *104*, 165.

Falk, T., Kilani, R. K., Yool, A. J., and Sherman, S. J. (2001). Viral vector-mediated expression of K+ channels regulates electrical excitability in skeletal muscle. Gene. Ther. *8*, 1372-1379.

Fehrentz, T., Schonberger, M., and Trauner, D. (2011). Optochemical genetics. Angew. Chem. Int. Ed. Engl. *50*, 12156-12182.

Fenno, L., Yizhar, O., and Deisseroth, K. (2011). The development and application of optogenetics. Annu. Rev. Neurosci. *34*, 389-412.

Flett, P. J., Stern, L. M., Waddy, H., Connell, T. M., Seeger, J. D., and Gibson, S. K. (1999). Botulinum toxin A versus fixed cast stretching for dynamic calf tightness in cerebral palsy. J. Paediatr. Child Health *35*, 71-77.

Fork, R. L. (1971). Laser stimulation of nerve cells in Aplysia. Science *171*, 907-908.

Garneau, L., Klein, H., Parent, L., and Sauvé, R. (2003). Contribution of cytosolic cysteine residues to the gating properties of the Kir2.1 inward rectifier. Biophys. J. *84*, 3717-3729.

Gradinaru, V., Zhang, F., Ramakrishnan, C., Mattis, J., Prakash, R., Diester, I., Goshen, I., Thompson, K. R., and Deisseroth, K. (2010). Molecular and cellular approaches for diversifying and extending optogenetics. Cell *141*, 154-165.

Grosse, W., Essen, L. O., and Koert, U. (2011). Strategies and perspectives in ion-channel engineering. Chembiochem. *12*, 830-839.

Grunbeck, A., Huber, T., Sachdev, P., and Sakmar, T.P. (2011). Mapping the ligand-binding site on a G protein-coupled receptor (GPCR) using genetically encoded photocrosslinkers. Biochemistry *50*, 3411-3413.

Grunewald, J., Tsao, M. L., Perera, R., Dong, L., Niessen, F., Wen, B. G., Kubitz, D. M., Smider, V. V., Ruf, W., Nasoff, M., Lerner, R. A., and Schultz, P. G. (2008).

Immunochemical termination of self-tolerance. Proc. Natl. Acad. Sci. USA *105*, 11276-11280.

Guo, J., Wang, J., Anderson, J. C., and Schultz, P. G. (2008). Addition of an alpha-hydroxy acid to the genetic code of bacteria. Angew. Chem. Int. Ed. Engl. *47*,722-725.

Han, X. (2012). In vivo application of optogenetics for neural circuit analysis. ACS Chem. Neurosci. *3*, 577-584.

Halverson, K. M., Panchal, R. G., Nguyen, T. L., Gussio, R., Little, S. F., Misakian, M., Bavari, S., and Kasianowicz, J. J. (2005). Anthrax biosensor, protective antigen ion channel asymmetric blockade. J. Biol. Chem. *280*, 34056-34062.

Hibino, H., Inanobe, A., Furutani, K., Murakami, S., Findlay, I., and Kurachi, Y. (2010). Inwardly rectifying potassium channels: their structure, function, and physiological roles. Physiol. Rev. *90*, 291-366.

Hino, N., Okazaki, Y., Kobayashi, T., Hayashi, A., Sakamoto, K., and Yokoyama, S. (2005). Protein photo-cross-linking in mammalian cells by site-specific incorporation of a photoreactive amino acid. Nat. Methods *2*, 201-206.

Ibanez-Tallon, I., Wen, H., Miwa, J. M., Xing, J., Tekinay, A. B., Ono, F., Brehm, P., and Heintz, N. (2004). Tethering naturally occurring peptide toxins for cell-autonomous modulation of ion channels and receptors in vivo. Neuron *43*, 305-311.

Ishii, K., Yamagishi, T., and Taira, N. (1994). Cloning and functional expression of a cardiac inward rectifier K+ channel. FEBS Lett. *338*, 107-111.

Janovjak, H., Szobota, S., Wyart, C., Trauner, D., and Isacoff, E. Y. (2010). A light-gated, potassium-selective glutamate receptor for the optical inhibition of neuronal firing. Nat. Neurosci. *13*, 1027-1032.

Johns, D. C., Marx, R., Mains, R. E., O'Rourke, B., and Marban, E. (1999). Inducible genetic suppression of neuronal excitability. J. Neurosci. *19*, 1691-1697.

Karpova, A. Y., Tervo, D. G., Gray, N. W., and Svoboda, K. (2005). Rapid and reversible chemical inactivation of synaptic transmission in genetically targeted neurons. Neuron *48*, 727-735.

Kang, X. F., Cheley, S., Guan, X., and Bayley, H. (2006). Stochastic detection of enantiomers. J. Am. Chem. Soc. *128*, 10684-10685.

Katz, B. (1949). Les constantes electriques de la membrane du muscle. Arch. Sci. Physiol. *3*, 285-299.

Kew, J. N. C. and Davies, C. H. (2010). Ion channels : from structure to function, 2nd edn (Oxford ; New York: Oxford University Press).

Kokaia, M., Andersson, M., and Ledri, M. (2013). An optogenetic approach in epilepsy. Neuropharmacology *69*, 89-95.

Koçer, A., Walko, M., Bulten, E., Halza, E., Feringa, B. L., and Meijberg, W. (2006). Rationally designed chemical modulators convert a bacterial channel protein into a pH-sensory valve. Angew. Chem. Int. Ed. Engl. *45*, 3126-3130.

Kubo, Y., Baldwin, T. J., Jan, Y. N., and Jan, L. Y. (1993). Primary structure and functional expression of a mouse inward rectifier potassium channel. Nature *362*, 127-133.

Kubo, Y., Yoshimichi, M., and Heinemann, S. H. (1998). Probing pore topology and conformational changes of Kir2.1 potassium channels by cysteine scanning mutagenesis. FEBS Lett*. 435*, 69-73.

Kuo, A., Gulbis, J. M., Antcliff, J. F., Rahman, T., Lowe, E. D., Zimmer, J., Cuthbertson, J., Ashcroft, F. M., Ezaki, T. & Doyle, D. A. (2003). Crystal structure of the potassium channel KirBac1.1 in the closed state. Science *300*, 1922-1926.

Kurata, H. T., Cheng, W. W., Arrabit, C., Slesinger, P. A., and Nichols, C. G. (2007). The role of the cytoplasmic pore in inward rectification of Kir2.1 channels. J. Gen. Physiol. *130*, 145-155.

Lacey, V. K., Parrish, A. R., Han, S., Shen, Z., Briggs, S. P., Ma, Y., and Wang, L. (2011). A fluorescent reporter of the phosphorylation status of the substrate protein STAT3. Angew. Chem. Int. Ed. Engl. *50*, 8692-8696.

Lechner, H. A., Lein, E. S., and Callaway, E. M. (2002). A genetic method for selective and quickly reversible silencing of Mammalian neurons. J. Neurosci. *22*, 5287-5290.

Lee, H. S., Spraggon, G., Schultz, P. G., and Wang, F. (2009). Genetic incorporation of a metal-ion chelating amino acid into proteins as a biophysical probe. J. Am. Chem. Soc*. 131*, 2481-2483.

Lemke, E. A., Summerer, D., Geierstanger, B. H., Brittain, S. M., and Schultz, P. G. (2007). Control of protein phosphorylation with a genetically encoded photocaged amino acid. Nat. Chem. Biol. *3*, 769-772.

Li, L., Zhong, W., Zacharias, N., Gibbs, C., Lester, H. A., and Dougherty, D. A. (2001). The tethered agonist approach to mapping ion channel proteins--toward a structural model for the agonist binding site of the nicotinic acetylcholine receptor. Chem. Biol. *8*, 47-58.

Liao, S. Y., Tse, H. F., Chan, Y. C., Mei-Chu Yip, P., Zhang, Y., Liu, Y., and Li, R. A. (2012). Overexpression of Kir2.1 channel in embryonic stem cell-derived cardiomyocytes attenuates posttransplantation proarrhythmic risk in myocardial infarction. Heart Rhythm. *10*, 273-282.

Liu, C. C., and Schultz, P. G. (2010). Adding new chemistries to the genetic code. Annu. Rev. Biochem. *79*, 413-444.

Liu, W., Brock, A., Chen, S., Chen, S., and Schultz, P. G. (2007). Genetic incorporation of unnatural amino acids into proteins in mammalian cells. Nat. Methods. *4*, 239-244.

Liu, Y., Himes, B. T., Moul, J., Huang, W., Chow, S. Y., Tessler, A., and Fischer, I. (1997). Application of recombinant adenovirus for in vivo gene delivery to spinal cord. Brain Res. *768*, 19-29.

Lopatin, A. N., Makhina, E. N., and Nichols, C. G. (1994). Potassium channel block by cytoplasmic polyamines as the mechanism of intrinsic rectification. Nature *372*, 366-369.

Lozano, A. M. and Lipsman, N. (2013). Probing and regulating dysfunctional circuits using deep brain stimulation. Neuron *77*, 406-424.

Lu, H. and Klaassen, C. (2006). Tissue distribution and thyroid hormone regulation of Pept1 and Pept2 mRNA in rodents. Peptides *27*, 850-857.

Lu, T., Nguyen, B., Zhang, X., and Yang, J. (1999a). Architecture of a K+ channel inner pore revealed by stoichiometric covalent modification. Neuron *22*, 571-580.

Lu, T., Zhu, Y. G., and Yang, J. (1999b). Cytoplasmic amino and carboxyl domains form a wide intracellular vestibule in an inwardly rectifying potassium channel. Proc. Natl. Acad. Sci. USA *96*, 9926-9931.

Lummis, S. C., Beene, D. L., Lee, L. W., Lester, H. A., Broadhurst, R. W., and Dougherty, D. A. (2005). Cis-trans isomerization at a proline opens the pore of a neurotransmitter-gated ion channel. Nature *438*, 248-252.

Ma, D., Taneja, T. K., Hagen, B. M., Kim, B. Y., Ortega, B., Lederer, W. J., and Welling, P. A. (2011). Golgi export of the Kir2.1 channel is driven by a trafficking signal located within its tertiary structure. Cell *145*, 1102-1115.

Macri, V., Angoli, D., and Accili, E. A. (2012). Architecture of the HCN selectivity filter and control of cation permeation. Sci Rep. *2*, 894.

Malandro, M. S. and Kilberg, M. S. (1996). Molecular biology of mammalian amino acid transporters. Annu. Rev. Biochem. *65*, 305-336.

Matsuda, H., Saigusa, A., and Irisawa, H. (1987). Ohmic conductance through the inwardly rectifying K channel and blocking by internal $Mg2^{+}$. Nature *325*, 156-159.

Matsuzaki, M., Ellis-Davies, G. C., Nemoto, T., Miyashita, Y., Iino, M., and Kasai, H. (2001). Dendritic spine geometry is critical for AMPA receptor expression in hippocampal CA1 pyramidal neurons. Nat. Neurosci. *4*, 1086-1092.

Meijler, M. M., Arad-Yellin, R., Cabantchik, Z. I., and Shanzer, A. (2002). Synthesis and evaluation of iron chelators with masked hydrophilic moieties. J. Am. Chem. Soc. *124*, 12666-12667.

Millar, C., Roy, S., Brown, A. R., and Asenov, A. (2007). Simulating the bio-nanoelectronic interface. J. Phys.: Condens. Matter. *19*, 215205.

Miller, J. C., Silverman, S. K., England, P. M., Dougherty, D. A., and Lester, H. A. (1998). Flash decaging of tyrosine sidechains in an ion channel. Neuron *20*, 619-624.

Minor, D. L., Jr., Masseling, S. J., Jan, Y. N., and Jan, L. Y. (1999). Transmembrane structure of an inwardly rectifying potassium channel. Cell *96*, 879-891.

Mulder, J., Aguado, T., Keimpema, E., Barabas, K., Ballester Rosado, C. J., Nguyen, L., Monory, K., Marsicano, G., Di Marzo, V., Hurd, Y. L.*, et al.* (2008). Endocannabinoid signaling controls pyramidal cell specification and long-range axon patterning. Proc. Natl. Acad. Sci. USA *105*, 8760-8765.

Nadeau, H., McKinney, S., Anderson, D. J., and Lester, H. A. (2000). ROMK1 (Kir1.1) causes apoptosis and chronic silencing of hippocampal neurons. J. Neurophysiol. *84*, 1062-1075.

Nagel, G., Ollig, D., Fuhrmann, M., Kateriya, S., Musti, A. M., Bamberg, E., and Hegemann, P. (2002). Channelrhodopsin-1: a light-gated proton channel in green algae. Science *296*, 2395-2398.

Neustadt, B. R. (1994). Facile preparation of N-(sulfonyl)carbamates. Tetrahedron Lett. *35*, 379-380.

Nichols, C. G., and Lopatin, A. N. (1997). Inward rectifier potassium channels. Annu. Rev. Physiol. *59*, 171-191.

Noren, es. . J., Anthony-Cahill, S. J., Griffith, M. C., and Schultz, P. G. (1989). A general method for site-specific incorporation of unnatural amino acids into proteins. Science *244*, 182-188.

Okazaki, A., Sudo, Y., and Takagi, S. (2012). Optical silencing of C. elegans cells with arch proton pump. PLoS One *7*, e35370.

Pantoja, R., Rodriguez, E. A., Dibas, M. I., Dougherty, D. A., and Lester, H. A. (2009). Single-molecule imaging of a fluorescent unnatural amino acid incorporated into nicotinic receptors. Biophys. J. *96*, 226-237.

Parrish, A. R., She, X., Xiang, Z., Coin, I., Shen, Z., Briggs, S. P., Dillin, A., and Wang, L. (2012). Expanding the Genetic Code of Caenorhabditis elegans Using Bacterial Aminoacyl-tRNA Synthetase/tRNA Pairs. ACS Chem. Biol. *7*, 1292-1302.

Pedersen, H., Holder, S., Sutherlin, D. P., Schwitter, U., King, D. S., and Schultz, P. G. (1998). A method for directed evolution and functional cloning of enzymes. Proc. Natl. Acad. Sci. USA *95*, 10523-10528.

Pegan, S., Arrabit, C., Zhou, W., Kwiatkowski, W., Collins, A., Slesinger, P. A. & Choe, S. (2008). Cytoplasmic domain structures of Kir2.1 and Kir3.1 show sites for modulating gating and rectification. Nat. Neurosci. *8*, 279-287.

Philipson, K. D., Gallivan, J. P., Brandt, G. S., Dougherty, D. A., and Lester, H. A. (2001). Incorporation of caged cysteine and caged tyrosine into a transmembrane segment of the nicotinic ACh receptor. Am. J. Physiol. Cell. Physiol. *281*, C195-206.

Plaster, N. M., Tawil, R., Tristani-Firouzi, M., Canun, S., Bendahhou, S., Tsunoda, A., Donaldson, M. R., Iannaccone, S. T., Brunt, E., Barohn, R., Clark, J., Deymeer, F., George, A. L. Jr, Fish, F. A., Hahn, A., Nitu, A., Ozdemir, C., Serdaroglu, P., Subramony, S. H., Wolfe, G., Fu, Y. H., Ptácek, L. J. (2001). Mutations in Kir2.1 cause the developmental and episodic electrical phenotypes of Andersen's syndrome. Cell *105*, 511-519.

Priori, S.G., Pandit, S.V., Rivolta, I., Berenfeld, O., Ronchetti, E., Dhamoon, A., Napolitano, C., Anumonwo, J., di Barletta, M.R., Gudapakkam, S., Bosi, G., Stramba-Badiale, M., and Jalife, J. (2005). A novel form of short QT syndrome (SQT3) is caused by a mutation in the KCNJ2 gene. Circ. Res. *96*, 800-807.

Raimondo, J. V., Kay, L., Ellender, T. J., and Akerman, C. J. (2012). Optogenetic silencing strategies differ in their effects on inhibitory synaptic transmission. Nat. Neurosci. *15*, 1102-1104.

Rautio, J., Kumpulainen, H., Heimbach, T., Oliyai, R., Oh, D., Järvinen, T., and Savolainen, J. (2008). Prodrugs: design and clinical applications. Nat. Rev. Drug Discovery *7*, 255-270.

Remple, M. S., Bradenham, C. H., Kao, C. C., Charles, P. D., Neimat, J. S., and Konrad, P. E. (2011). Subthalamic nucleus neuronal firing rate increases with Parkinson's disease progression. Mov Disord. *26*, 1657-1662.

Rhee, H., Lee, J. S., Lee, J., Joo, C., Han, H., and Cho, M. (2008). Photolytic control and infrared probing of amide I mode in the dipeptide backbone-caged with the 4,5-dimethoxy-2-nitrobenzyl group. J. Phys. Chem. B *112*, 2128-2135.

Riggsbee, C. W., and Deiters, A. (2010). Recent advances in the photochemical control of protein function. Trends Biotechnol. *28*, 468-475.

Rodriguez, M. C., Obeso, J. A., and Olanow, C. W. (1998). Subthalamic nucleus-mediated excitotoxicity in Parkinson's disease: a target for neuroprotection. Ann. Neurol. *44*, S175-188.

Sakai, N., Mareda, J., Matile, S. (2005). Rigid-Rod Molecules in Biomembrane Models: From Hydrogen-Bonded Chains to Synthetic Multifunctional Pores. Acc. Chem. Res. *38*, 79-87.

Sakamoto, K., Hayashi, A., Sakamoto, A., Kiga, D., Nakayama, H., Soma, A., Kobayashi, T., Kitabatake, M., Takio, K., Saito, K., Shirouzu, M., Hirao, I., and Yokoyama, S. (2002). Site-specific incorporation of an unnatural amino acid into proteins in mammalian cells. Nucleic Acids Res. *30*, 4692-4699.

Saito, T. (2006). In vivo electroporation in the embryonic mouse central nervous system. Nat. Protoc. *1*, 1552-1558.

Sandoz, G., Levitz, J., Kramer, R. H., and Isacoff, E. Y. (2012). Optica control of endogenous proteins with a photoswitchable conditional subunit reveals a role for TREK1 in GABA(B) signaling. Neuron *74*, 1005-1014.

Schlieker, C., Weibezahn, J., Patzelt, H., Tessarz, P., Strub, C., Zeth, K., Erbse, A., Schneider-Mergener, J., Chin, J. W., Schultz, P. G., Bukau, B., and Mogk, A. (2004). Substrate recognition by the AAA+ chaperone ClpB. Nat. Struct. Mol. Biol. *11*, 607-615.

Schultz, C., Vajanaphanich, M., Harootunian, A. T., Sammak, P. J., Barrett, K. E., and Tsien, R. Y. (1993). Acetoxymethyl esters of phosphates, enhancement of the permeability and potency of cAMP. J. Biol. Chem. *268*, 6316-6322.

Schultz, K. C., Supekova, L., Ryu, Y., Xie, J., Perera, R., and Schultz, P. G. (2006). A genetically encoded infrared probe. J. Am. Chem. Soc. *128*, 13984-13985

Sekar, R. B., Kizana, E., Smith, R. R., Barth, A. S., Zhang, Y., Marban, E., and Tung, L. (2007). Lentiviral vector-mediated expression of GFP or Kir2.1 alters the electrophysiology of neonatal rat ventricular myocytes without inducing cytotoxicity. Am. J. Physiol. Heart Circ. Physiol. *293*, H2757-2770.

Seyedsayamdost, M. R., Xie, J., Chan, C. T., Schultz, P. G., and Stubbe, J. (2007). Site-specific insertion of 3-aminotyrosine into subunit α2 of *E. coli* ribonucleotide reductase: direct evidence for involvement of Y730 and Y731 in radical propagation. J. Am. Chem. Soc. *129*,15060-15071.

Shen, B., Xiang, Z., Miller, B., Louie, G., Wang, W., Noel, J.P., Gage, F. H., and Wang, L. (2011). Genetically encoding unnatural amino acids in neural stem cells and optically reporting voltage-sensitive domain changes in differentiated neurons. Stem Cells *29*, 1231-1240.

Slimko, E. M., McKinney, S., Anderson, D. J., Davidson, N., and Lester, H. A. (2002). Selective electrical silencing of mammalian neurons in vitro by the use of invertebrate ligand-gated chloride channels. J. Neurosci. *22*, 7373-7379.

Sobolevsky, A. I., Yelshansky, M. V., and Wollmuth, L. P. (2003). Different gating mechanisms in glutamate receptor and K+ channels. J. Neurosci. *23*, 7559-7568.

Sobolevsky, A. I., Rosconi, M. P., and Gouaux, E. (2009). X-ray structure, symmetry and mechanism of an AMPA subtype glutamate receptor. Nature *462*, 745-756.

Summerer, D., Chen. S., Wu. N., Deiters. A., Chin, J. W., and Schultz, P. G. (2006). A genetically encoded fluorescent amino acid. Proc. Natl. Acad. Sci. USA *103*, 9785-9789.

Szobota, S., and Isacoff, E. Y. (2010). Optical control of neuronal activity. Annu. Rev. Biophys. *39*, 329-348.

Tabata, H., and Nakajima, K. (2001). Efficient in utero gene transfer system to the developing mouse brain using electroporation: visualization of neuronal migration in the developing cortex. Neuroscience *103*, 865-872.

Takimoto, J. K., Adams, K. L., Xiang, Z., and Wang, L. (2009). Improving orthogonal tRNA-synthetase recognition for efficient unnatural amino acid incorporation and application in mammalian cells. Mol. BioSyst. *5*, 931-934.

Tan, E. M., Yamaguchi, Y., Horwitz, G. D., Gosgnach, S., Lein, E. S., Goulding, M., Albright, T. D., and Callaway, E. M. (2006). Selective and quickly reversible inactivation of mammalian neurons in vivo using the Drosophila allatostatin receptor. Neuron *51*, 157-170.

Tao, X., Avalos, J. L., Chen, J., and MacKinnon, R. (2009). Crystal structure of the eukaryotic strong inward-rectifier K+ channel Kir2.2 at 3.1 A resolution. Science *326*, 1668-1674.

Tao, X., Lee, A., Limapichat, W., Dougherty, D. A., and MacKinnon, R. (2010). A gating charge transfer center in voltage sensors. Science *328*, 67-73.

Tervo, D. and Karpova, A. Y. (2007). Rapidly inducible, genetically targeted inactivation of neural and synaptic activity in vivo. Curr Opin Neurobiol *17*, 581-586.

Thomas, P. and Smart, T. G. (2005). HEK293 cell line: a vehicle for the expression of recombinant proteins. J. Pharmacol. Toxicol. Methods *51*, 187-200.

Thum, A. S., Knapek, S., Rister, J., Dierichs-Schmitt, E., Heisenberg, M., and Tanimoto, H. (2006). Differential potencies of effector genes in adult Drosophila. J. Comp. Neurol. *498*, 194-203.

Tiscornia, G., Singer, O., and Verma, I. M. (2006). Production and purification of lentiviral vectors. Nat. Protocol *1*, 241-245.

Tong, Y., Brandt, G. S., Li, M., Shapovalov, G., Slimko, E., Karschin, A., Dougherty, D. A., and Lester, H. A. (2001). Tyrosine decaging leads to substantial membrane trafficking during modulation of an inward rectifier potassium channel. J Gen Physiol *117*, 103-118.

Tsien, R. Y. (1981) A non-disruptive technique for loading calcium buffers and indicators into cells. Nature *290*, 527-528.

Valiyaveetil, F. I., Sekedat, M., MacKinnon, R., and Muir, T. W. (2006). Structural and functional consequences of an amide-to-ester substitution in the selectivity filter of a potassium channel. J. Am. Chem. Soc. *128*, 11591-11599.

Volgraf, M., Gorostiza, P., Numano, R., Kramer, R. H., Isacoff, E. Y., Trauner, D. (2006). Allosteric control of an ionotropic glutamate receptor with an optical switch. Nat. Chem. Biol. *2*, 47-52.

Wang, L., Brock, A., Herberich, B., and Schultz, P. G. (2001). Expanding the genetic code of Escherichia coli. Science *292*, 498-500.

Wang, L., and Schultz, P. G. (2005). Expanding the genetic code. Angew. Chem. Int. Ed. Engl. *44*, 34-66.

Wang, L., Xie, J., and Schultz, P. G. (2006). Expanding the genetic code. Annu. Rev. Biophys. Biomol. Struct. *35*, 225-249.

Wang, Q., Parrish, A. R., and Wang, L. (2009). Expanding the genetic code for biological studies. Chem. Biol. *16*, 323-336.

Wang, W., Takimoto, J. K., Louie, G. V., Baiga, T. J., Noel, J. P., Lee, K. F., Slesinger, P. A., and Wang, L. (2007). Genetically encoding unnatural amino acids for cellular and neuronal studies. Nat. Neurosci. *10*, 1063-1072.

White, B., Osterwalder, T., and Keshishian, H. (2001). Molecular genetic approaches to the targeted suppression of neuronal activity. Curr. Biol. *11*, R1041-1053.

Wulff, H., Castle, N. A., and Pardo, L. A. (2009). Voltage-gated potassium channels as therapeutic targets. Nat. Rev. Drug Discov. *8*, 982-1001.

Xiao, J., Zhen, X. G., and Yang, J. (2003). Localization of PIP2 activation gate in inward rectifier K+ channels. Nat. Neurosci. *6*, 811-818.

Yamada, K. A., Tang, C. M. (1993). Benzothiadiazides inhibit rapid glutamate receptor desensitization and enhance glutamatergic synaptic currents. J. Neurosci. *13*, 3904-3915.

Yamamoto, M., Wada, N., Kitabatake, Y., Watanabe, D., Anzai, M., Yokoyama, M., Teranishi, Y., and Nakanishi, S. (2003). Reversible suppression of glutamatergic neurotransmission of cerebellar granule cells in vivo by genetically manipulated expression of tetanus neurotoxin light chain. J. Neurosci. *23*, 6759-6767.

Yizhar, O., Fenno, L. E., Davidson, T. J., Mogri, M., and Deisseroth, K. (2011). Optogenetics in neural systems. Neuron *71*, 9-34.

Yoshimura, Y., Dantzker, J. L., and Callaway, E. M. (2005). Excitatory cortical neurons form fine-scale functional networks. Nature *433*, 868-873.

Yu, C. R., Power, J., Barnea, G., O'Donnell, S., Brown, H. E., Osborne, J., Axel, R., and Gogos, J. A. (2004). Spontaneous neural activity is required for the

establishment and maintenance of the olfactory sensory map. Neuron *42*, 553-566.

Zaddam, S., Sacconi, S., Desnuelle, C., Amri, E., and Said, B. (2012). The Potassium Channel Kir2.1 Activity is Required for Osteoblastogenesis. Biophys. J. *102*, 538a.

Zeitelhofer, M., Vessey, J. P., Xie, Y., Tubing, F., Thomas, S., Kiebler, M., and Dahm, R. (2007). High-efficiency transfection of mammalian neurons via nucleofection. Nat. Protocol *2*, 1692-1704.

Zemelman, B. V., Nesnas, N., Lee, G. A., and Miesenbock, G. (2003). Photochemical gating of heterologous ion channels: remote control over genetically designated populations of neurons. Proc. Natl. Acad. Sci. USA *100*, 1352-1357.

Zhang, F., Wang, L. P., Brauner, M., Liewald, J. F., Kay, K., Watzke, N., Wood, P. G., Bamberg, E., Nagel, G., Gottschalk, A., and Deisseroth, K. (2007). Multimodal fast optical interrogation of neural circuitry. Nature *446*, 633-639.